Structural Diversity of Mixed Polypnictogen Complexes: Dicationic $E_2E'_2$ (E ≠ E' = P, As, Sb, Bi) Chains, Cycles and Cages Stabilized by Transition Metals

– SUPPORTING INFORMATION –

Luis Dütsch, Christoph Riesinger, Gábor Balázs, Michael Seidl, and Manfred Scheer*

Institute of Inorganic Chemistry
University of Regensburg
D-93040 Regensburg
Germany

Email: manfred.scheer@ur.de

Contents

1 General considerations

All manipulations were carried out under an inert atmosphere of dried nitrogen/argon using standard Schlenk and glovebox techniques. The used Schlenk flask were heated at 550 °C for at least 15-30 minutes under reduced pressure prior to use to get rid of water traces adhered to the glass surface. The starting materials Li[TEF^{Cl}],[1] [Thia][TEF],[2] and [{CpMo(CO)$_2$}$_2$(μ,η^2:η^2-EE')] (EE' = PAs (**A**), PSb (**B**), AsSb (**C**), AsBi (**D**), SbBi(**E**))[3] were synthesized via the respective literature procedures. The reagents thianthrene and [NO][SbF$_6$] are commercially available and were used without further purification. Solvents were freshly distilled under nitrogen after drying over CaH_2 (CH_2Cl_2, CD_2Cl_2), K or Na/K alloy (alkanes), P_4O_{10} (*ortho*-difluorobenzene = *o*-DFB) or NaH (toluene). Dried solvents were also taken from a solvent purification system from MBraun. For reactions in liquid SO_2, SO_2 gas cylinders were bought from Linde and SO_2 was condensed into Schlenk flasks with a Young valve at −196 °C under reduced pressure. Diatomaceous earth used for filtrations was stored at 130 °C for at least 24 h prior to use. NMR spectra were recorded at 300 K (if not stated otherwise) on a Bruker Avance 300 MHz NMR spectrometer (^{1}H: 300.132 MHz, ^{31}P: 121.495 MHz, ^{13}C: 75.468 MHz, ^{19}F: 282.404 MHz) or a Bruker Avance 400 MHz NMR spectrometer (^{1}H: 400.130 MHz, ^{31}P: 161.976 MHz, ^{13}C: 100.613 MHz, ^{19}F: 376.498 MHz) with external references of $SiMe_4$ (^{1}H, ^{13}C), CCl_3F (^{19}F) and H_3PO_4 (85%, ^{31}P). The chemical shifts δ are presented in parts per million (ppm) and coupling constants *J* in Hz. X-Band EPR spectra were recorded on a MiniScope MS400 device from Magnettech GmbH with a frequency of 9.5 GHz equipped with a rectangular resonator TE102. Cyclic voltammetry (CV) measurements were performed in CH_2Cl_2 solution containing [NBu_4][PF_6] (c = 0.1 mol·L^{-1}) as supporting electrolyte. Ferrocene (Cp_2Fe) was added to the samples after the complete measurements and Cp_2Fe was used as an internal reference (E($Cp_2Fe^{0/+}$) = 0 V). ESI-MS spectra were either measured on a Finnigan Thermoquest TSQ 7000 mass-spectrometer by the MS department of the University of Regensburg or on a Waters Micromass LCT ESI-TOF mass-spectrometer by the first author. IR spectra were recorded either as solids using a ThermoFisher Nicolet iS5 FT-IR spectrometer with an iD7 ATR module and an ITX Germanium or ITX Diamond crystal, or grinded together with dried KBr and pressed to pellets and measured on a VARIAN FTS-800 FR-IR spectrometer. Elemental analyses (EA) were performed by the micro analytical laboratory of the University of Regensburg.

2 Experimental details

2.1 Synthesis of $[Thia]^{\cdot+}$ with $[TEF^{Cl}]^-$ as counterion

In order to vary the weakly coordinating anion (= WCA) of the desired products and to investigate their influence on the solid-state structures, the used strong one-electron oxidant thianthrenium $[C_{12}H_8S_2]^{\cdot+}$ (= $[Thia]^+$, E^0 = 0.86 V vs $Cp_2Fe^{0/+}$)[4] was synthesized with the WCA $[Al\{OC(CF_3)_2(CCl_3)\}_4]^-$ (=$[TEF^{Cl}]^-$). A simple one-step synthesis starting from commercially available reagents afford the deep purple salt $[Thia][TEF^{Cl}]$ in excellent yields and in a multigram scale (Scheme S1). The reaction is performed in liquid SO_2 to ensure the solubility of all components.

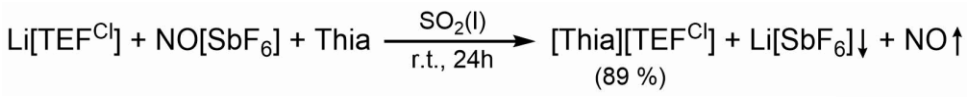

Scheme S1: Synthesis of $[Thia][TEF^{Cl}]$.

A Schlenk flask equipped with a Young valve was loaded with a stirring bar, thianthrene (1.00 g, 4.62 mmol, 1.0 eq.), $NO[SbF_6]$ (1.22 g, 4.59 mmol, 1 eq.) and $Li[TEF^{Cl}]$ (5.44 g, 4.65 mmol, 1.0 eq.). 60 mL SO_2 were condensed onto these solids under reduced pressure at –196 °C. The flask was closed under reduced pressure and the cooling was removed. Upon dissolution the reaction turns from light blue to dark blue and finally to dark violet. After stirring at room temperature for 24 h the SO_2 was removed. The residue was dissolved/suspended in 30 mL CH_2Cl_2 and transferred onto a frit with diatomaceous earth. The dark purple solution was filtered, and the residue washed with CH_2Cl_2 till the filtrate is colourless. The amount of solvent was reduced to 15 mL and addition of 200 mL *n*-hexane leads to precipitation of dark purple $[Thia][TEF^{Cl}]$, which was washed twice with 60 mL of a 1:1 mixture of *n*-hexane/toluene. Recrystallization via layering a CH_2Cl_2 solution with *n*-hexane (1:6) affords dark purple crystals. These were washed again with 50 mL toluene and dried in vacuum for 3 hours.Yield 5.61 g (4.06 mmol = 89 %). ^1H NMR (400 MHz, CD_2Cl_2) no signals detectable for $[Thia]^{\cdot+}$; $^{19}F\{^1H\}$ NMR (282.4 MHz, CD_2Cl_2) δ/ppm = –67.4 (s). Anal. calcd. for $[Thia][TEF^{Cl}]$: C: 24.35; H: 0.58, S: 4.64; found: C: 24.61, H: 0.68, S: 4.72. Positive ion ESI-MS *m/z* (%): 215.97 (100) $[Thia]^+$. Negative ion ESI-MS *m/z* (%): 1162.59 (100) $[TEF^{Cl}]^-$.

2.2 Oxidation of A–E with [Thia][TEF]

2.2.1 Preparation of $[\{CpMo(CO)_2\}_4(\mu_4,\eta^2{:}\eta^2{:}\eta^2{:}\eta^2\text{-AsPPAs})][TEF]_2$ (1)

A dark purple solution of [Thia][TEF] (203 mg, 0.17 mmol, 1.0 eq.) in 15 mL CH_2Cl_2 was transferred to an orange red solution of $[\{CpMo(CO)_2\}_2(\mu,\eta^2{:}\eta^2\text{-PAs})]$ (**A**) (98 mg, 0.18 mmol, 1.05 eq.) in 10 mL CH_2Cl_2 at room temperature causing an immediate colour change to a dark greenish red solution. After stirring for 120 minutes, addition of 60 mL *n*-hexane led to precipitation of a dark green powder of crude **1**. The slightly orange supernatant solution was removed and the precipitate washed twice with 20 mL of pure toluene. The crude product was dried in vacuum. Recrystallization via layering a CH_2Cl_2 solution with *n*-hexane (1:5) and storage at +4 °C afforded pure **1** as dark red blocks, which were suitable for single crystal X-ray diffraction. The supernatant was removed and the crystals were dried in vacuum. Yield 189 mg (0.062 mmol =

73 %). ^{1}H NMR (300 MHz, CD_2Cl_2) δ/ppm = 5.66 (s, Cp). ^{31}P{^{1}H} NMR (121.5 MHz, CD_2Cl_2) δ/ppm = −28.8 (s). ^{31}P NMR (121.5 MHz, CD_2Cl_2) δ/ppm = −29.1 (s); for ^{31}P{^{1}H} VT-NMR see NMR section below. ^{13}C{^{1}H} NMR (75.5 MHz, CD_2Cl_2) δ/ppm = 219.2 (small, br, CO), 121.65 (q, $^{1}J_{CF}$ = 293 Hz; CF_3), 90.98 (s, Cp). ^{19}F{^{1}H} NMR (282.4 MHz, CD_2Cl_2) δ/ppm = −75.5 (s, CF_3). Compound **1** is silent in the X-band EPR spectra in the solid-state and in CH_2Cl_2 solution at room temperature and at 77 K. Anal. calcd. for $[(C_{14}H_{10}O_4Mo_2PAs)_2][TEF]_2$: C: 23.91; H: 0.67. Found: (crystalline product **1**): C: 24.26; H: 0.82. Positive ion ESI-MS *m/z* (%): 539.63 (15) [**A**]$^{+}$, 511.71 (3) [**A**–1·CO]$^{+}$, 483.68 (37) [**A**–2·CO]$^{+}$, 455.68 (100) [**A**–3·CO]$^{+}$, 427.69 (70) [**A**–4·CO]$^{+}$; in very concentrated solutions: 511,71 (5) [**A**-1·CO]$_2^{2+}$. Negative ion ESI-MS *m/z* (%): 966.9 (100) [TEF]$^{-}$. **1** (crystalline): IR(KBr) $\tilde{\nu}$/cm^{-1} = 3136 (w), 2344 (vw), 2062(s), 2050 (s), 2032 (vs), 1991 (s), 1955 (m), 1624 (vw), 1426 (w), 1354 (s), 1302 (vs), 1277 (vs), 1243 (vs), 1219 (vs), 1172 (m), 973 (vs), 841 (m), 727 (s). **1** (precipitate): IR(KBr) $\tilde{\nu}$/cm^{-1} = 3133 (w), 2960 (vw), 2925 (w), 2854 (vw), 2360 (w), 2343 (w), 2062 (s), 2051 (vs), 2037 (vs), 2023 (vs), 1995 (s, br), 1955 (m, br), 1627 (w), 1426 (w), 1384 (w), 1353 (m), 1302 (vs), 1277 (vs), 1244 (vs), 1220 (vs), 1173 (m), 974 (vs), 841 (m), 728 (s).

2.2.2 Preparation of [{CpMo(CO)$_2$}$_4$(μ_4,η^2:η^2:η^2-SbPPSb)][TEF]$_2$ (2)

A dark purple solution of [Thia][TEF] (121 mg, 0.10 mmol, 1.0 eq.) in 7 mL CH_2Cl_2 was transferred to an orange red solution of [{CpMo(CO)$_2$}$_2$(μ,η^2:η^2-PSb)] (**B**) (60 mg, 0.10 mmol, 1.0 eq.) in 3 mL CH_2Cl_2 at room temperature causing an immediate colour change to a dark orange brown solution. After stirring for 30 minutes, addition of 40 mL *n*-hexane led to precipitation of a brown, fluffy powder of crude **2**. The slightly orange supernatant solution was removed and the precipitate washed twice with 20 mL of pure toluene leading to an oily solid. The crude product was dried in vacuum, redissolved in 5 mL CH_2Cl_2 and precipitated with 30 mL *n*-hexane yielding again a fluffy, brown powder. Recrystallization via layering a CH_2Cl_2 solution with *n*-hexane (1:5) and storage at +4 °C afforded pure **2** as thin orange red plates, which were not suitable for good single crystal X-ray diffraction (several attempts to get suitable crystals by changing the solvents, crystallization methods or crystallization temperatures were unsuccessful). The supernatant was removed and the crystals were dried in vacuum. Yield 137 mg (0.044 mmol = 88 %). ^{1}H NMR (400 MHz, CD_2Cl_2) δ/ppm = 5.61 (s, Cp). ^{31}P{^{1}H} NMR (162.0 MHz, CD_2Cl_2) δ/ppm = 34.7 (s). ^{31}P NMR (162.0 MHz, CD_2Cl_2) δ/ppm = 34.6 (s). ^{19}F{^{1}H} NMR (376.6 MHz, CD_2Cl_2) δ/ppm = −75.5 (s). ^{31}P{^{1}H} NMR of crude solution of **2** (162.0 MHz, CH_2Cl_2/C_6D_6) δ/ppm = 35.0 (s). ^{31}P NMR of crude solution of **2** (162.0 MHz, CH_2Cl_2/C_6D_6) δ/ppm = 35.0 (s); for ^{31}P{^{1}H} VT-NMR see NMR section below. Compound **2** is silent in the X-band EPR spectra in CH_2Cl_2 solution at room temperature and at 77 K. Anal. calcd. for $[(C_{14}H_{10}O_4Mo_2PSb)_2][TEF]_2\cdot(toluene)_{0.7}$: C: 24.57; H: 0.81. Found: C: 24.55; H: 0.60. Mass spectrometric investigations were unsuccessful due to decomposition of **2** during the measurement.

2.2.3 Preparation of [{CpMo(CO)$_2$}$_4$(μ_4,η^2:η^2:η^2-AsSbSbAs)][TEF]$_2$ (3a)

A dark purple solution of [Thia][TEF] (56 mg, 0.048 mmol, 1.0 eq.) in 7 mL CH_2Cl_2 was transferred to a red solution of [{CpMo(CO)$_2$}$_2$(μ,η^2:η^2-AsSb)] (**C**) (41 mg, 0.048 mmol, 1.0 eq.) in 5 mL CH_2Cl_2 at room temperature causing an immediate colour change to a dark greenish brown solution. After stirring for 15 minutes, addition

of 50 mL *n*-hexane led to precipitation of a green to black powder. The slightly orange supernatant solution was removed and the precipitate washed twice with 30 mL of pure toluene. Recrystallization via layering a CH_2Cl_2 solution with *n*-hexane (1:5) and storage at +4 °C afforded pure **3a** as dark red to black blocks, which were suitable for single crystal X-ray diffraction. The supernatant was removed and the crystals were dried in vacuum. Yield 70 mg (0.022 mmol = 92 %). ^{1}H NMR (400 MHz, CD_2Cl_2) δ/ppm = 5.68 (s, Cp). ^{19}F{^{1}H} NMR (376.5 MHz, CD_2Cl_2) δ/ppm = −75.5 (s, CF_3). Compound **3a** is silent in the X-band EPR spectra in CH_2Cl_2 solution at room temperature, but shows a very weak axial signal (g_{iso} = 1.954) at 77 K. Anal. calcd. for $[(C_{14}H_{10}O_4Mo_2AsSb)_2][TEF]_2$: C: 22.55; H: 0.63. Found: C: 22.94; H: 0.72. Positive ion ESI-MS *m/z* (%): 629.63 (80) [**C**]$^+$, 601.67 (3) [**C**–CO]$^+$, 573.68 (20) [**C**–2·CO]$^+$, 545.67 (100) [**C**–3·CO]$^+$, 517.68 (50) [**C**–4·CO]$^+$. IR (ATR) $\tilde{\nu}$/cm^{-1} = 2055 (w), 2048 (w), 2038 (w), 1999 (m), 1988 (m), 1961 (w), 1934 (vw), 1352 (w), 1297 (m), 1274 (s), 1240 (s), 1213 (vs), 1173 (w), 971 (vs), 841 (w), 727 (s); C-H around 3000 not observed (too small).

2.2.4 Preparation of [{CpMo(CO)$_2$}$_4$(μ_4,η^2:η^2:η^2-AsBiBiAs)][TEF]$_2$ (4a)

A dark purple solution of [Thia][TEF] (118 mg, 0.10 mmol, 1.0 eq.) in 5 mL CH_2Cl_2 was transferred to a dark red solution of [{CpMo(CO)$_2$}$_2$(μ,η^2:η^2-AsBi)] (**D**) (72 mg, 0.10 mmol, 1.0 eq.) in 3 mL CH_2Cl_2 at room temperature causing an immediate colour change to a dark brown solution. After stirring for 30 minutes, addition of 40 mL *n*-pentane led to precipitation of a brown to black powder. The slightly orange supernatant solution was removed and the precipitate washed twice with 20 mL of pure toluene and twice with 20 mL *n*-pentane. The crude product was dried in vacuum and recrystallization via layering a CH_2Cl_2 solution with *n*-hexane (1:5) and storage at room temperature under exclusion of light afforded pure **4a** as black blocks, which were suitable for single crystal X-ray diffraction. The supernatant was removed and the crystals were dried in vacuum. Yield 150 mg (0.0445 mmol = 89 %). ^{1}H NMR (400 MHz, CD_2Cl_2) δ/ppm = 5.69 (s, Cp). ^{13}C{^{1}H} NMR (100.6 MHz, CD_2Cl_2) δ/ppm = 89.80 (s, Cp), 121.25 (q, $^1J_{CF}$ = 291 Hz; CF_3), 214.33 (s, CO), 215.65 (s, CO). ^{19}F{^{1}H} NMR (376.6 MHz, CD_2Cl_2) δ/ppm = −75.5 (s, CF_3). Compound **4a** is silent in the X-band EPR spectra in CH_2Cl_2 solution at room temperature and at 77 K. Anal. calcd. for $[(C_{14}H_{10}O_4Mo_2AsBi)_2][TEF]_2$: C: 21.38; H: 0.60. Found: C: 21.82; H: 0.56. Positive ion ESI-MS *m/z* (%): 717.77 (100) [**D**]$^+$, 734.77 (15) [**D**+O]$^+$. Negative ion ESI-MS *m/z* (%): 966.91 (100) [TEF]$^-$.

2.2.5 Preparation of [{CpMo(CO)$_2$}$_4$(μ_4,η^2:η^2:η^2-BiSbSbBi)][TEF]$_2$ (5)

A dark purple solution of [Thia][TEF] (59 mg, 0.05 mmol, 1.0 eq.) in 10 mL *o*-DFB was transferred to a dark bordeaux red solution of [{CpMo(CO)$_2$}$_2$(μ,η^2:η^2-SbBi)] (**E**) (38 mg, 0.05 mmol, 1.0 eq.) in a mixture of 10 mL *o*-DFB and 1 mL CH_2Cl_2 at −20 °C causing an immediate colour change to a dark brown to black solution. After stirring for 60 minutes at −20 °C, addition of 80 mL *n*-hexane led to precipitation of a dark green to black powder. The slightly red supernatant solution was removed and the precipitate washed twice with 20 mL of pure toluene. The crude product was dried in vacuum and recrystallization via layering an *o*-DFB solution with *n*-hexane (1:4) and storage at +4 °C afforded pure **5** as black blocks, which were suitable for single crystal X-ray diffraction. The supernatant was removed and the crystals were dried in vacuum. Yield 73 mg (0.021 mmol = 84 %). ^{1}H NMR (400 MHz, CD_2Cl_2) δ/ppm = 5.64 (s, Cp, traces of **XI**), 5.72 (s, Cp of **5**), 5.78 (s,

Cp, traces of **XII**). $^{19}F\{^{1}H\}$ NMR (376.6 MHz, CD_2Cl_2) δ/ppm = −75.5 (s, CF_3). Compound **5** is silent in the X-band EPR spectra in CH_2Cl_2 solution at room temperature and at 77 K. Anal. calcd. for $[(C_{14}H_{10}O_4Mo_2SbBi)_2][TEF]_2$: C: 20.80; H: 0.58. Found: C: 21.38; H: 0.45. Mass spectrometric investigations were unsuccessful due to decomposition of **5** during the measurement.

2.3 Oxidation of C and D with [Thia][TEF^{Cl}]

2.3.1 Preparation of [{CpMo(CO)$_2$}$_4$(μ_4,η^2:η^2:η^2:η^2-AsSbAsSb)][TEF^{Cl}]$_2$ (3b)

A dark purple solution of [Thia][TEF^{Cl}] (89 mg, 0.065 mmol, 1.0 eq.) in 5 mL CH_2Cl_2 was transferred to a red solution of [{CpMo(CO)$_2$}$_2$(μ,η^2:η^2-AsSb)] (**C**) (41 mg, 0.065 mmol, 1.0 eq.) in 5 mL CH_2Cl_2 at room temperature causing an immediate colour change to a dark brown solution. After stirring for 15 minutes, addition of 40 mL toluene led to precipitation of a dark greenish brown powder. The slightly brown supernatant solution was removed and the precipitate dried in vacuum. Recrystallization via layering a CH_2Cl_2 solution with *n*-hexane (1:5) and storage at +4 °C afforded pure **3b** as dark red blocks, which were suitable for single crystal X-ray diffraction. The supernatant was removed and the crystals were dried in vacuum. Yield 89 mg (0.025 mmol = 77 %). ^{1}H NMR (400 MHz, CD_2Cl_2) δ/ppm = 5.70 (s, Cp). $^{19}F\{^{1}H\}$ NMR (376.6 MHz, CD_2Cl_2) δ/ppm = −68.5 (s, CF_3). Anal. calcd. for $[(C_{14}H_{10}O_4Mo_2AsSb)_2][TEF^{Cl}]_2$: C: 20.07; H: 0.56. Found: C: 20.31; H: 0.74. Positive ion ESI-MS *m/z* (%): 629.65 (100) [**C**]$^+$, 584.7 (37) [**VI**]$^+$, 573.7 (8) [**C**–2·CO]$^+$, 556.7 (8) [**VI**−CO]$^+$, 545.7 (18) [**C**–3·CO]$^+$, 528.7 (10) [**VI**–2·CO]$^+$, 517.7 (6) [**C**–4·CO]$^+$, 500.7 (7) [**VI**–3·CO]$^+$, 472.7 (4) [**VI**–4·CO]$^+$. Negative ion ESI-MS *m/z* (%): 1162.64 (100) [TEF^{Cl}]$^-$. IR (ATR) $\tilde{\nu}$/cm^{-1} = 3145 (vw), 3138 (vw), 3122 (vw), 2360 (w), 2344 (w), 2053 (w), 2032 (w), 1998 (m), 1983 (m), 1970 (w), 1954 (w), 1943 (w), 1310 (w), 1243 (m), 1194 (vs), 1145 (w), 1010 (w), 964 (w), 858 (m), 787 (m), 725 (m), 712 (s).

2.3.2 Preparation of [{CpMo(CO)$_2$}$_4$(μ_4,η^2:η^2:η^2:η^2-AsBiBiAs)][TEF^{Cl}]$_2$ (4b)

A dark purple solution of [Thia][TEF^{Cl}] (58 mg, 0.042 mmol, 1.0 eq.) in 3 mL CH_2Cl_2 was transferred to a dark red solution of [{CpMo(CO)$_2$}$_2$(μ,η^2:η^2-AsBi)] (**D**) (30 mg, 0.042 mmol, 1.0 eq.) in 5 mL CH_2Cl_2 at −50 °C causing an immediate colour change to a dark greenish brown solution. After stirring for 60 minutes, addition of 40 mL *n*-hexane led to precipitation of a dark green to black powder. The slightly brown supernatant solution was removed and washed twice with pure toluene. The crude product was dried in vacuum and recrystallization via layering a CH_2Cl_2 solution with *n*-hexane (1:4) and storage at +4 °C afforded pure **4b** as dark red blocks, which were suitable for single crystal X-ray diffraction. The supernatant was removed and the crystals were dried in vacuum. Yield 64 mg (0.017 mmol = 81 %). Compound **4b** is silent in the X-band EPR spectra in CH_2Cl_2 solution at room temperature and at 77 K. Anal. calcd. for $[(C_{14}H_{10}O_4Mo_2AsBi)_2][TEF^{Cl}]_2$: C: 19.14; H: 0.54. Found: C: 19.30; H: 0.40. Mass spectrometric investigations were unsuccessful due to decomposition of **4b** during the measurement.

3 Cyclovoltammetry

3.1.1 CV of A

The CV of **A** in CH_2Cl_2 solution is depicted in Figure S1. The complex undergoes a pseudo-reversible oxidation with the peak of the anodic wave at +0.19 V vs. $Cp_2Fe^{0/+}$, while the corresponding cathodic wave is significantly shifted to –0.31 V vs. $Cp_2Fe^{0/+}$. This suggests that after the first oxidation of **A**, the shifted peak for the reduction corresponds to the dication of $[\mathbf{A\text{-}A}]^{2+}$. During this study, no decline of the cathodic wave of $[\mathbf{A\text{-}A}]^{2+}$ or the observation of any reduction assignable to the monocation $[\mathbf{A}]^{+}$ could be observed in the CV regardless of the scan rates, the temperature and the concentration of **A**. This points to a rapid dimerization to the dication. The full CV of **A** (Figure S2) reveals also a second (+0.45 V vs. $Cp_2Fe^{0/+}$) and a third oxidation (+0.71 V vs. $Cp_2Fe^{0/+}$), which are irreversible.

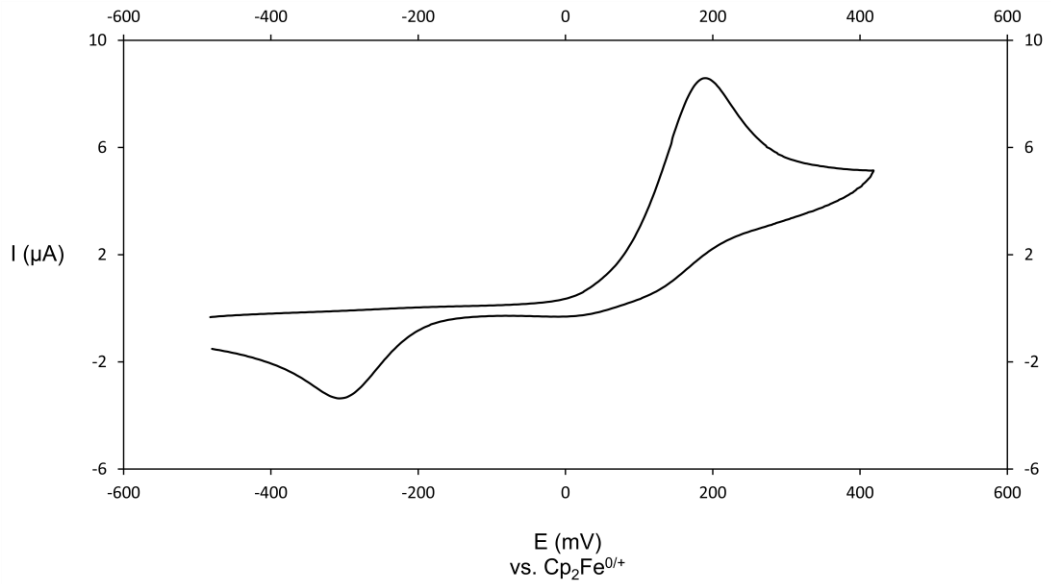

Figure S1. CV of **A** showing only the first (pseudo-reversible) oxidation.

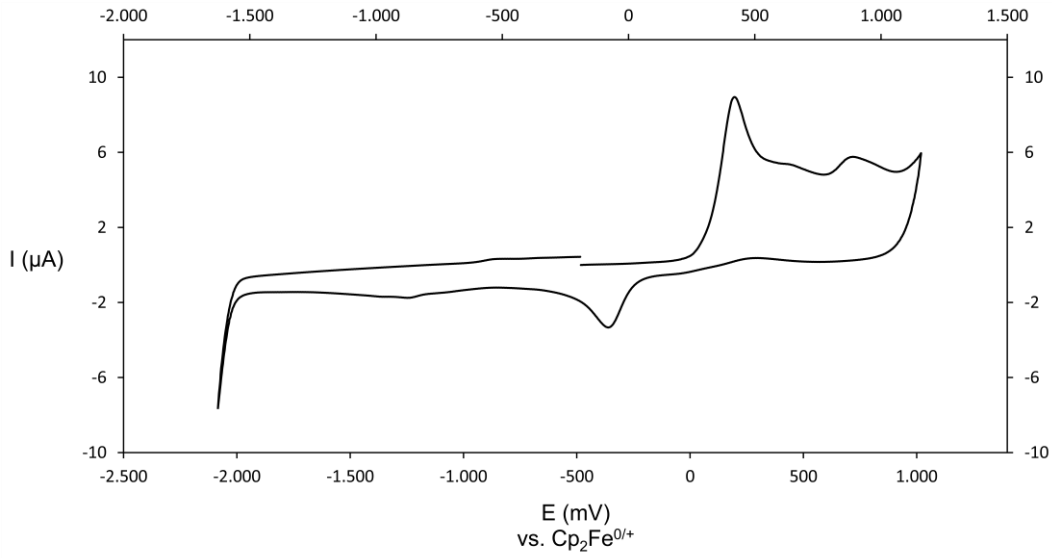

Figure S2. Full CV of **A**.

3.1.2 CV of B

The CV of **B** in CH_2Cl_2 solution is depicted in Figure S3. The complex undergoes a pseudo-reversible oxidation with the peak of the anodic wave at +0.08 V vs. $Cp_2Fe^{0/+}$, while the corresponding cathodic wave is significantly shifted to –0.43 V vs. $Cp_2Fe^{0/+}$. This suggests that after the first oxidation of **B**, the shifted peak for the reduction corresponds to the dication of $[\mathbf{B}\text{-}\mathbf{B}]^{2+}$. During this study, no decline of the cathodic wave of $[\mathbf{B}\text{-}\mathbf{B}]^{2+}$ or the observation of any reduction assignable to the monocation $[\mathbf{B}]^{+}$ could be observed in the CV regardless of the scan rates, the temperature and the concentration of **B**. This points to a rapid dimerization to the dication. The full CV of **B** (Figure S4) reveals also a second oxidation (+0.56 V vs. $Cp_2Fe^{0/+}$) and a reduction (−2.16 V vs. $Cp_2Fe^{0/+}$), which are irreversible.

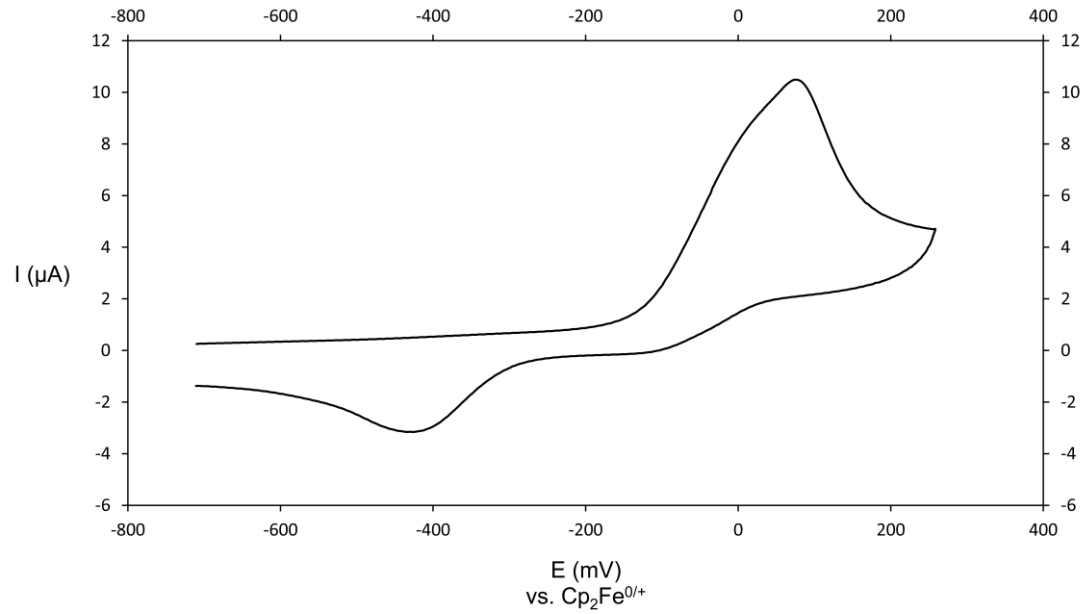

Figure S3. CV of **B** showing only the first (pseudo-reversible) oxidation.

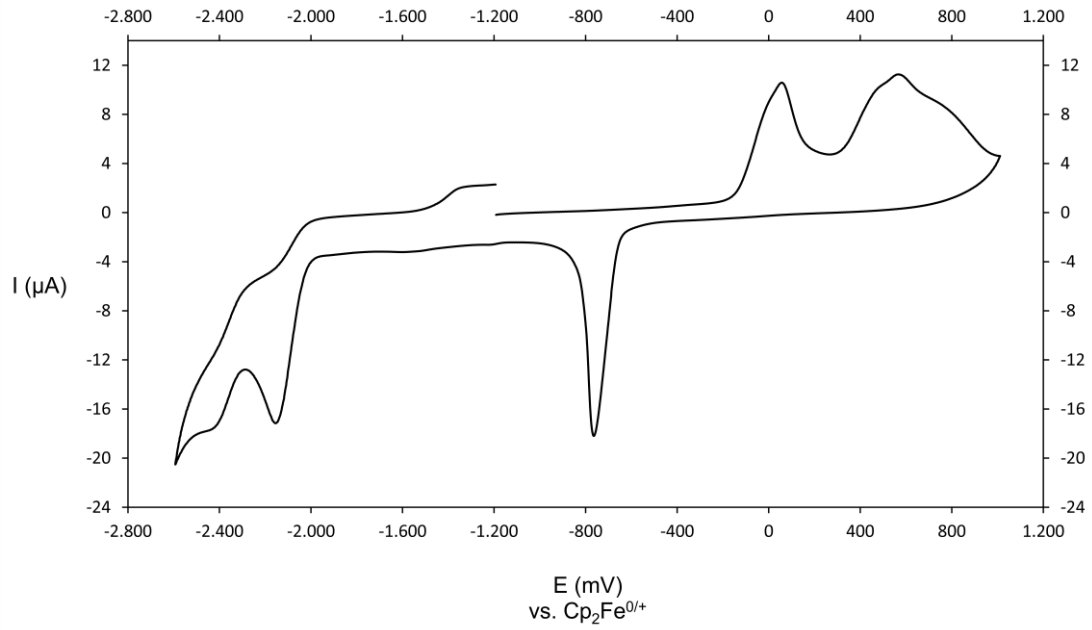

Figure S4. Full CV of **B**.

3.1.3 CV of C

The CV of **C** in CH_2Cl_2 solution is depicted in Figure S5. The complex undergoes a pseudo-reversible oxidation with the peak of the anodic wave at +0.12 V vs. $Cp_2Fe^{0/+}$, while the corresponding cathodic wave is significantly shifted to –0.20 V vs. $Cp_2Fe^{0/+}$. This suggests that after the first oxidation of **C**, the shifted peak for the reduction corresponds to the dication of $[\mathbf{C\text{-}C}]^{2+}$. During this study, no decline of the cathodic wave of $[\mathbf{C\text{-}C}]^{2+}$ or the observation of any reduction assignable to the monocation $[\mathbf{C}]^{+}$ could be observed in the CV regardless of the scan rates, the temperature and the concentration of **C**. This points to a rapid dimerization to the dication. The full CV of **C** (Figure S6) reveals also a second (+0.55 V vs. $Cp_2Fe^{0/+}$) and a third oxidation (+1.26 V vs. $Cp_2Fe^{0/+}$) as well as a reduction (−2.17 V vs. $Cp_2Fe^{0/+}$), which are irreversible.

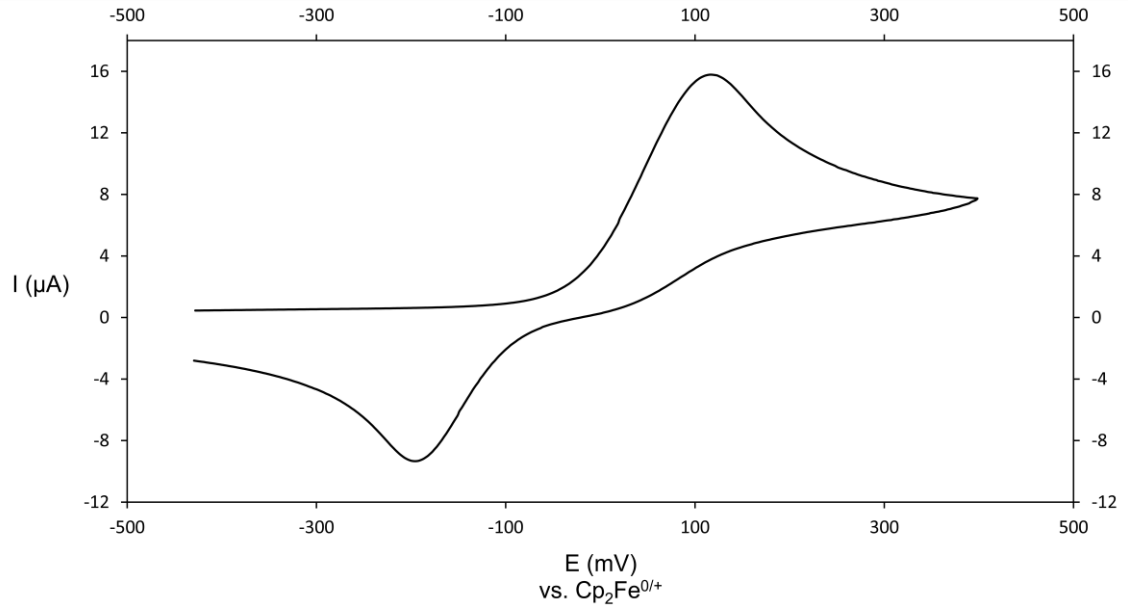

Figure S5. CV of **C** showing only the first (pseudo-reversible) oxidation.

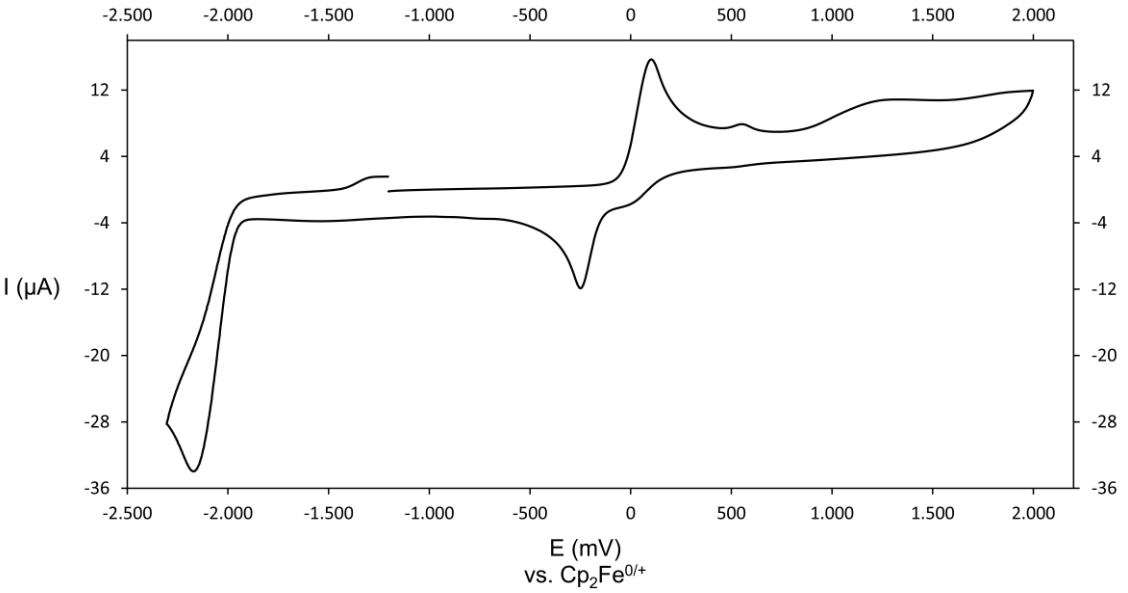

Figure S6. Full CV of **C**.

3.1.4 CV of D

The CV of **D** in CH_2Cl_2 solution is depicted in Figure S7. The complex undergoes a pseudo-reversible oxidation with the peak of the anodic wave at –0.10 V vs. $Cp_2Fe^{0/+}$, while the corresponding cathodic wave is significantly shifted to –0.36 V vs. $Cp_2Fe^{0/+}$. This suggests that after the first oxidation of **D**, the shifted peak for the reduction corresponds to the dication of $[\mathbf{D\text{-}D}]^{2+}$. During this study, no decline of the cathodic wave of $[\mathbf{D\text{-}D}]^{2+}$ or the observation of any reduction assignable to the monocation $[\mathbf{D}]^{+}$ could be observed in the CV regardless of the scan rates, the temperature and the concentration of **D**. This points to a rapid dimerization to the dication. The full CV of **D** (Figure S8) reveals also a second (+0.19 V vs. $Cp_2Fe^{0/+}$) and a third oxidation (+0.88 V vs. $Cp_2Fe^{0/+}$) as well as a reduction (−2.26 V vs. $Cp_2Fe^{0/+}$), which are irreversible.

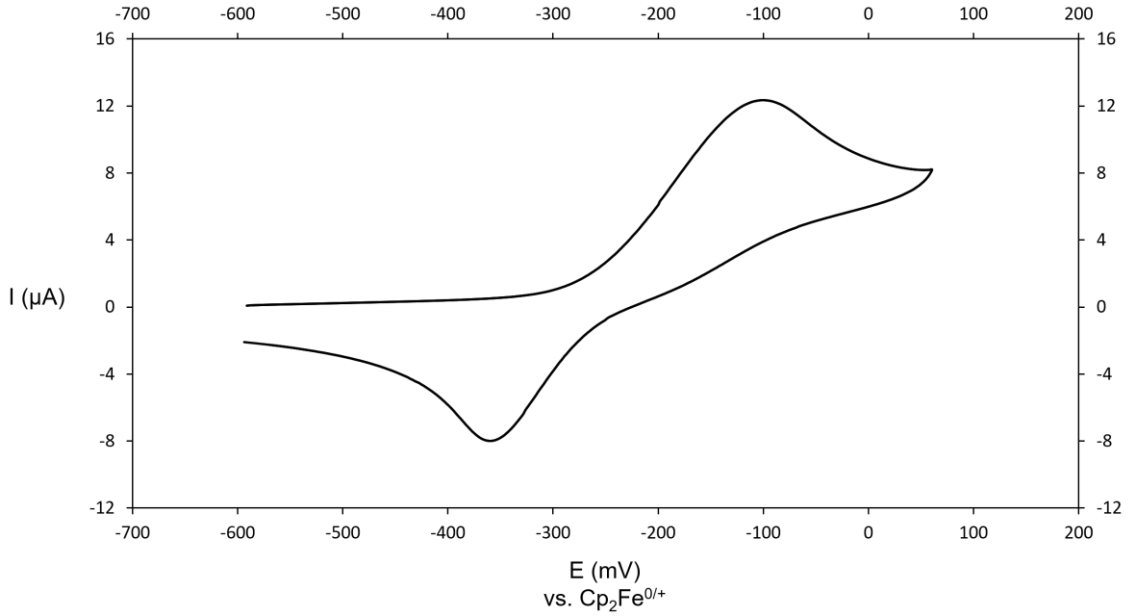

Figure S7. CV of **D** showing only the first (pseudo-reversible) oxidation.

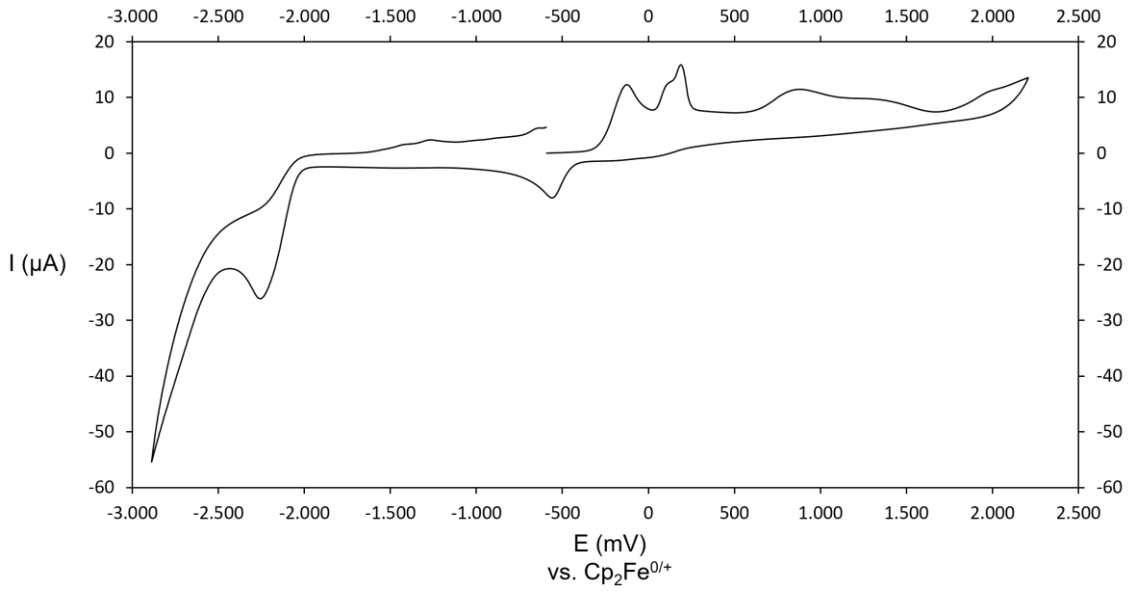

Figure S8. Full CV of **D**.

3.1.5 CV of E

The CV of **E** in CH_2Cl_2 solution is depicted in Figure S9. The complex undergoes a pseudo-reversible oxidation with the peak of the anodic wave at −0.07 V vs. $Cp_2Fe^{0/+}$, while the corresponding cathodic wave is significantly shifted to –0.44 V vs. $Cp_2Fe^{0/+}$. This suggests that after the first oxidation of **E**, the shifted peak for the reduction corresponds to the dication of [**E-E**]$^{2+}$. During this study, no decline of the cathodic wave of [**E-E**]$^{2+}$ or the observation of any reduction assignable to the monocation [**E**]$^{+}$ could be observed in the CV regardless of the scan rates, the temperature and the concentration of **E**. This points to a rapid dimerization to the dication. Besides the oxidation, also a small shoulder at (+0.05 V vs. $Cp_2Fe^{0/+}$), which can be attributed to small trace impurities of **VI**, which are formed during its synthesis.[2] The full CV of **E** (Figure S10) reveals also a second (+0.48 V vs. $Cp_2Fe^{0/+}$) and a third oxidation (+0.89 V vs. $Cp_2Fe^{0/+}$) as well as a reduction (−2.11 V vs. $Cp_2Fe^{0/+}$), which are irreversible.

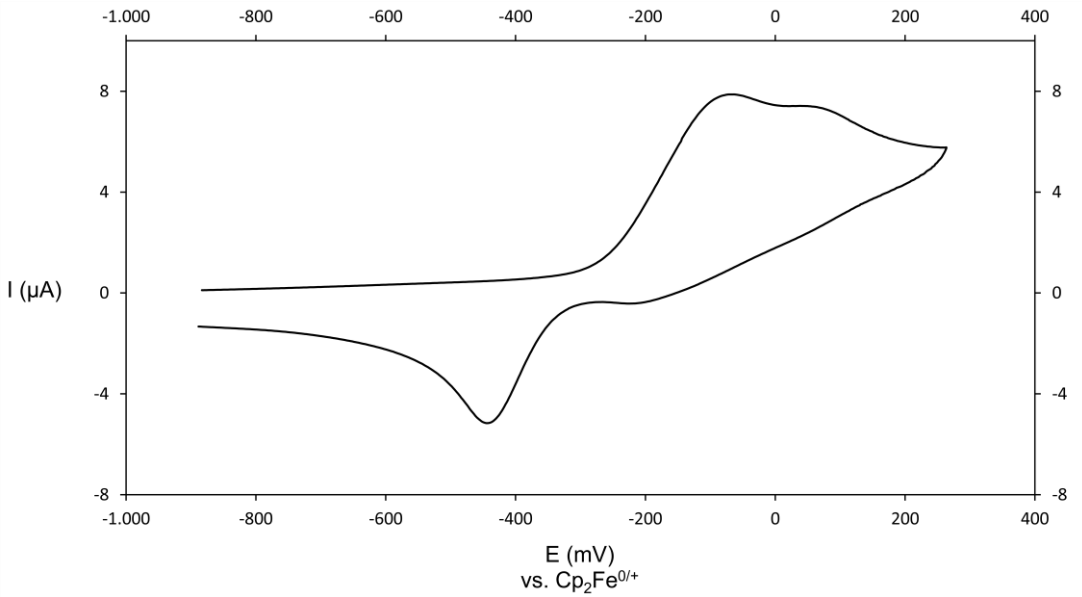

Figure S9. CV of **E** showing only the first (pseudo-reversible) oxidation.

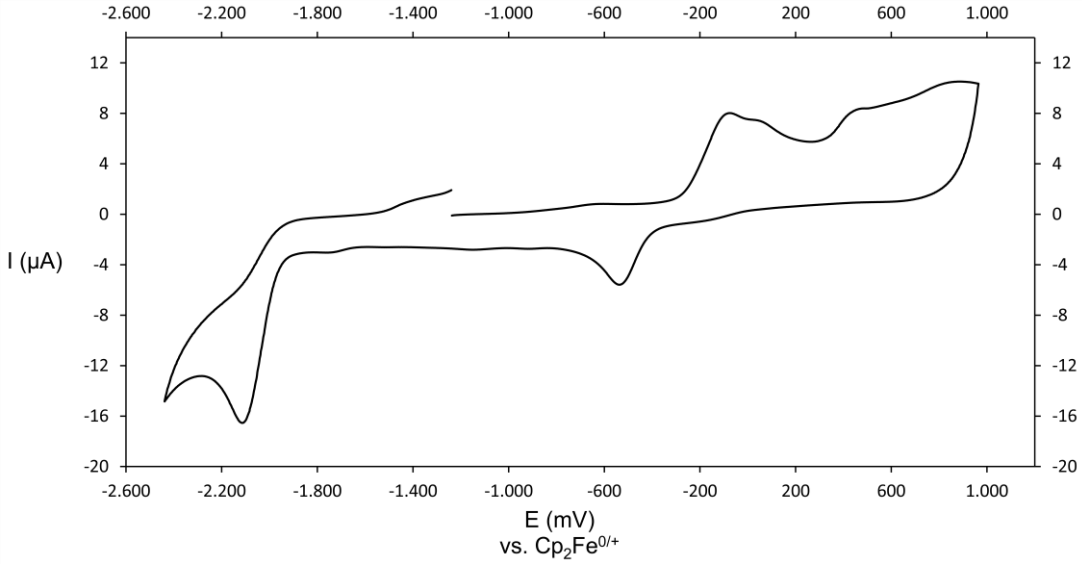

Figure S10. Full CV of **E**.

4 NMR spectra

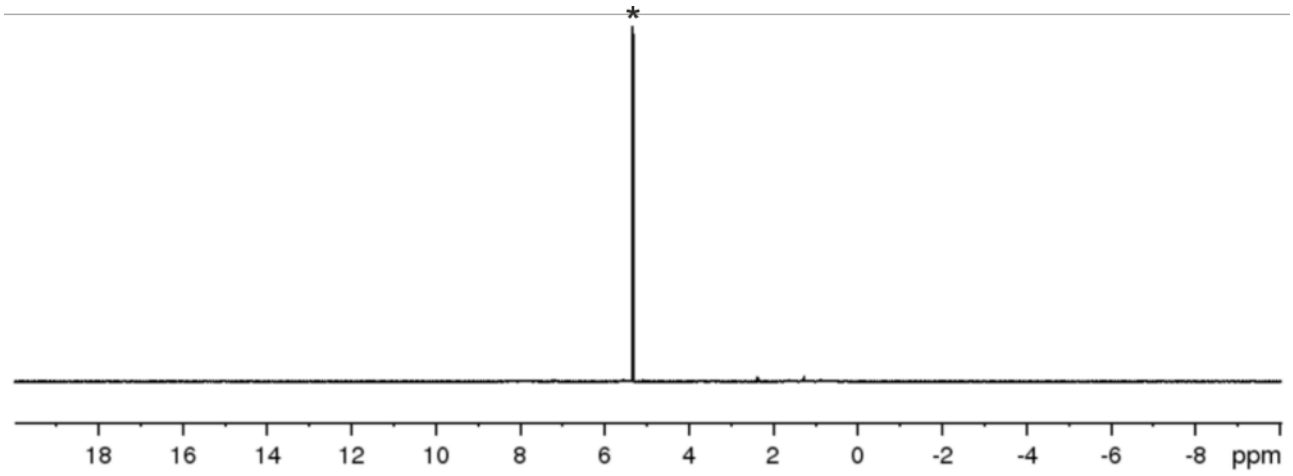

Figure S11: ^{1}H NMR spectrum of [Thia][TEF^{Cl}] in CD_2Cl_2; * = CD_2Cl_2.

The ^{1}H NMR spectrum of [Thia][TEF^{Cl}] reveals no signals for $[Thia]^{\cdot+}$ affirming the paramagnetic character of the radical cation.

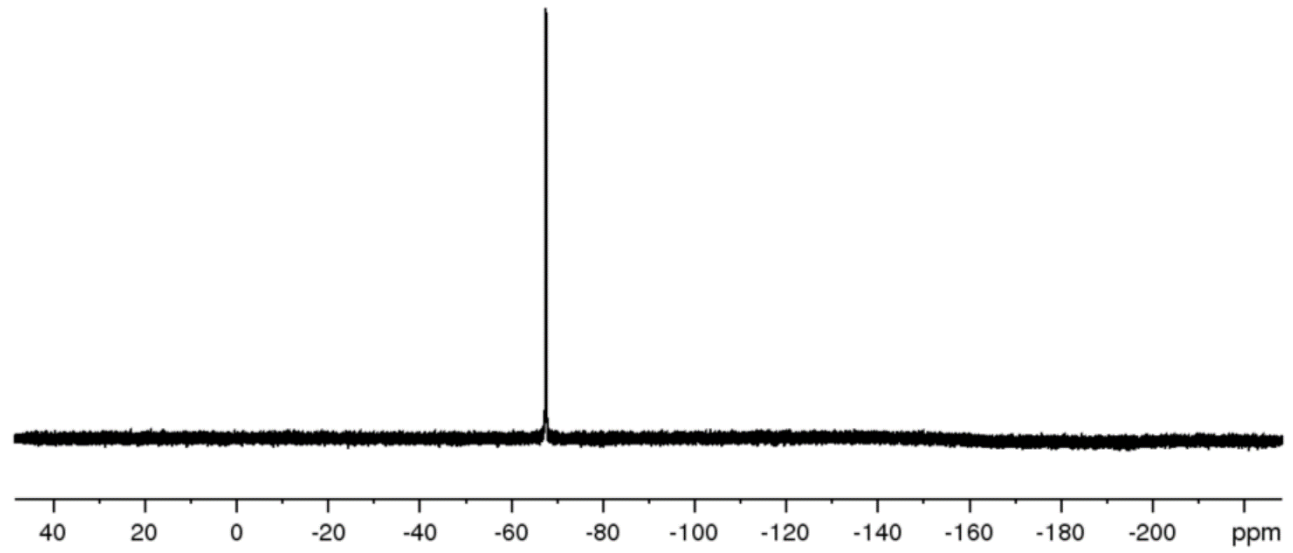

Figure S12: $^{19}F\{^{1}H\}$ NMR spectrum of [Thia][TEF^{Cl}] in CD_2Cl_2.

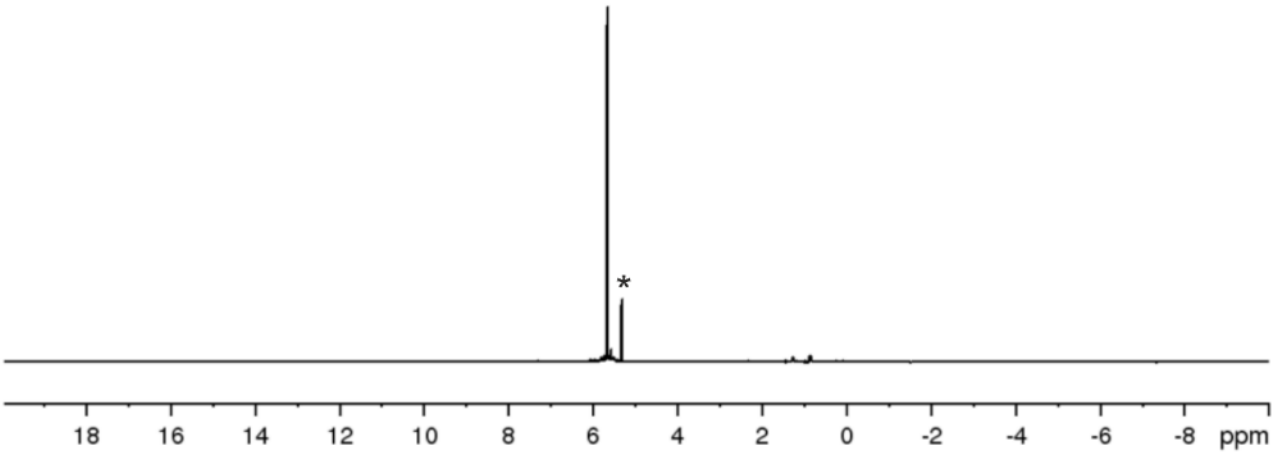

Figure S13: ^{1}H NMR spectrum of [{CpMo(CO)$_2$}$_4$(μ_4,η^2:η^2:η^2:η^2-AsPPAs)][TEF]$_2$ (**1**) in CD_2Cl_2; * = CD_2Cl_2.

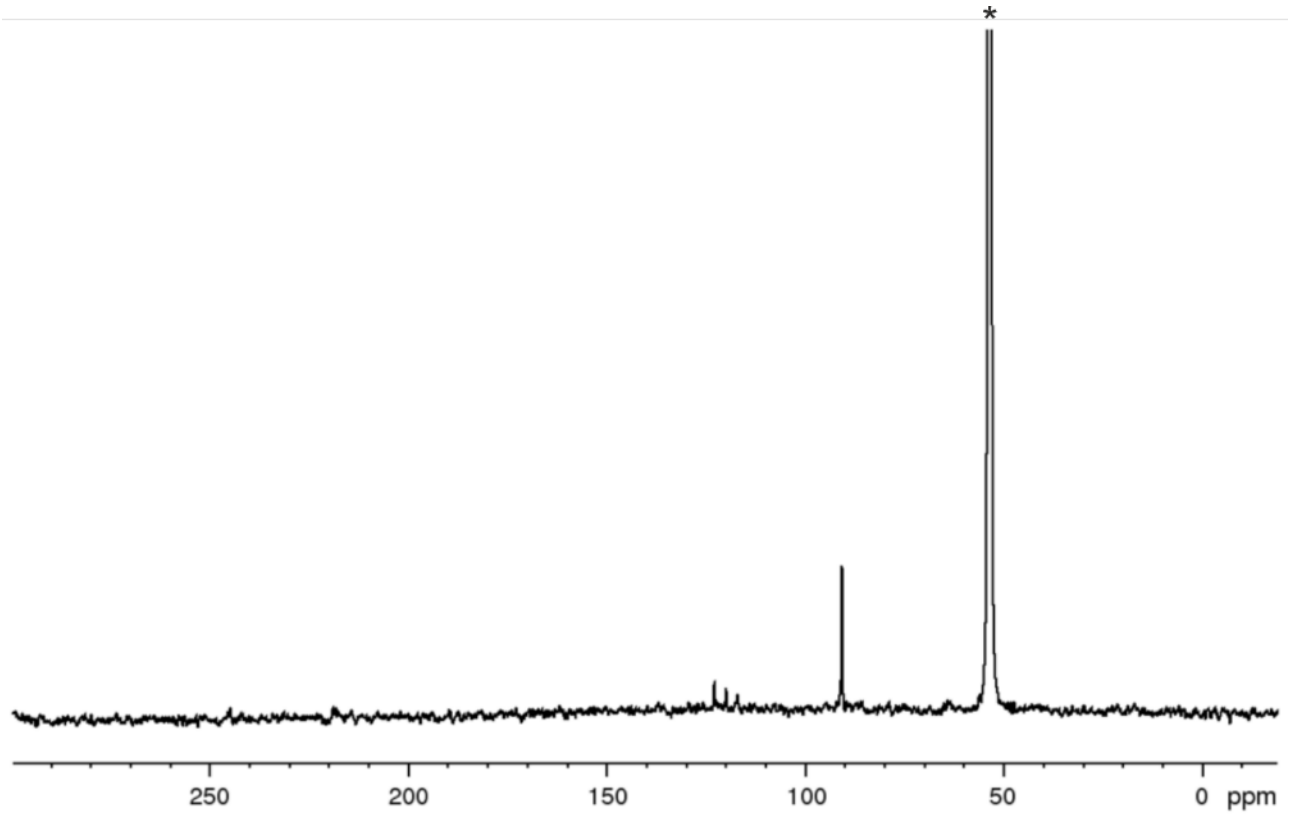

Figure S14: $^{13}C\{^{1}H\}$ NMR spectrum of [{CpMo(CO)$_2$}$_4$(μ_4,η^2:η^2:η^2:η^2-AsPPAs)][TEF]$_2$ (**1**) in CD_2Cl_2; * = CD_2Cl_2.

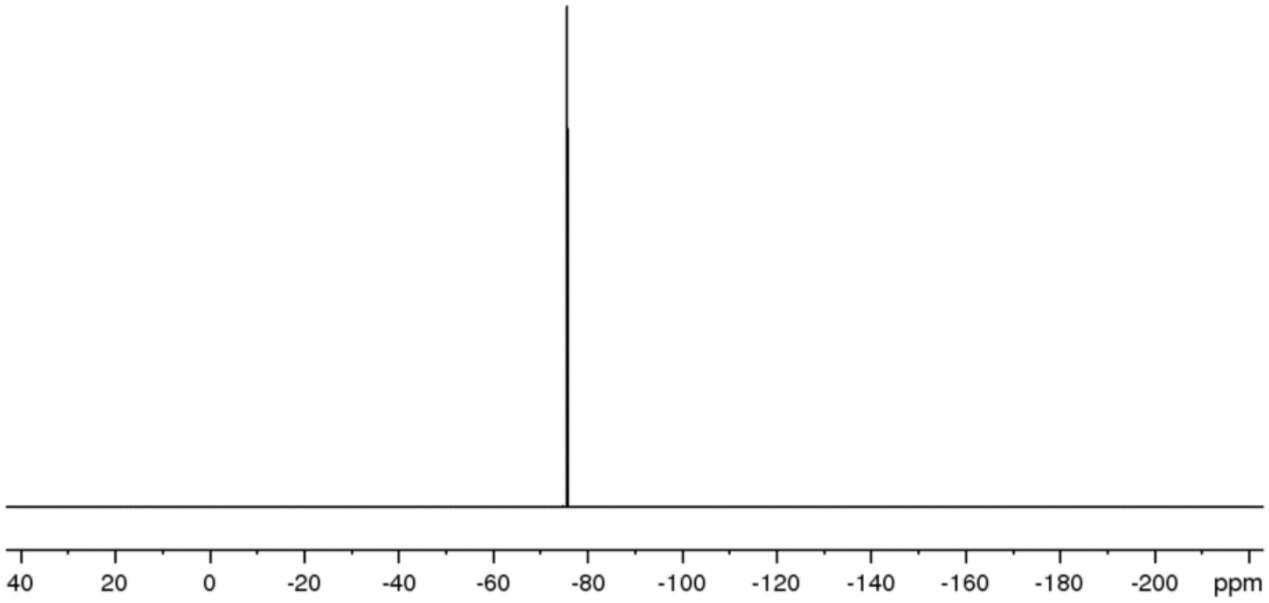

Figure S15: $^{19}F\{^{1}H\}$ NMR spectrum of [{CpMo(CO)$_2$}$_4$(μ_4,η^2:η^2:η^2:η^2-AsPPAs)][TEF]$_2$ (**1**) in CD_2Cl_2.

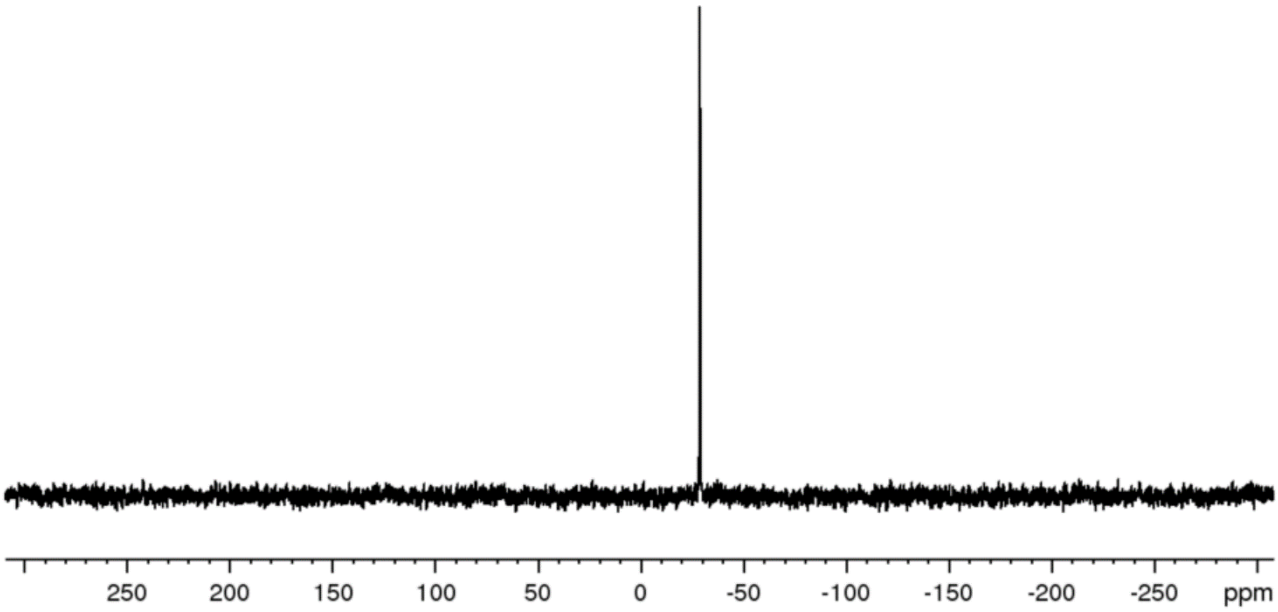

Figure S16: $^{31}P\{^{1}H\}$ NMR spectrum of [{CpMo(CO)$_2$}$_4$(μ_4,η^2:η^2:η^2:η^2-AsPPAs)][TEF]$_2$ (**1**) in CD_2Cl_2.

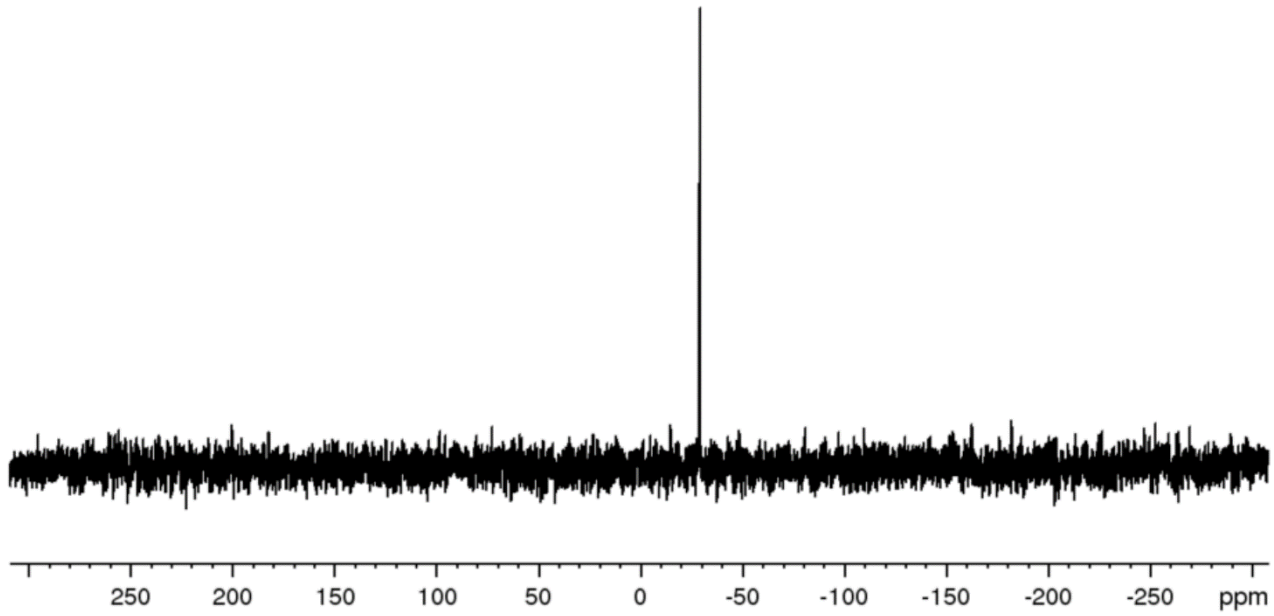

Figure S17: ^{31}P NMR spectrum of [{CpMo(CO)$_2$}$_4$(μ_4,η^2:η^2:η^2:η^2-AsPPAs)][TEF]$_2$ (**1**) in CD_2Cl_2.

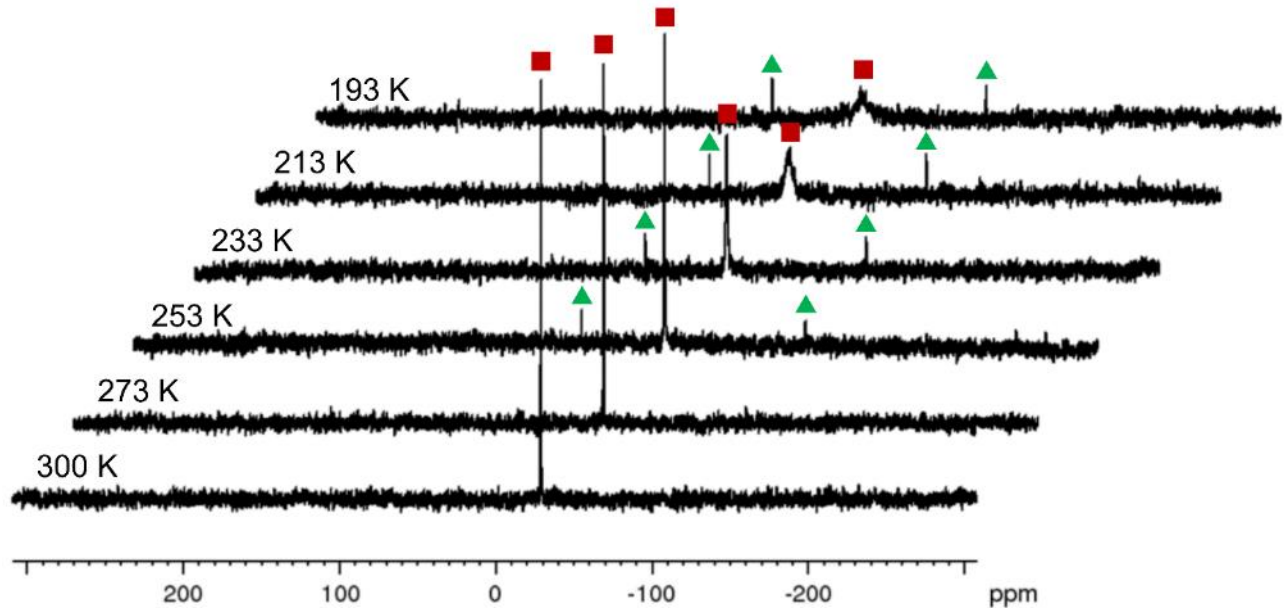

Figure S18: ^{31}P{^{1}H} VT-NMR spectrum of [{CpMo(CO)$_2$}$_4$(μ_4,η^2:η^2:η^2:η^2-AsPPAs)][TEF]$_2$ (**1**) in CD_2Cl_2.

In Figure S18 the ^{31}P{^{1}H} variable temperature (VT) NMR spectrum of **1** from 300 K to 193 K is shown. At room temperature a relatively sharp singlet at δ = –28.8 ppm ($\omega_{1/2}$ = 11 Hz) is observed, which is shifted to lower frequencies by 60 ppm compared to the starting material **A** (δ = 30.1 ppm).[3] Upon cooling to 193 K, the signal (■) moves farther to lower frequencies (δ = –39.4 ppm) and undergoes broadening ($\omega_{1/2}$ ~ 1700 Hz). Additionally, two new signals (▲) at δ = –119.7 ppm and 21.4 ppm arise below 253 K indicating the formation of a new, unidentified species.

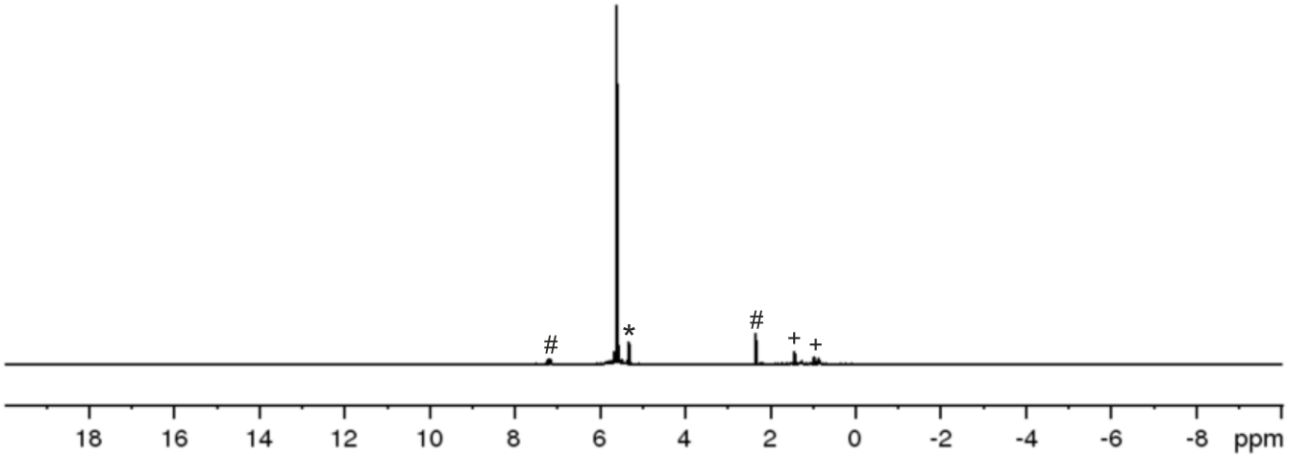

Figure S19: ^{1}H NMR spectrum of [{CpMo(CO)$_2$}$_4$(μ_4,η^2:η^2:η^2:η^2-SbPPSb)][TEF]$_2$ (**2**) in CD_2Cl_2; + = H grease, # = toluene, * = CD_2Cl_2.

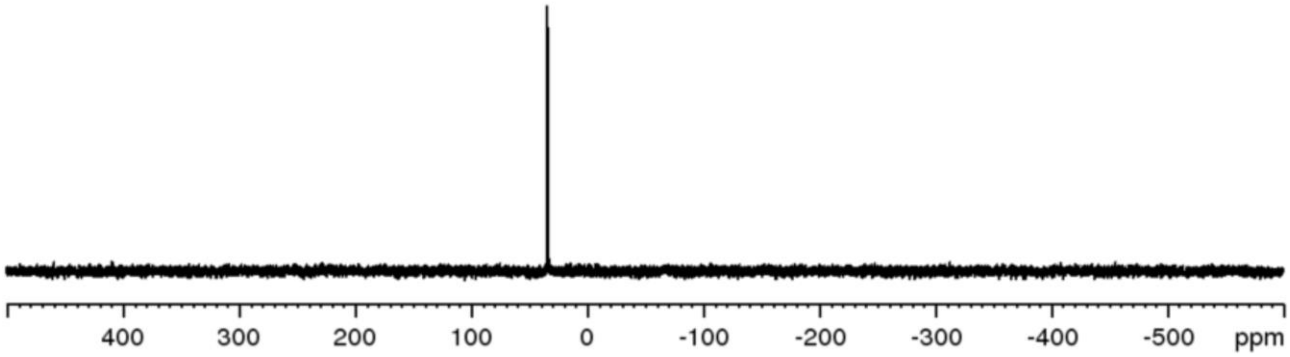

Figure S20: ^{31}P{^{1}H} NMR spectrum of [{CpMo(CO)$_2$}$_4$(μ_4,η^2:η^2:η^2:η^2-SbPPSb)][TEF]$_2$ (**2**) in CD_2Cl_2.

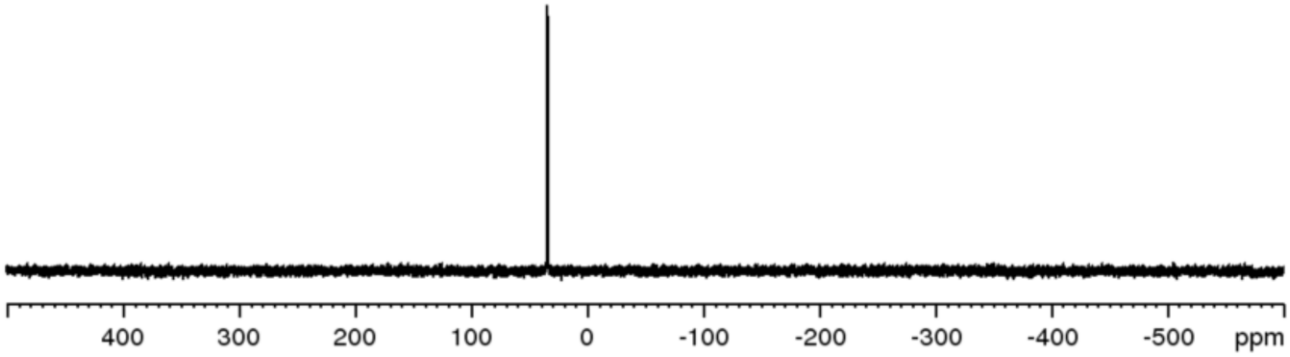

Figure S21: ^{31}P NMR spectrum of [{CpMo(CO)$_2$}$_4$(μ_4,η^2:η^2:η^2:η^2-SbPPSb)][TEF]$_2$ (**2**) in CD_2Cl_2.

The ^{31}P{^{1}H} and ^{31}P NMR spectra of **2** (Figure S20 and Figure S21) reveal a sole singlet at δ = 35.0 ppm, which again is shifted to lower frequencies by 55 ppm in comparison to the starting material **B** (δ = 90.7 ppm).[3] This affirms the suggestion that analogue to **1** a P–P coupled dicationic product is formed.

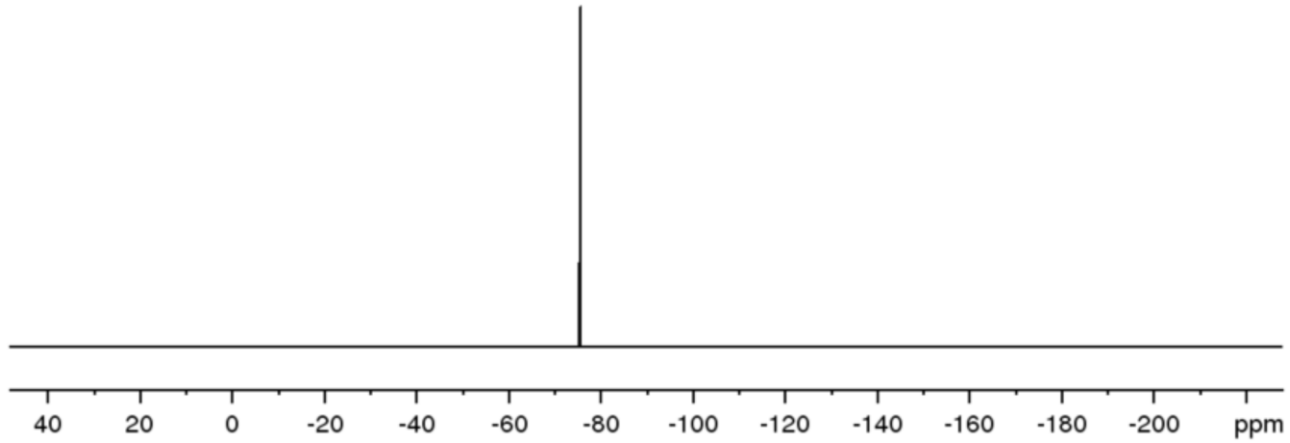

Figure S22: $^{19}F\{^{1}H\}$ NMR spectrum of [{CpMo(CO)$_2$}$_4$(μ_4,η^2:η^2:η^2:η^2-SbPPSb)][TEF]$_2$ (**2a**) in CD_2Cl_2.

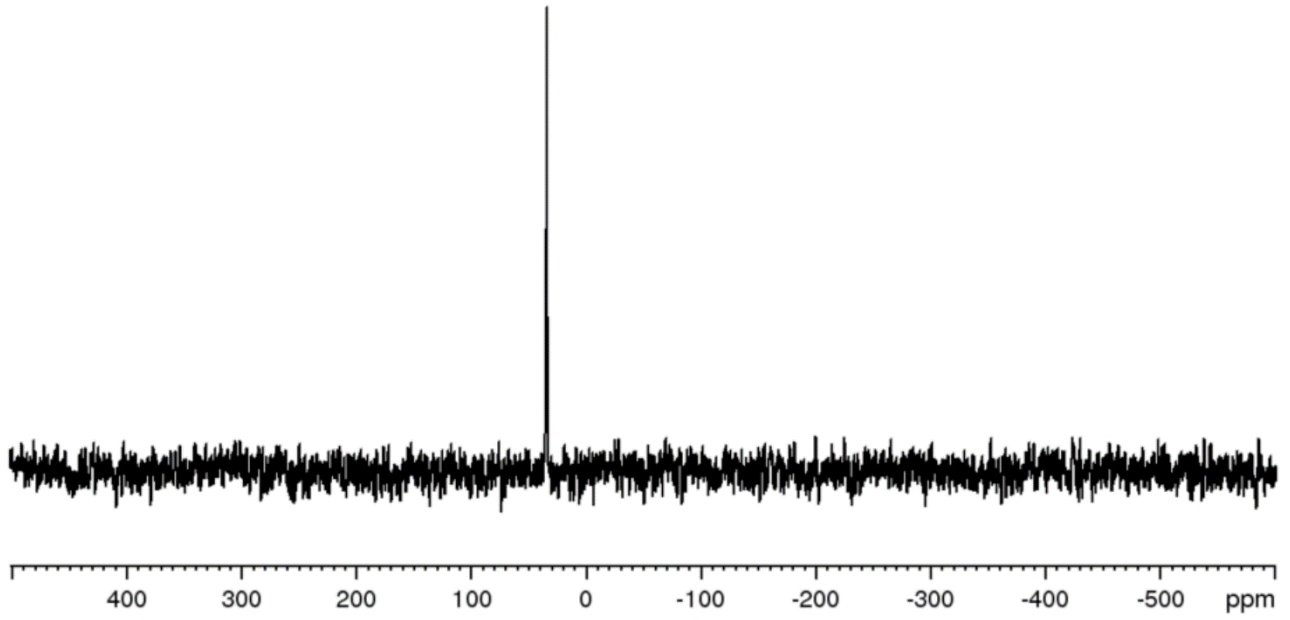

Figure S23: $^{31}P\{^{1}H\}$ NMR spectrum of the crude solution of [{CpMo(CO)$_2$}$_4$(μ_4,η^2:η^2:η^2:η^2-SbPPSb)][TEF]$_2$ (**2**) in CH_2Cl_2/C_6D_6.

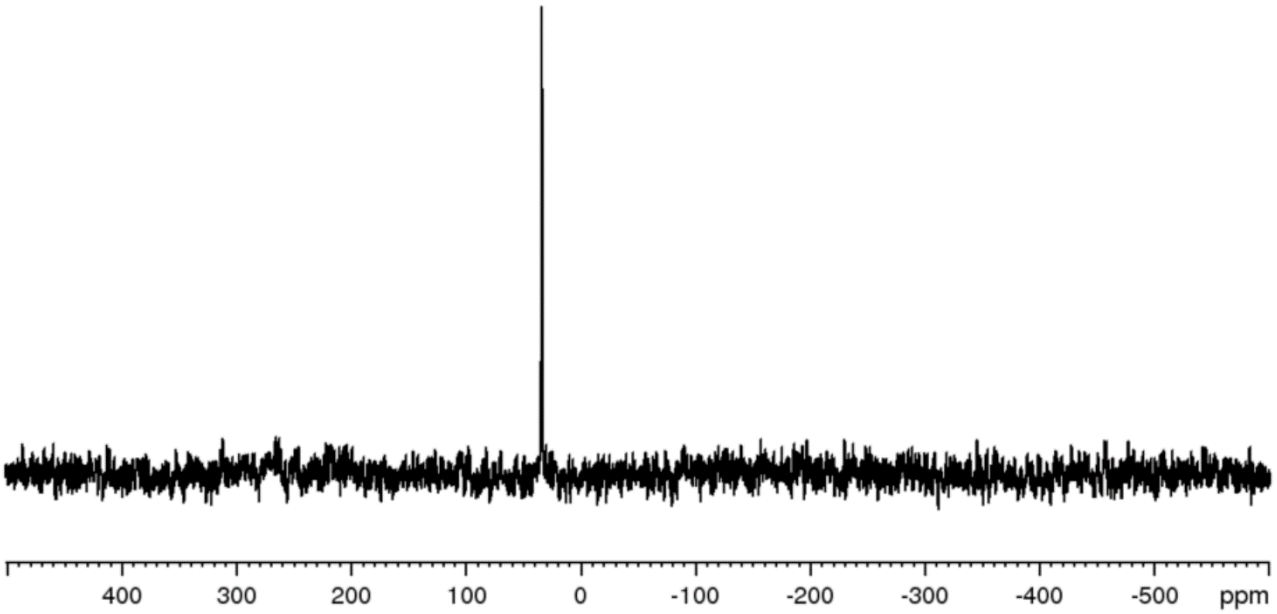

Figure S24: $^{31}P\{^{1}H\}$ NMR spectrum of the crude solution of [{CpMo(CO)$_2$}$_4$(μ_4,η^2:η^2:η^2:η^2-SbPPSb)][TEF]$_2$ (**2**) in CH_2Cl_2/C_6D_6.

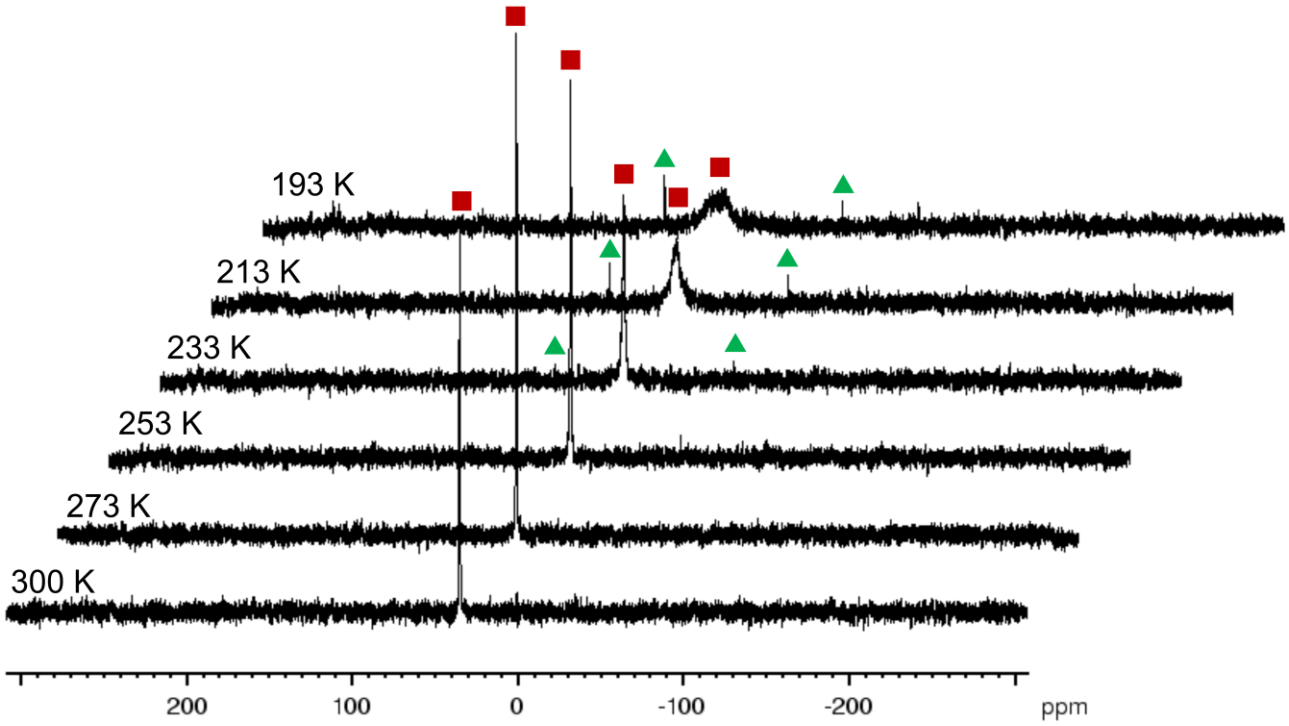

Figure S25: $^{31}P\{^{1}H\}$ VT-NMR spectrum of [{CpMo(CO)$_2$}$_4$(μ_4,η^2:η^2:η^2:η^2-SbPPSb)][TEF]$_2$ (**2**) in CD_2Cl_2.

In Figure S25 the $^{31}P\{^{1}H\}$ variable temperature (VT) NMR spectrum of **2** from 300 K to 193 K is shown. At room temperature a relatively sharp singlet at δ = 35.0 ppm ($\omega_{1/2}$ = 72 Hz), which is shifted to lower frequencies by 55 ppm compared to the starting material **B** (δ = 90.7 ppm).[3] The same behaviour was also observed for **1**. Upon cooling to 193 K, the signal (■) moves farther to lower frequencies (δ = 28.4 ppm) and undergoes broadening ($\omega_{1/2}$ ~ 17000 Hz). Additionally, two new signals (▲) at δ = –40.9 ppm and 66.5 ppm arise below 233 K indicating the formation of a new, unidentified species, like it was described for **1**.

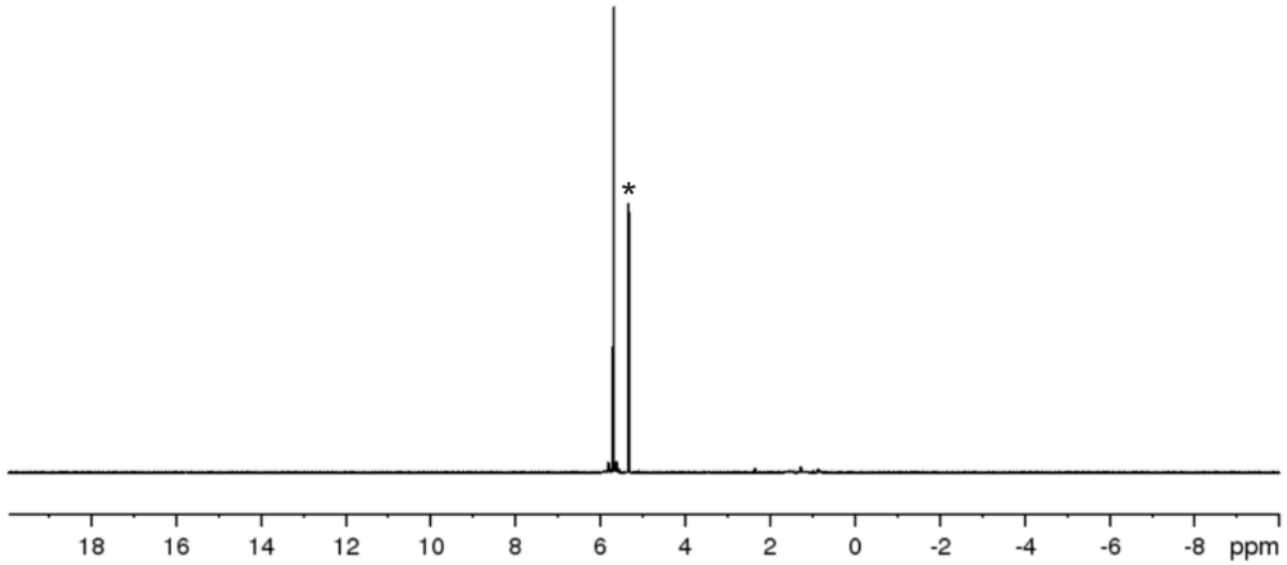

Figure S26: ^{1}H NMR spectrum of [{CpMo(CO)$_2$}$_4$(μ_4,η^2:η^2:η^2:η^2-AsSbSbAs)][TEF]$_2$ (**3a**) in CD_2Cl_2; * = CD_2Cl_2.

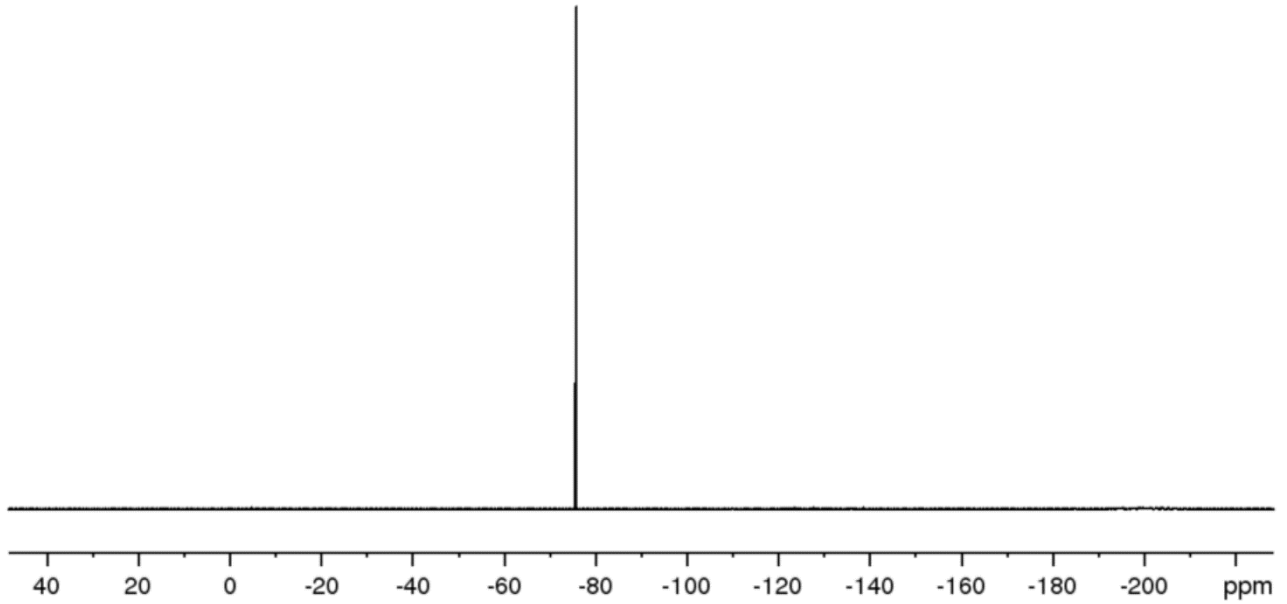

Figure S27: $^{19}F\{^{1}H\}$ spectrum of [{CpMo(CO)$_2$}$_4$(μ_4,η^2:η^2:η^2:η^2-AsSbSbAs)][TEF]$_2$ (**3a**) in CD_2Cl_2.

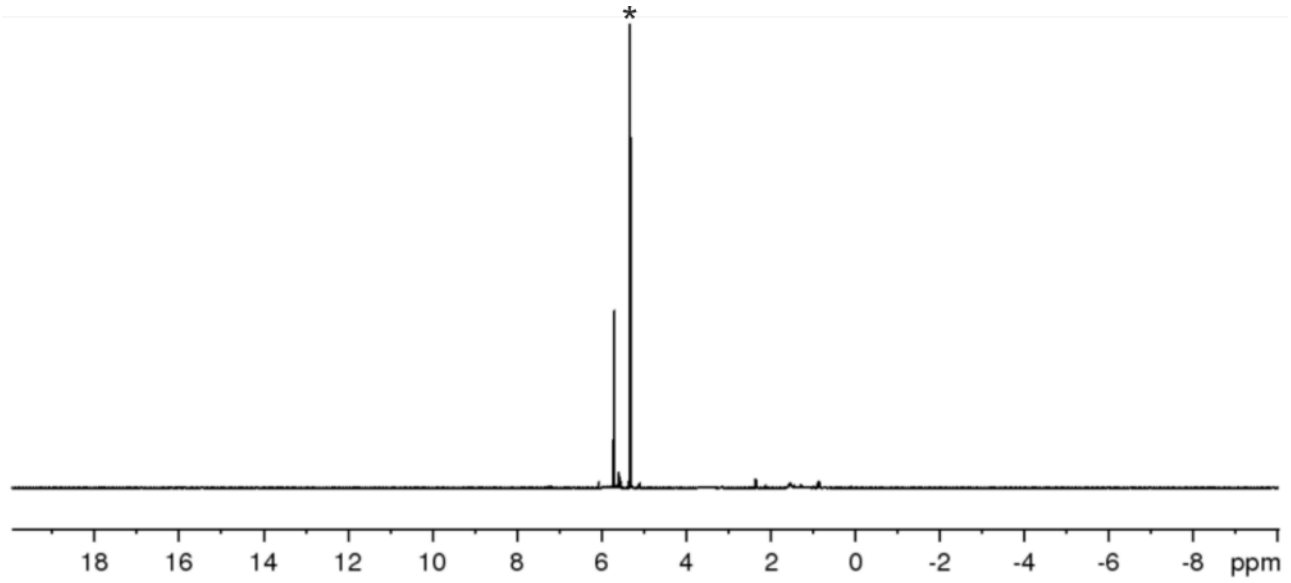

Figure S28: ^{1}H NMR spectrum of [{CpMo(CO)$_2$}$_4$(μ_4,η^2:η^2:η^2:η^2-AsSbAsSb)][TEF^{Cl}]$_2$ (**3b**) in CD_2Cl_2, * = CD_2Cl_2.

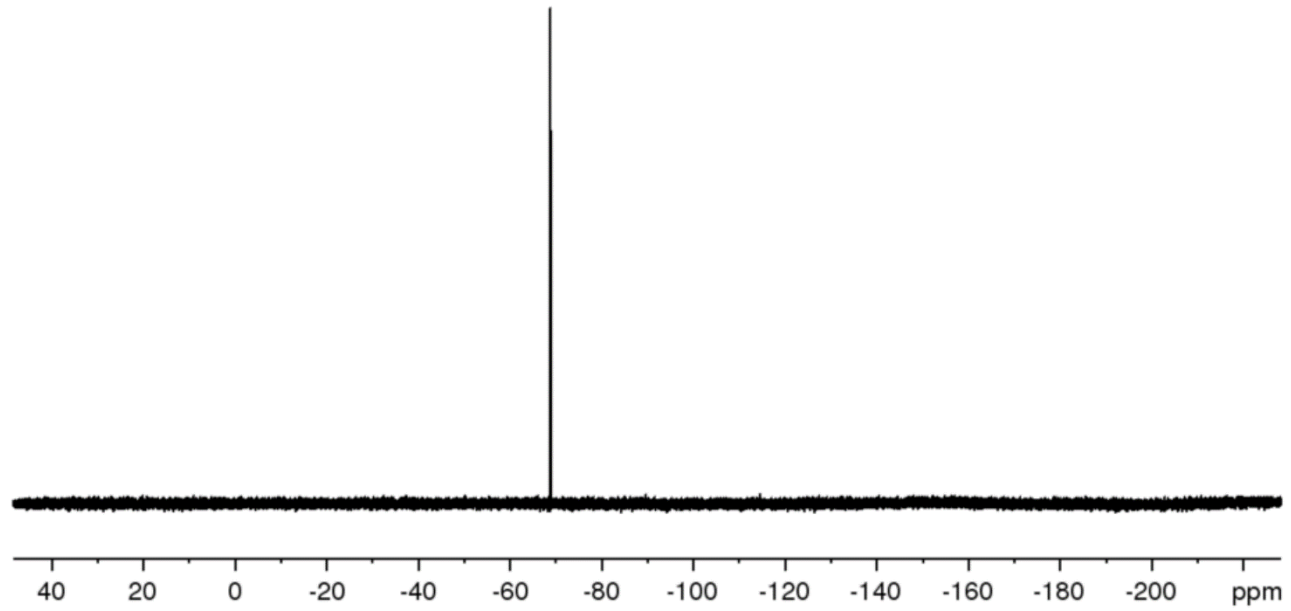

Figure S29: $^{19}F\{^{1}H\}$ NMR spectrum of [{CpMo(CO)$_2$}$_4$(μ_4,η^2:η^2:η^2:η^2-AsSbAsSb)][TEF^{Cl}]$_2$ (**3b**) in CD_2Cl_2.

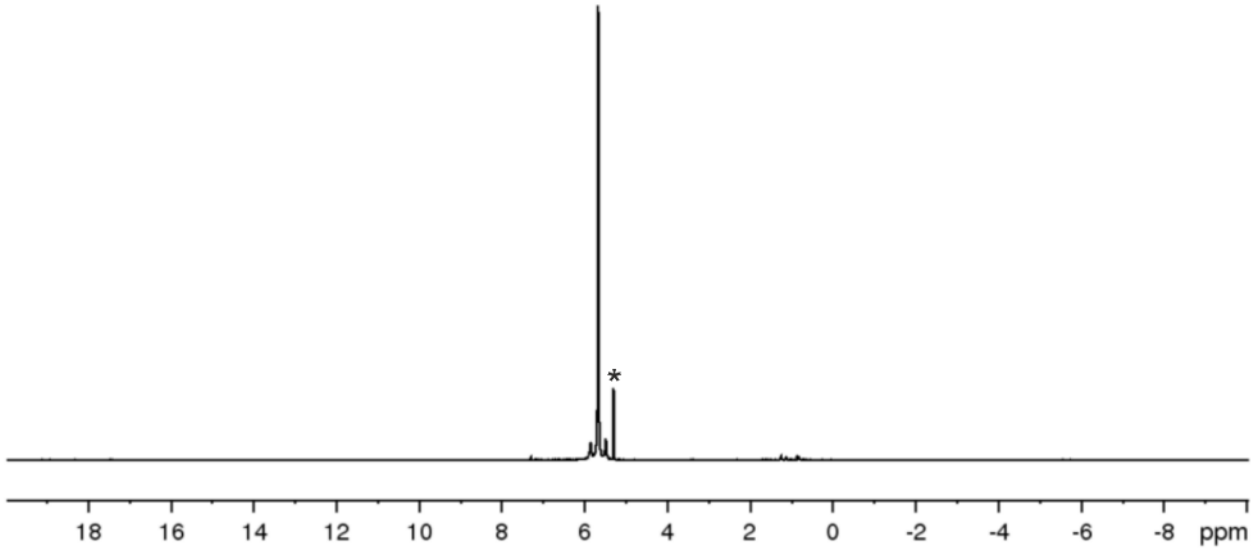

Figure S30: ^{1}H NMR spectrum of [{CpMo(CO)$_2$}$_4$(μ_4,η^2:η^2:η^2:η^2-AsBiBiAs)][TEF]$_2$ (**4a**) in CD_2Cl_2; * = CD_2Cl_2.

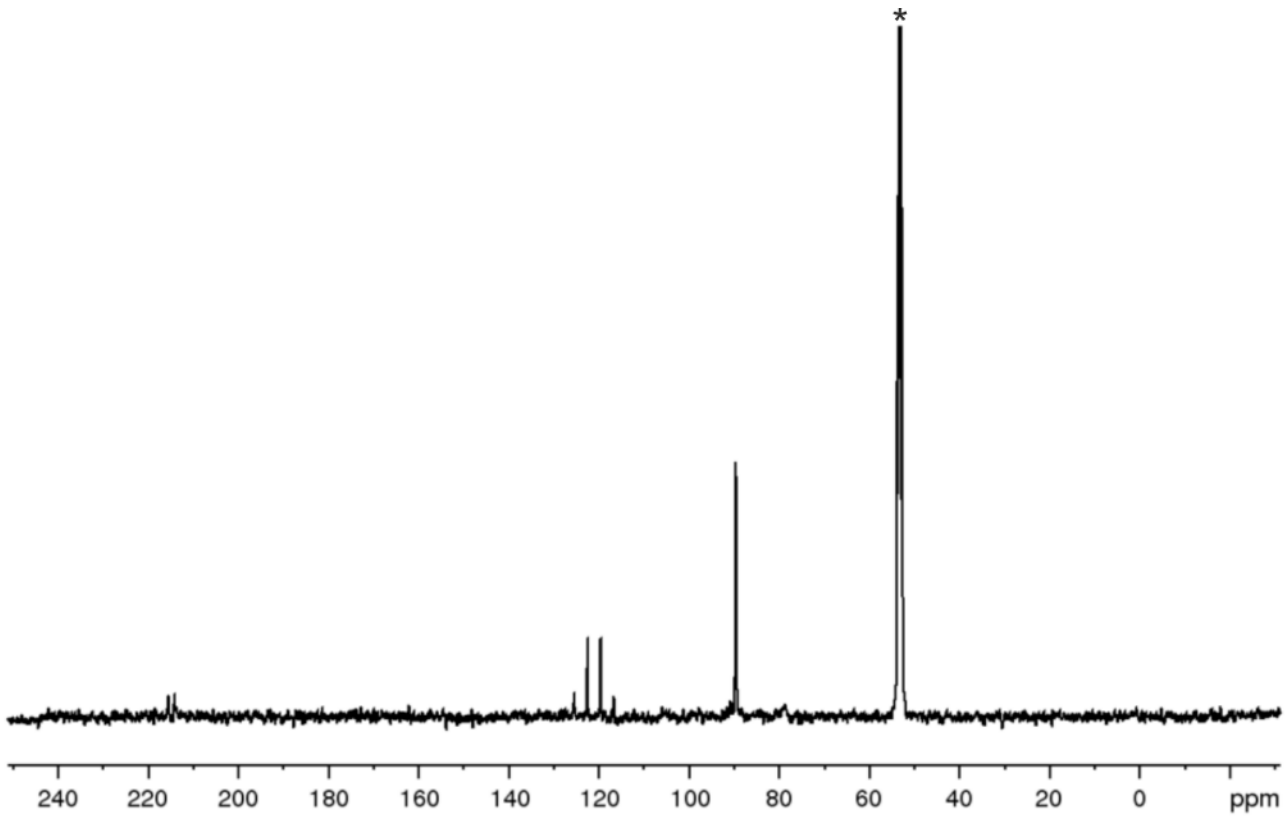

Figure S31: $^{13}C\{^{1}H\}$ NMR spectrum of [{CpMo(CO)$_2$}$_4$(μ_4,η^2:η^2:η^2:η^2-AsBiBiAs)][TEF]$_2$ (**4a**) in CD_2Cl_2; * = CD_2Cl_2.

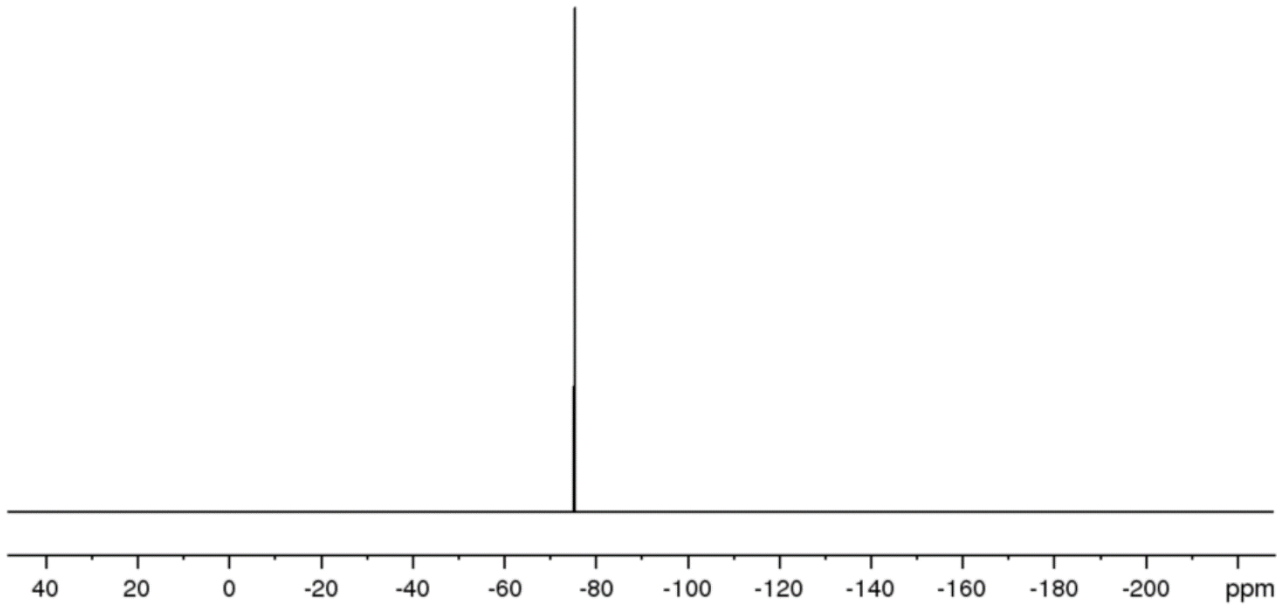

Figure S32: $^{19}F\{^{1}H\}$ NMR spectrum of [{CpMo(CO)$_2$}$_4$(μ_4,η^2:η^2:η^2:η^2-AsBiBiAs)][TEF]$_2$ (**4a**) in CD_2Cl_2.

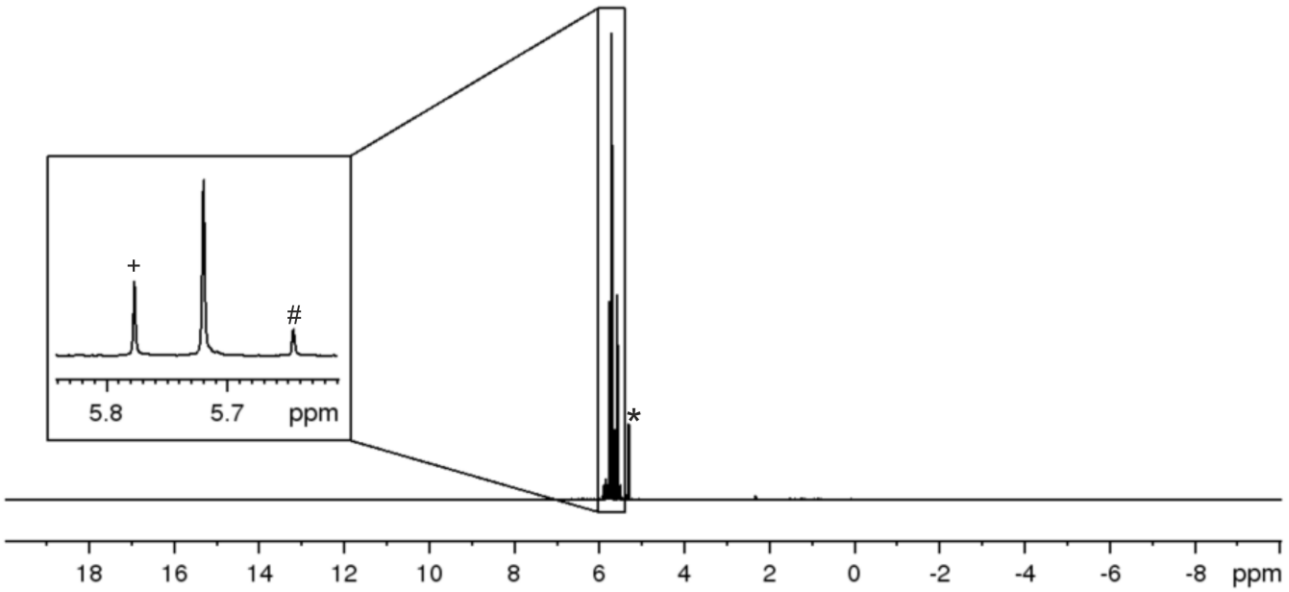

Figure S33: ^{1}H NMR spectrum of [{CpMo(CO)$_2$}$_4$(μ_4,η^2:η^2:η^2:η^2-BiSbSbBi)][TEF]$_2$ (**5**) in CD_2Cl_2; * = CD_2Cl_2, # = **XI**, + = **XII**.

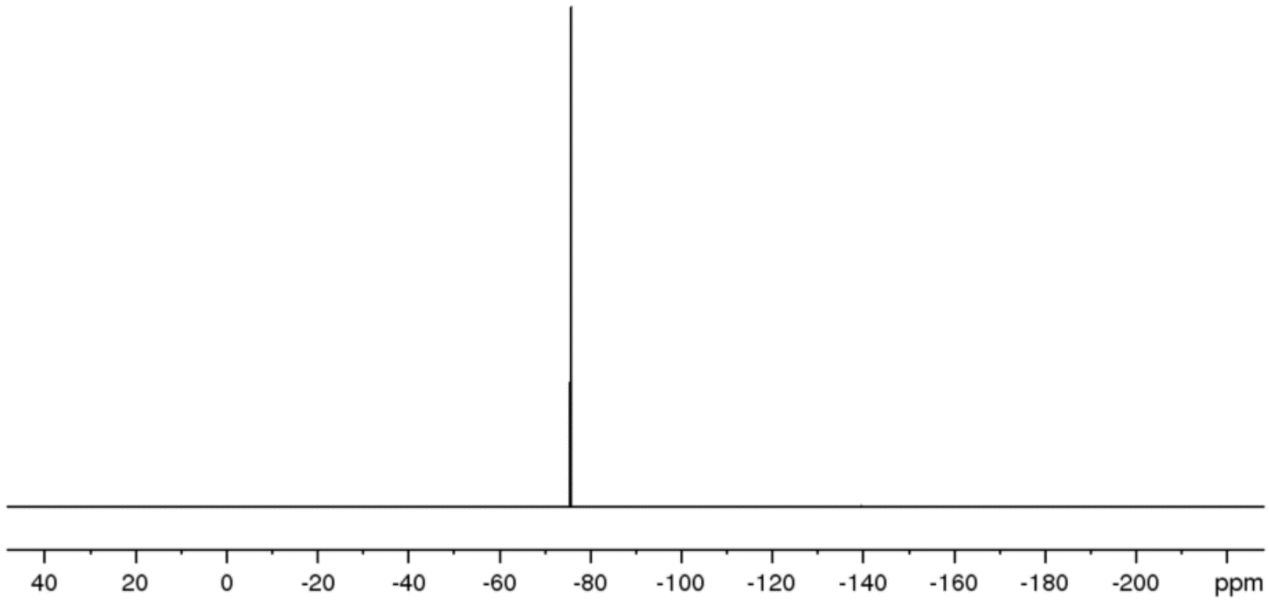

Figure S34: $^{19}F\{^{1}H\}$ NMR spectrum of [{CpMo(CO)$_2$}$_4$(μ_4,η^2:η^2:η^2:η^2-BiSbSbBi)][TEF]$_2$ (**5**) in CD_2Cl_2.

5 Mass spectrometry

The mass spectra, which were recorded by the mass spectrometry department of the University of Regensburg, are not available to the authors in a digital format and, therefore, could not be displayed in the following.

5.1 ESI mass spectrometry of [Thia][TEF^{Cl}]

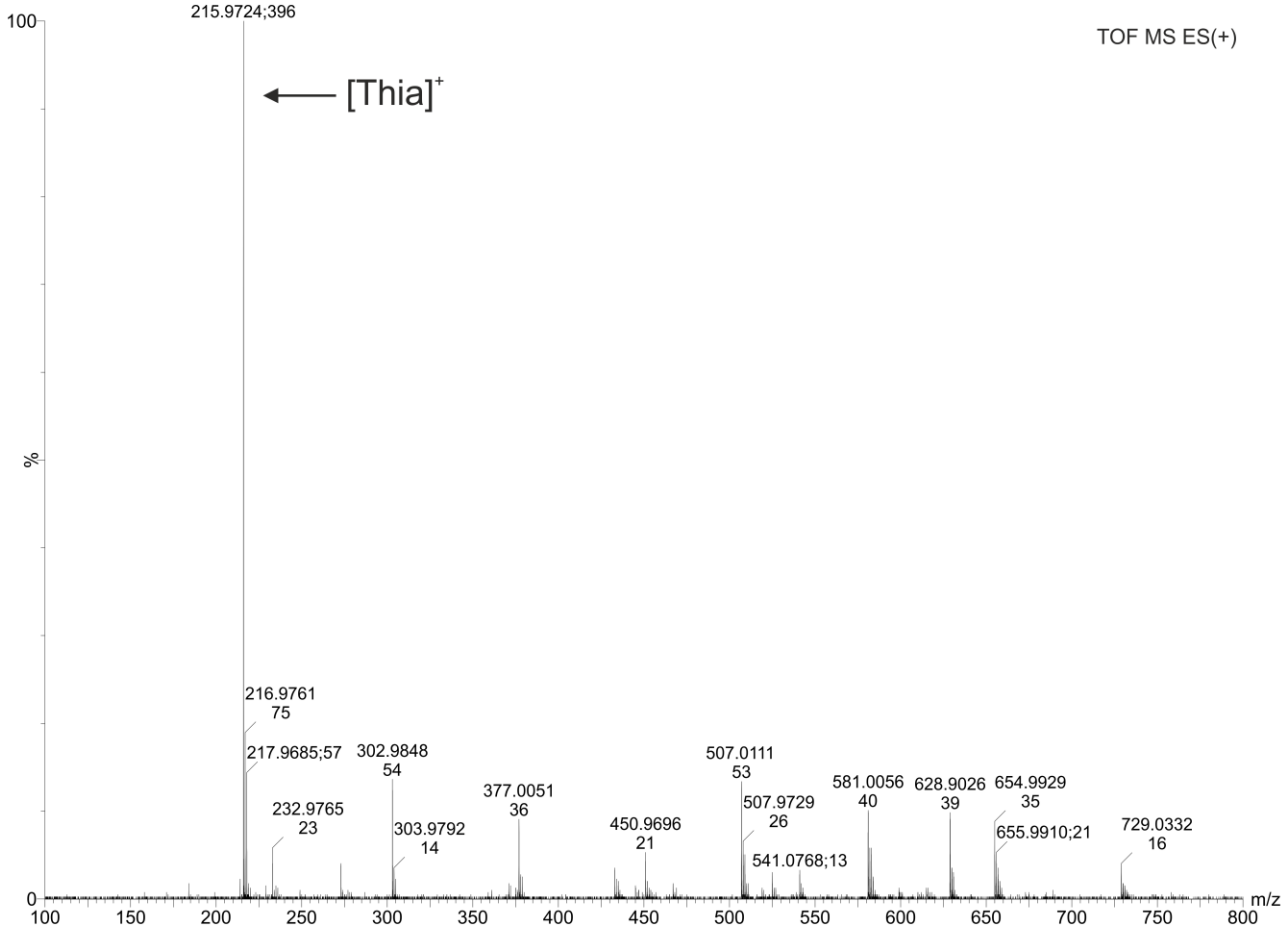

Figure S35: ESI(+) MS spectrum of [Thia][TEF^{Cl}].

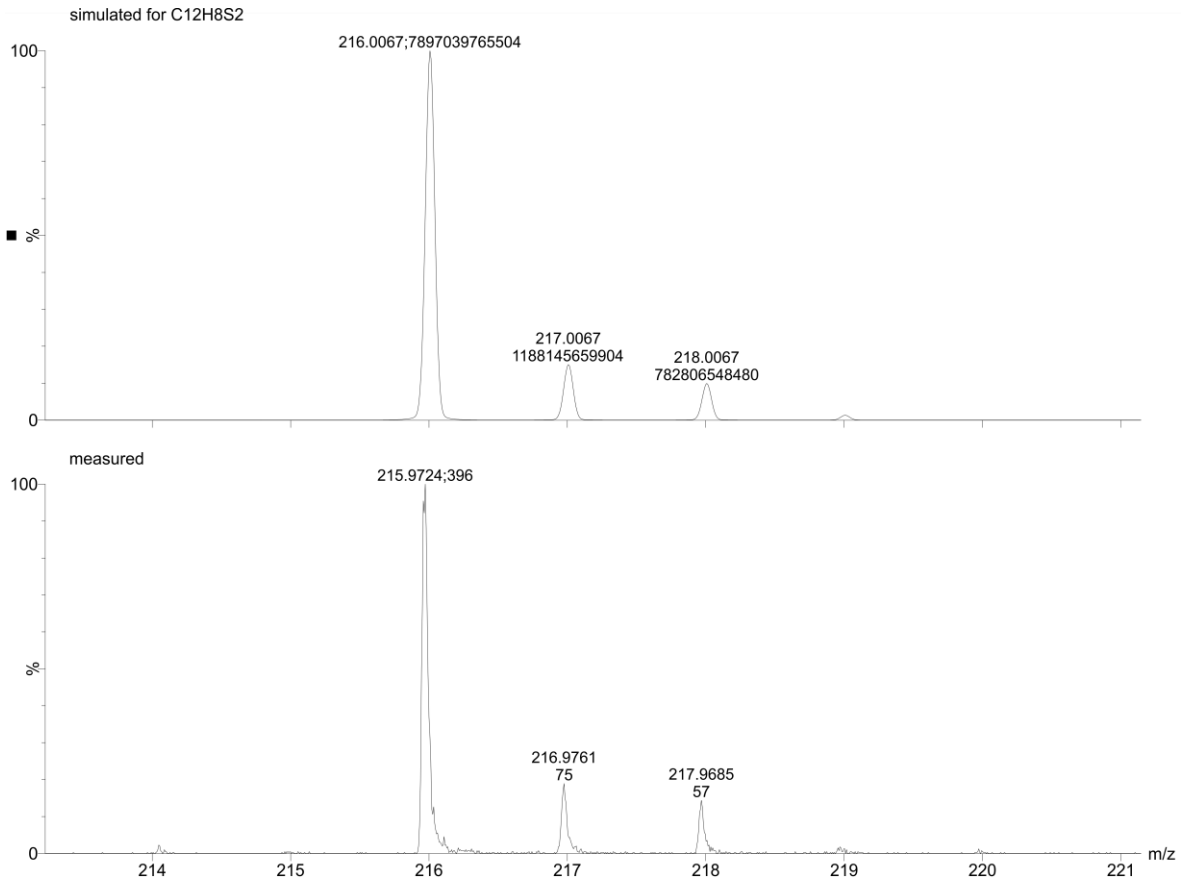

Figure S36: Molecular ion peak of $[Thia]^+$. Bottom: measured spectrum, top: simulated spectrum.

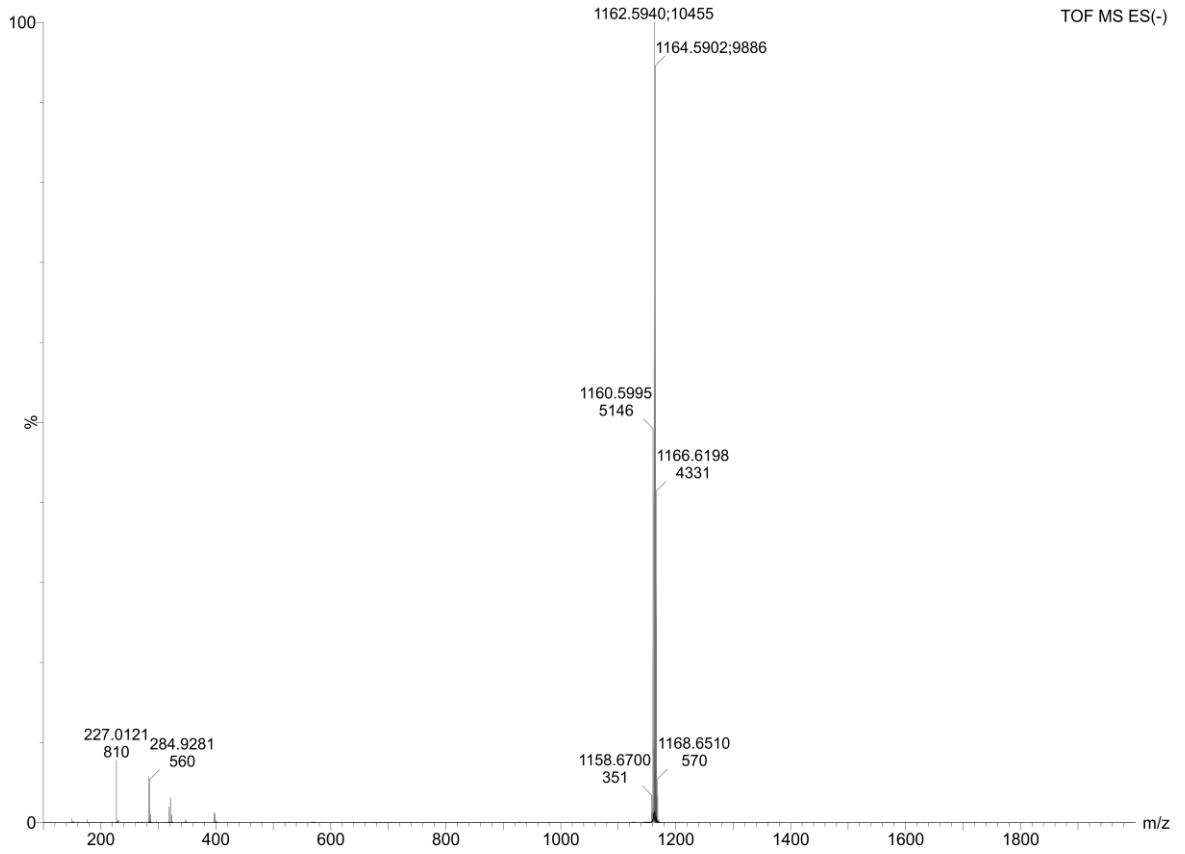

Figure S37: ESI(−) MS spectrum of $[Thia][TEF^{Cl}]$.

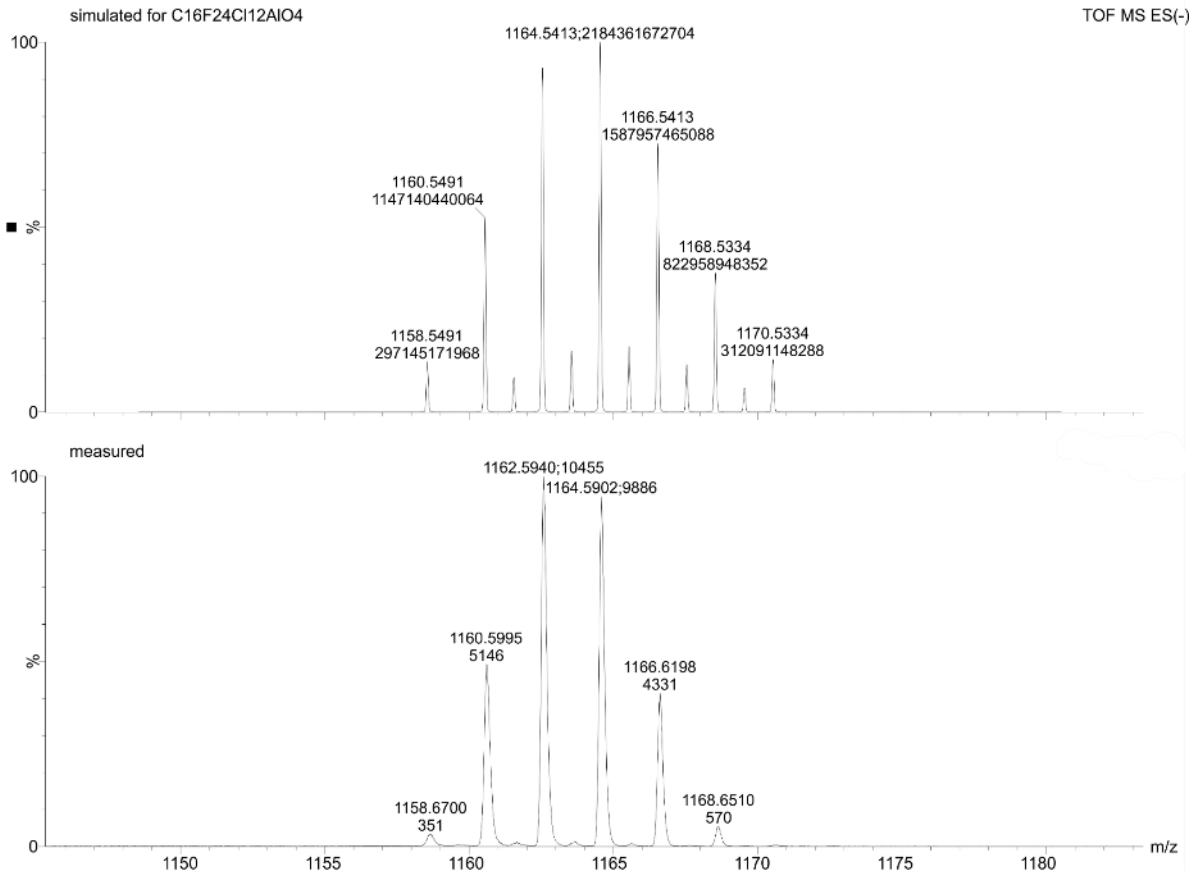

Figure S38: Molecular ion peak of $[TEF^{Cl}]^-$. Bottom: measured spectrum, top: simulated spectrum.

5.2 ESI mass spectrometry of 1:

The ESI mass spectrum of a CH_2Cl_2 solution of crystalline **1** (Figure S39) clearly shows signals assignable to the monocationic species $[\mathbf{A}]^+$, $[\mathbf{A}–1(CO)]^+$, $[\mathbf{A}–2(CO)]^+$, $[\mathbf{A}–3(CO)]^+$ and $[\mathbf{A}–4(CO)]^+$. However, by varying the extraction cone voltages one can also record signals for a dicationic species, which can be assigned to $[\mathbf{A_2}\text{-}2(CO)]^{2+}$ (Figure S40). Additionally, some small peaks (≈7:1 intensity, shifted by ≈0.5 Da) are detected in the *m/z* regions for signals, which may be assigned to $[\mathbf{A}–CO–O]^+$ and $[\mathbf{A}–2(CO)]^+$. The overlay of the latter signals with monocationic species though does not allow a reliable assignment by isotopic distribution modelling of these species and the reported formulas in Figure S40 should be regarded as suggested species.

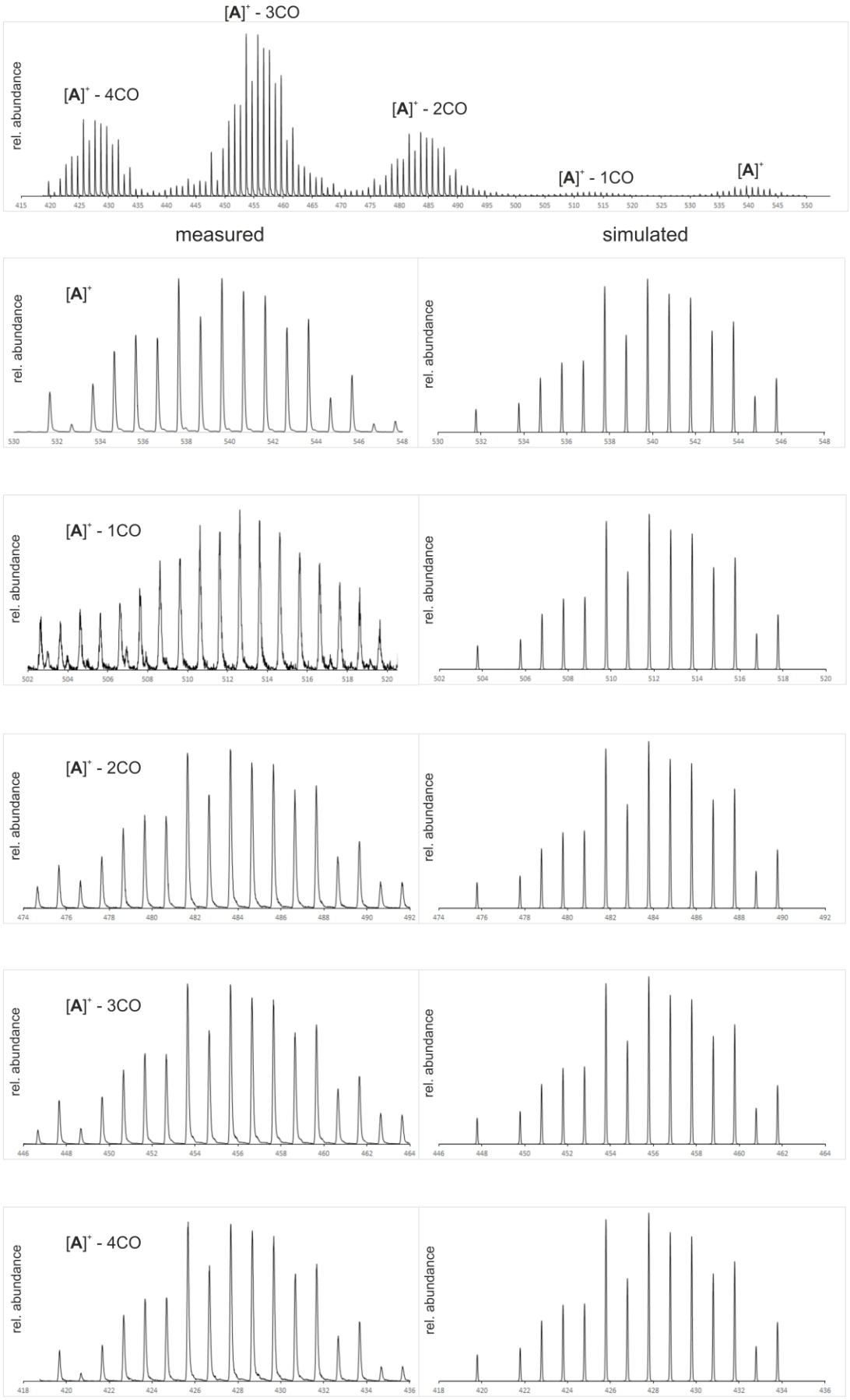

Figure S39: (top) ESI MS spectrum of **1** from CH_2Cl_2. Measured (left) and simulated (right) isotopic distribution for the assignable peaks.

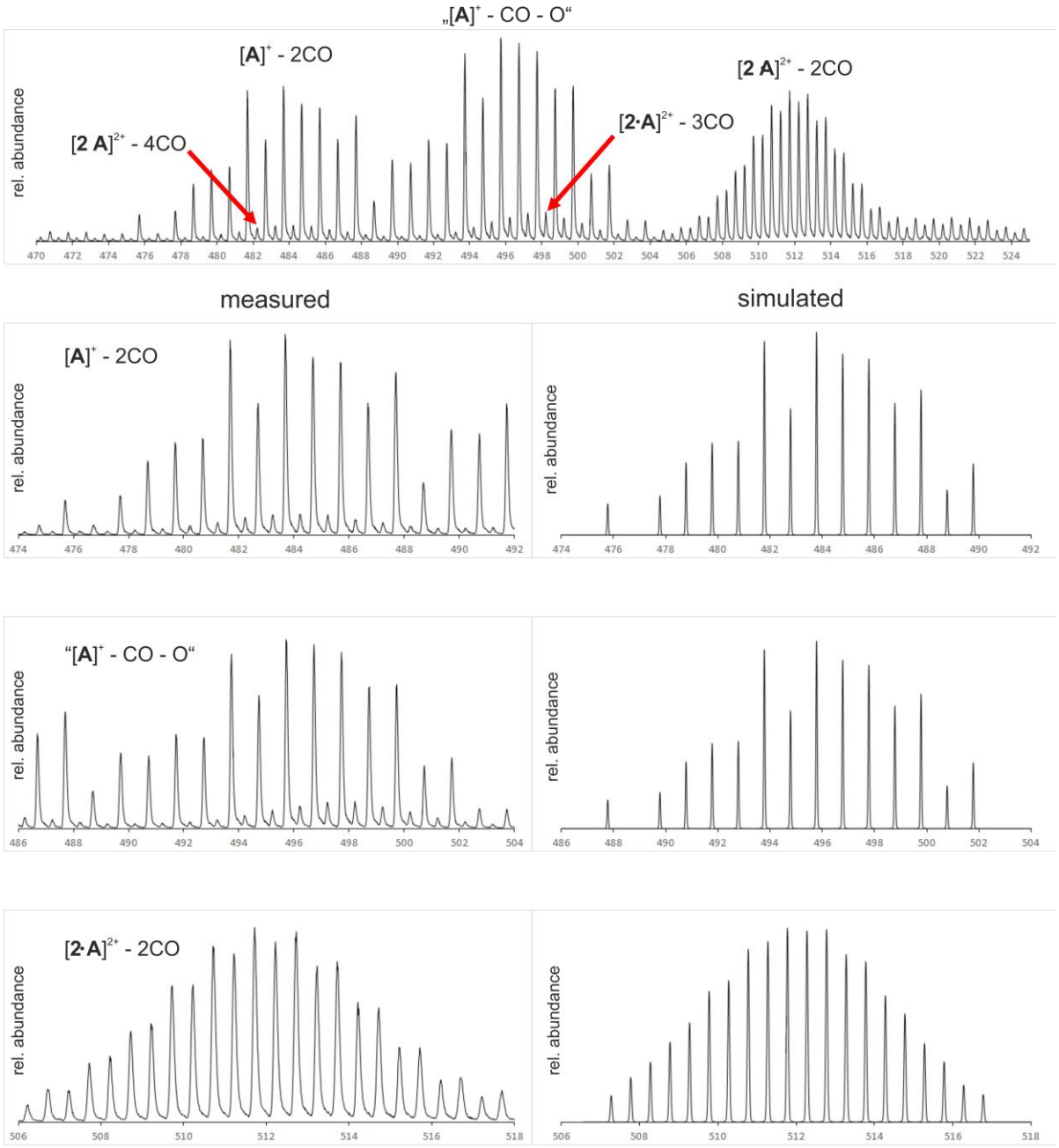

Figure S40: (top) ESI MS spectrum of **1** from CH_2Cl_2 after varying the extraction cone voltage. Measured (left) and simulated (right) isotopic distribution for the assignable peaks.

5.3 ESI mass spectrometry of 3a:

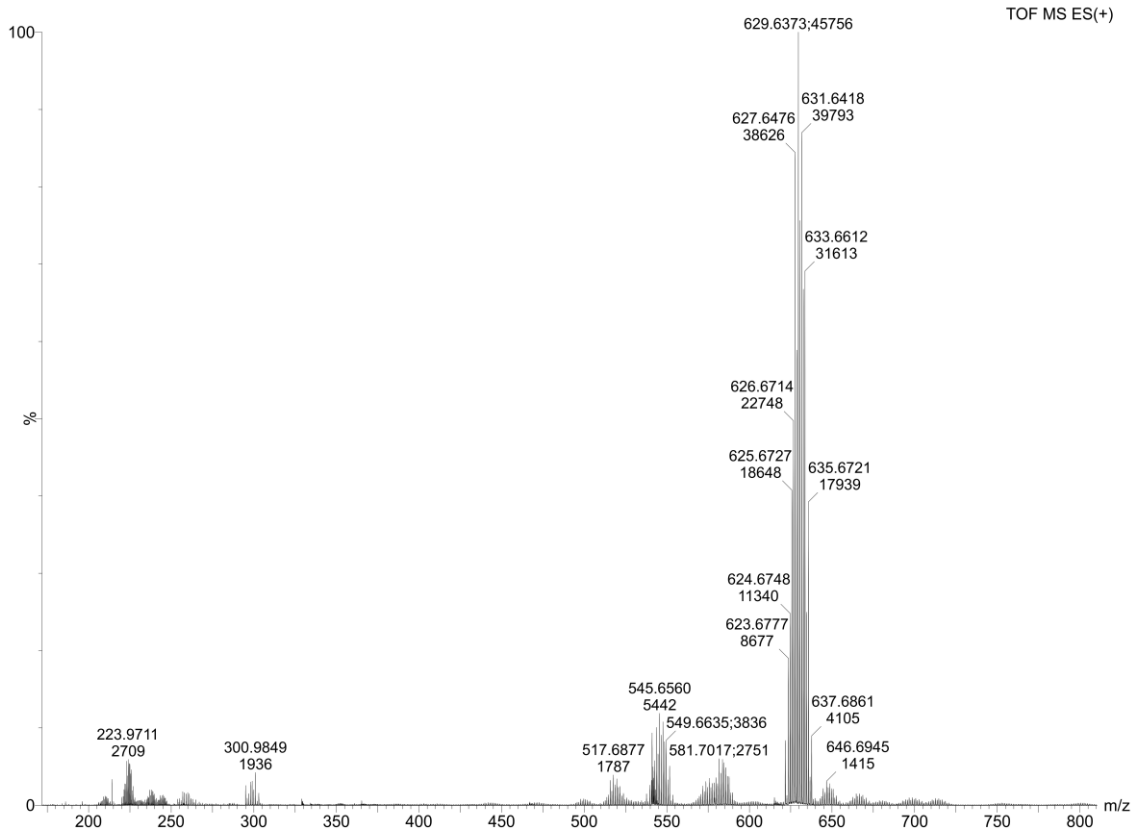

Figure S41: ESI(+) MS spectrum of **3a**.

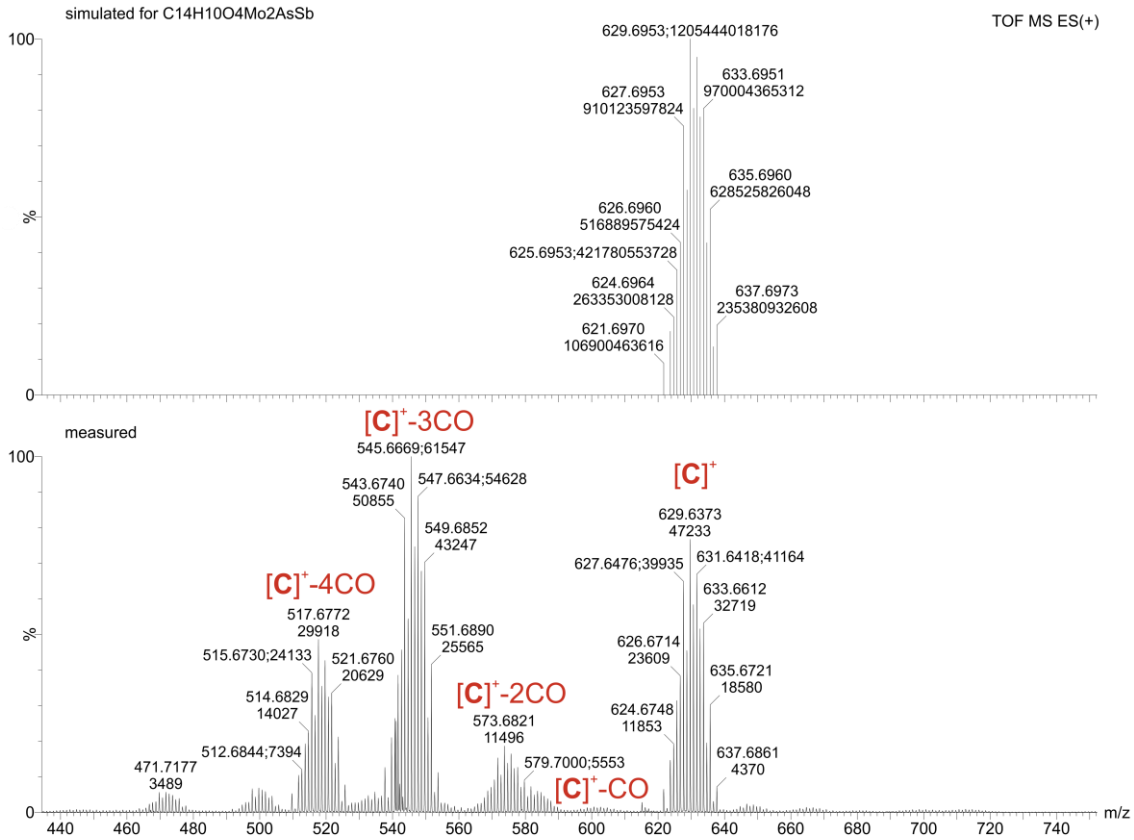

Figure S42: Assignable signals in the ESI(+) MS spectrum of **3a**. Bottom: measured spectrum, top: simulated molecular ion peak [**C**]$^+$.

5.4 ESI mass spectrometry of 3b:

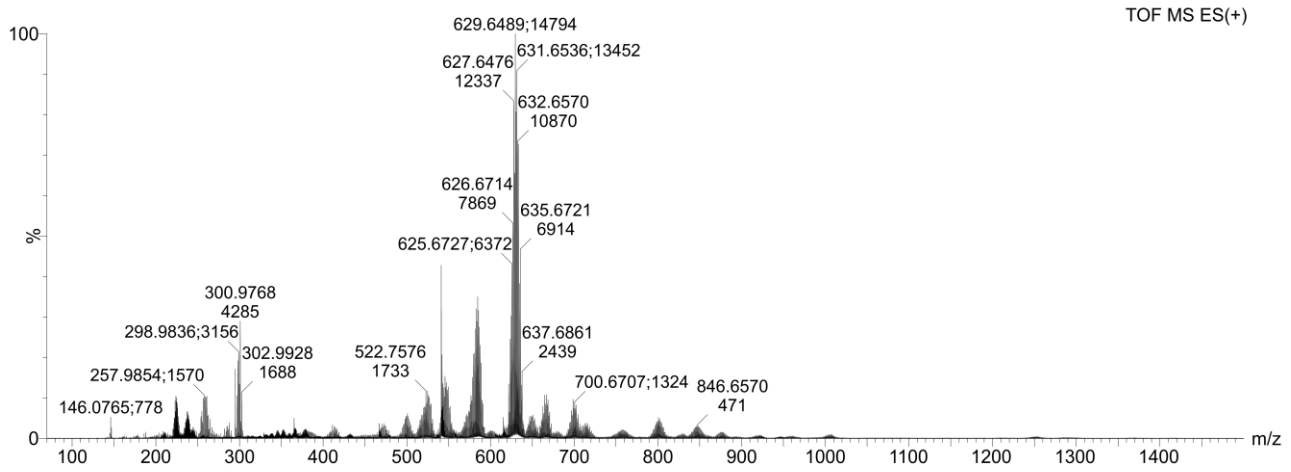

Figure S43: ESI(+) MS spectrum of **3b**.

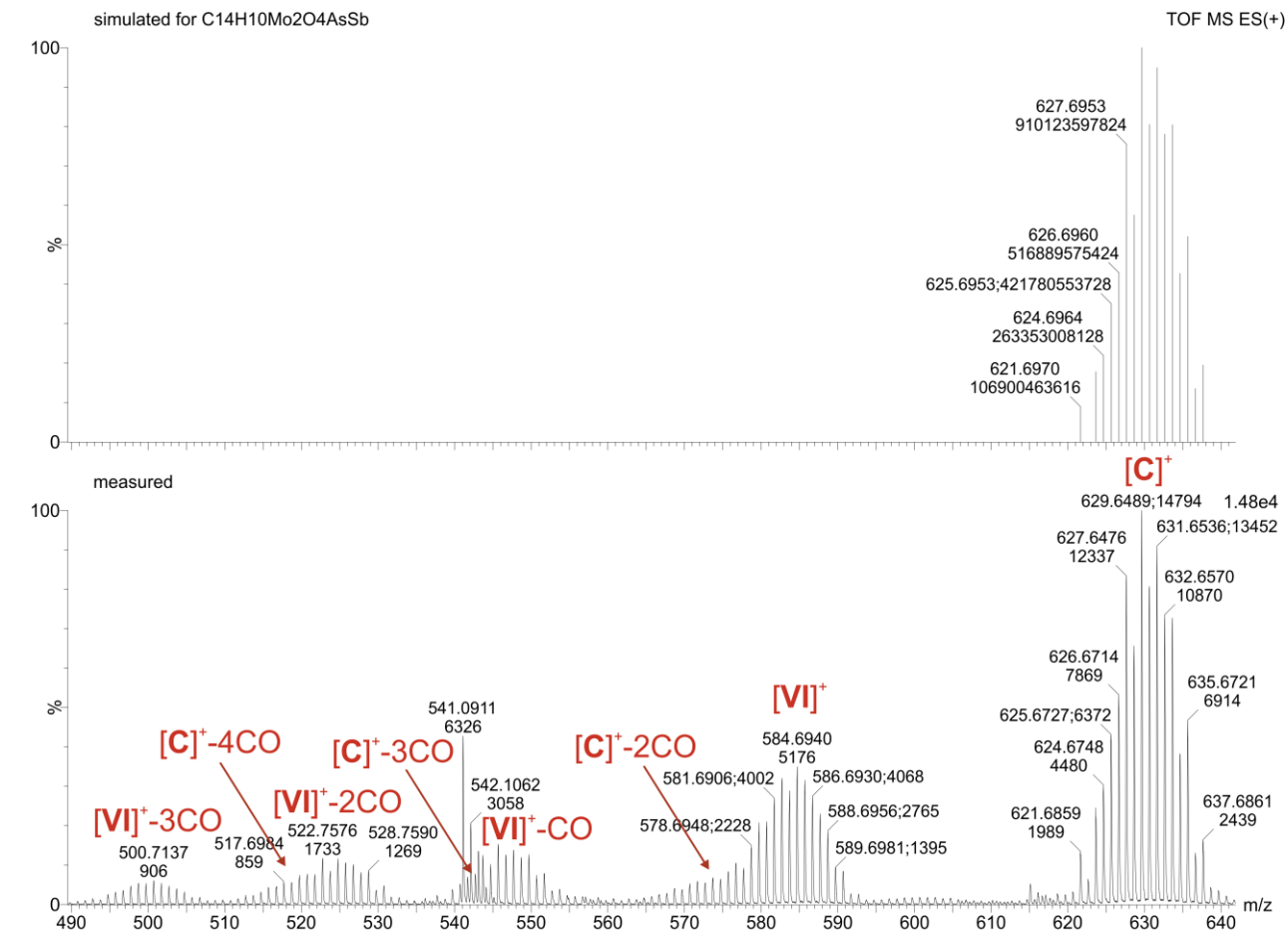

Figure S44: Assignable signals in the ESI(+) MS spectrum of **3b**. Bottom: measured spectrum, top: simulated molecular ion peak of [**C**]$^+$.

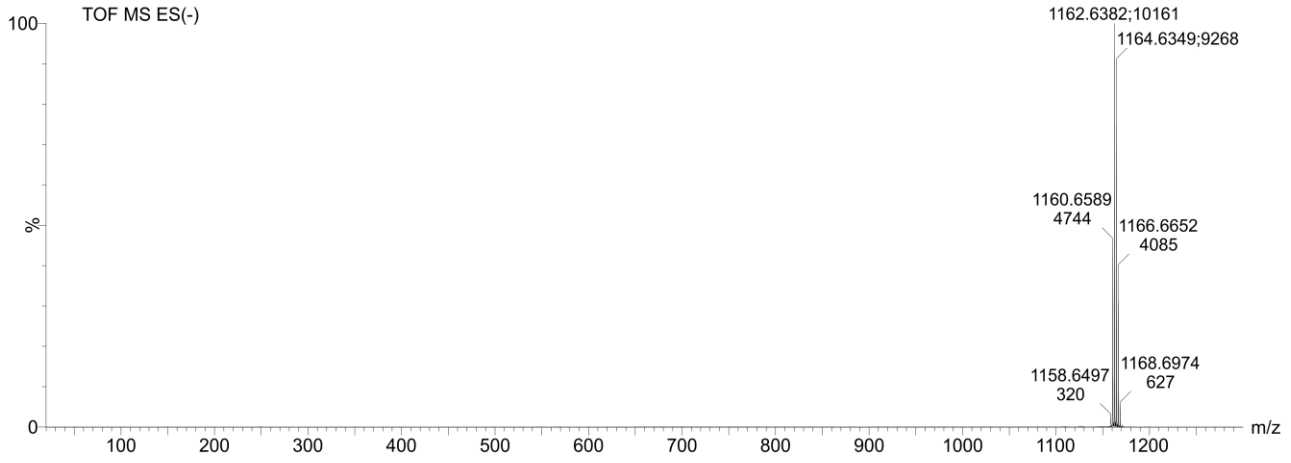

Figure S45: ESI(−) MS spectrum of **3b**.

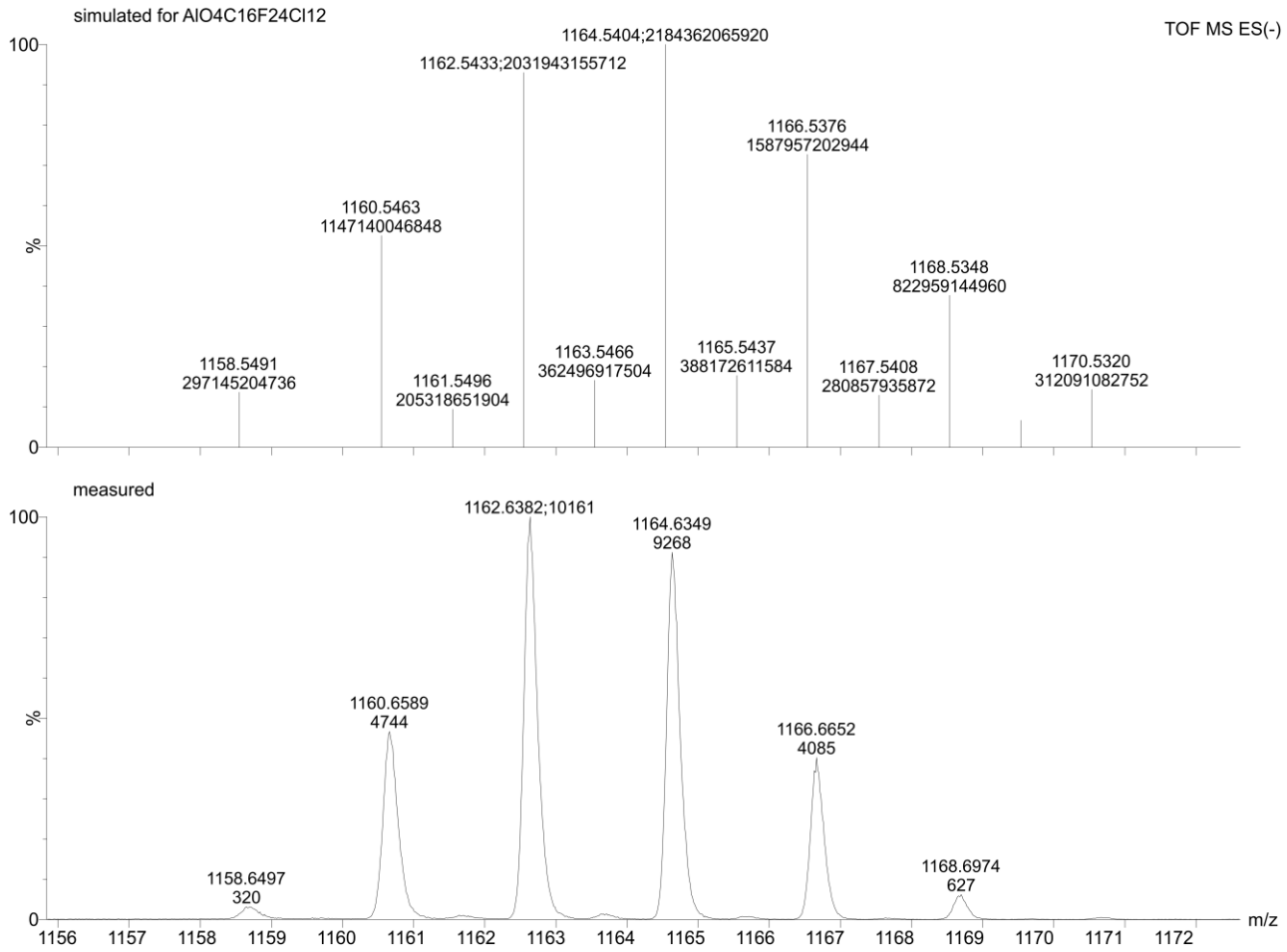

Figure S46: Molecular ion peak of $[TEF^{Cl}]^-$ in the ESI(−) MS spectrum of **3b**. Bottom: measured spectrum, top: simulated spectrum.

6 EPR spectra

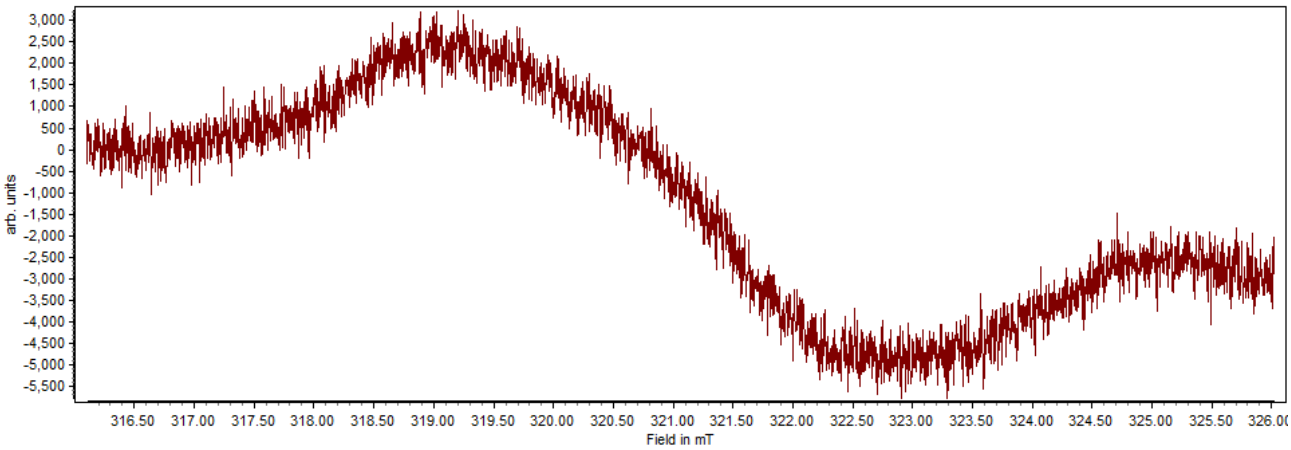

Figure S47: X-Band EPR spectrum of **1** at room temperature showing no signal.

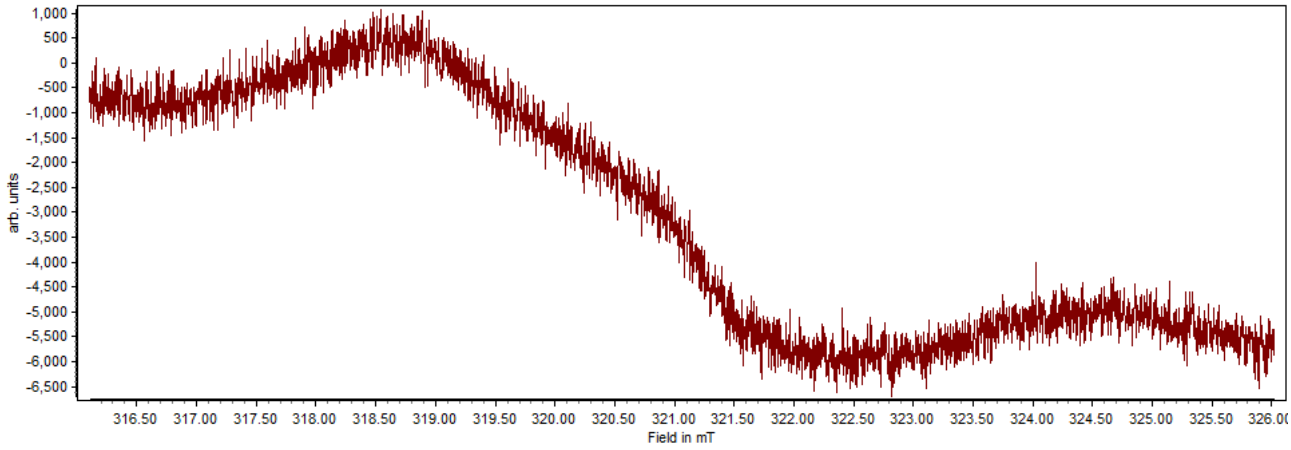

Figure S48: X-Band EPR spectrum of **1** at 77 K showing no signal.

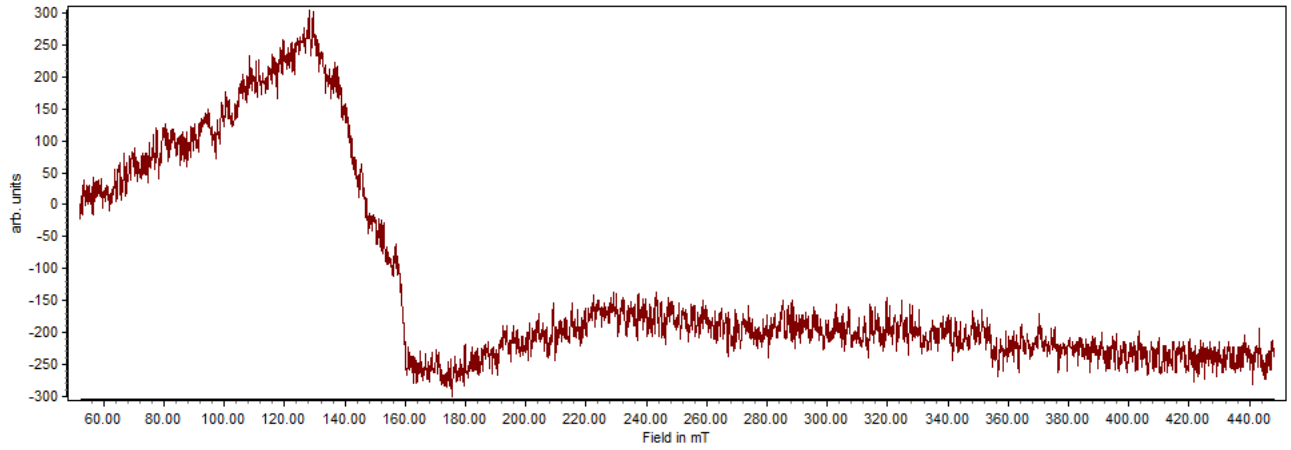

Figure S49: X-Band EPR spectrum of **2** at room temperature showing no signal. The "signal" at ~145 mT arises from the glas measuring apparatus, which was used and contains Fe.

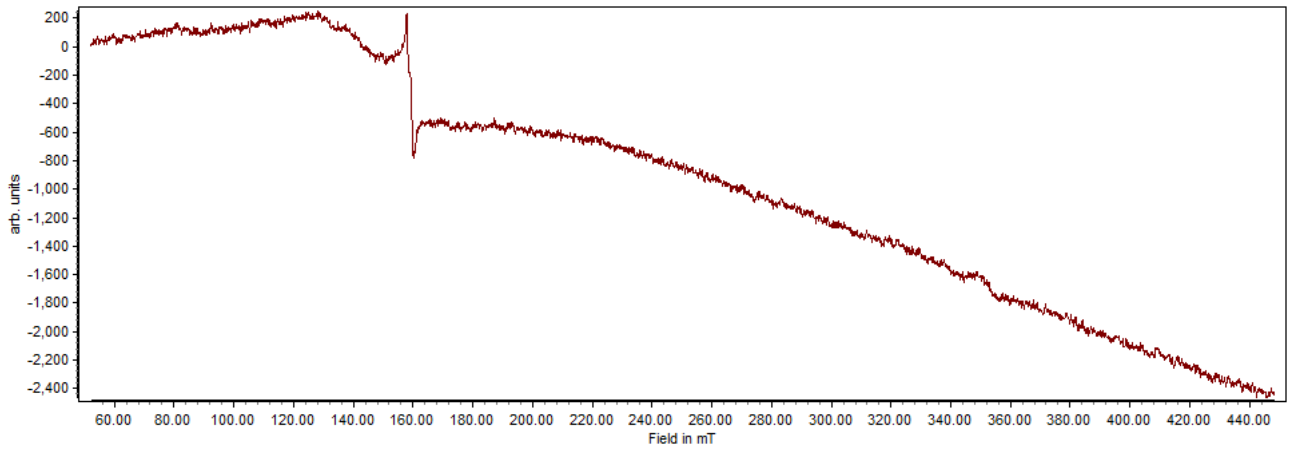

Figure S50: X-Band EPR spectrum of **2** at 77 K showing no signal. The "signal" at ~145 mT arises from the glas measuring apparatus, which was used and contains Fe.

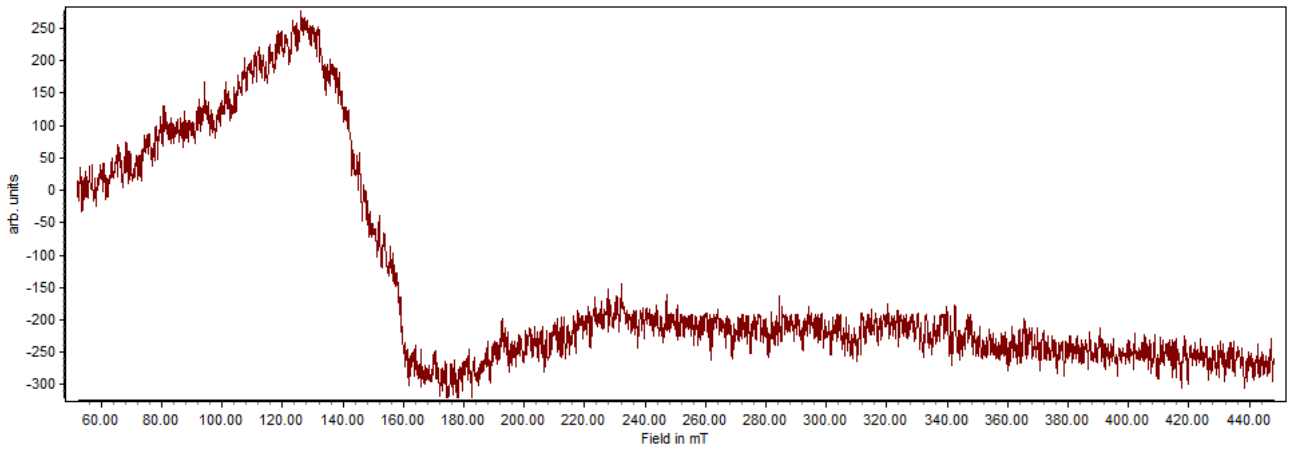

Figure S51: X-Band EPR spectrum of **3a** at room temperature showing no signal. The "signal" at ~145 mT arises from the glas measuring apparatus, which was used and contains Fe.

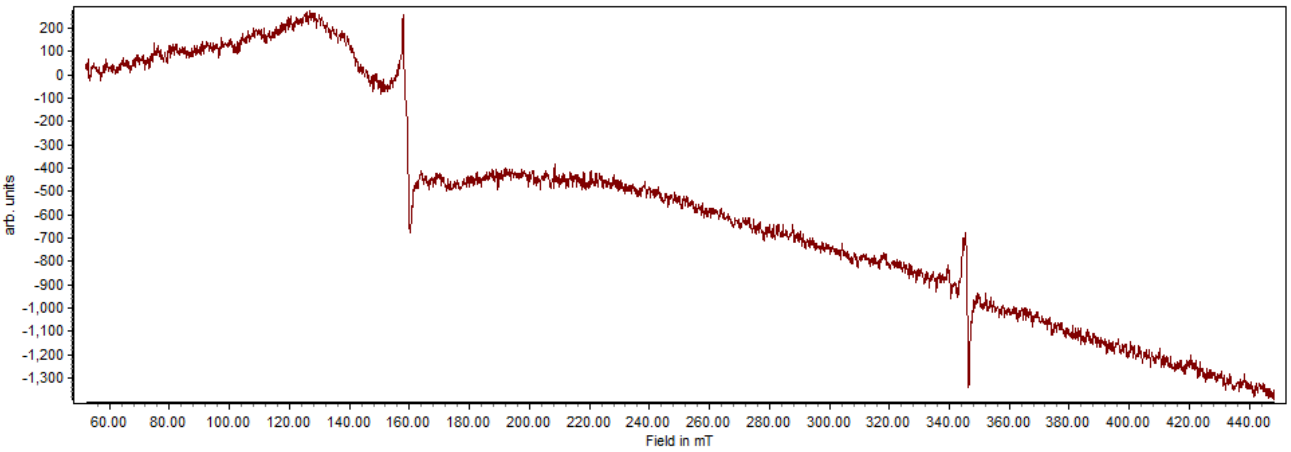

Figure S52: X-Band EPR spectrum of **3a** at 77 K showing a very weak axial signal (g_{iso} = 1.954). The "signal" at ~145 mT arises from the glas measuring apparatus, which was used and contains Fe.

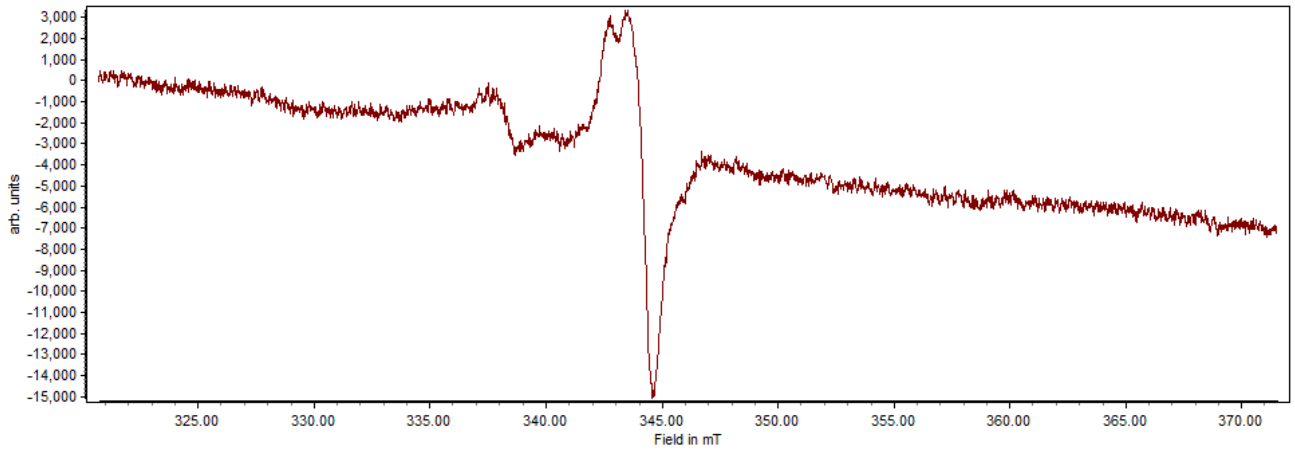

Figure S53: X-Band EPR spectrum of **3a** at 77 K from 320–370 mT showing a very weak axial signal (g_{iso} = 1.954).

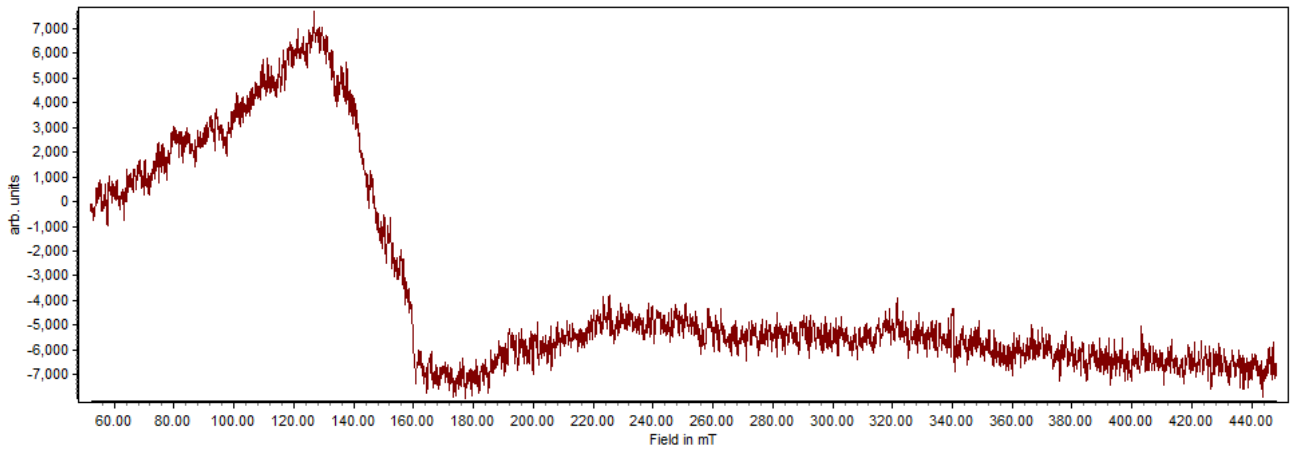

Figure S54: X-Band EPR spectrum of **4a** at room temperature showing no signal. The "signal" at ~145 mT arises from the glas measuring apparatus, which was used and contains Fe.

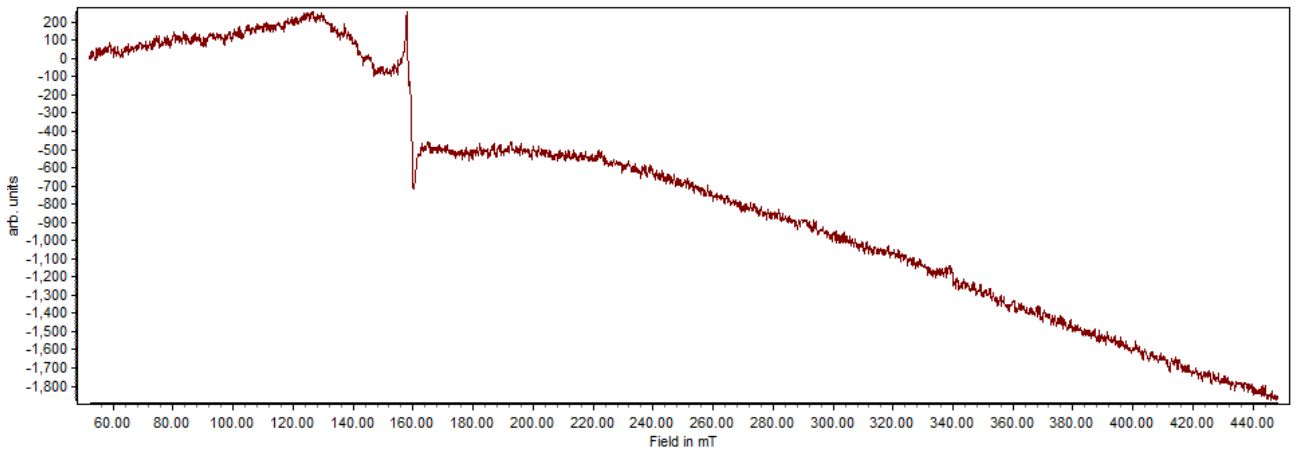

Figure S55: X-Band EPR spectrum of **4a** at 77 K showing no signal. The "signal" at ~145 mT arises from the glas measuring apparatus, which was used and contains Fe.

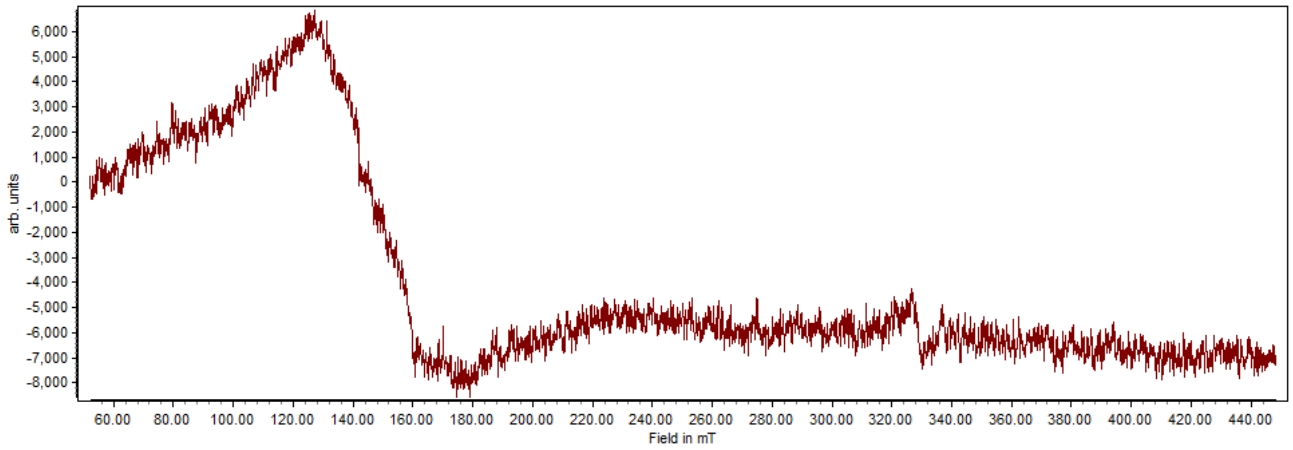

Figure S56: X-Band EPR spectrum of **4b** at room temperature showing no signal. The "signal" at ~145 mT arises from the glas measuring apparatus, which was used and contains Fe.

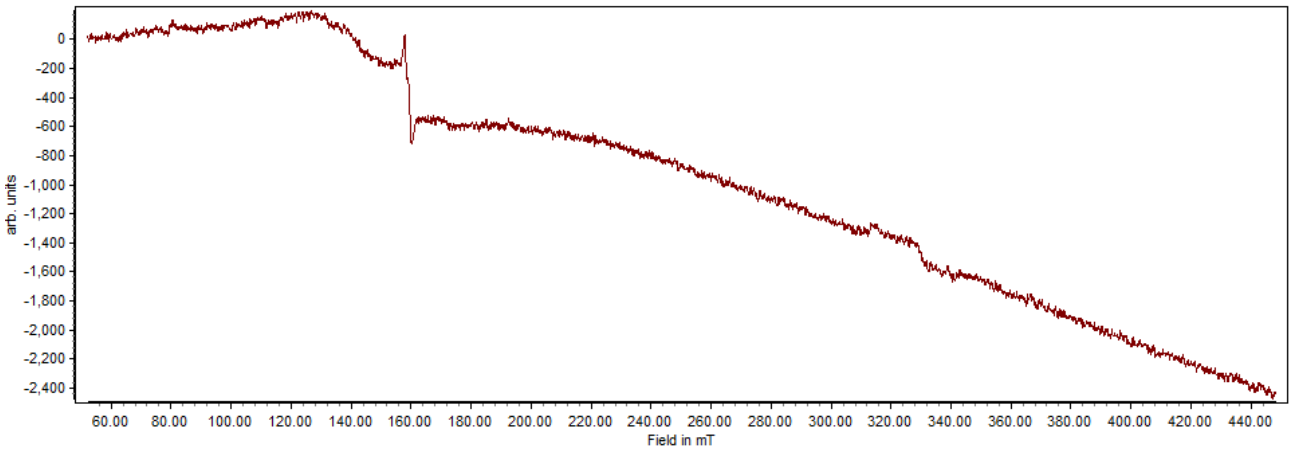

Figure S57: X-Band EPR spectrum of **4b** at 77 K showing no signal. The "signal" at ~145 mT arises from the glas measuring apparatus, which was used and contains Fe.

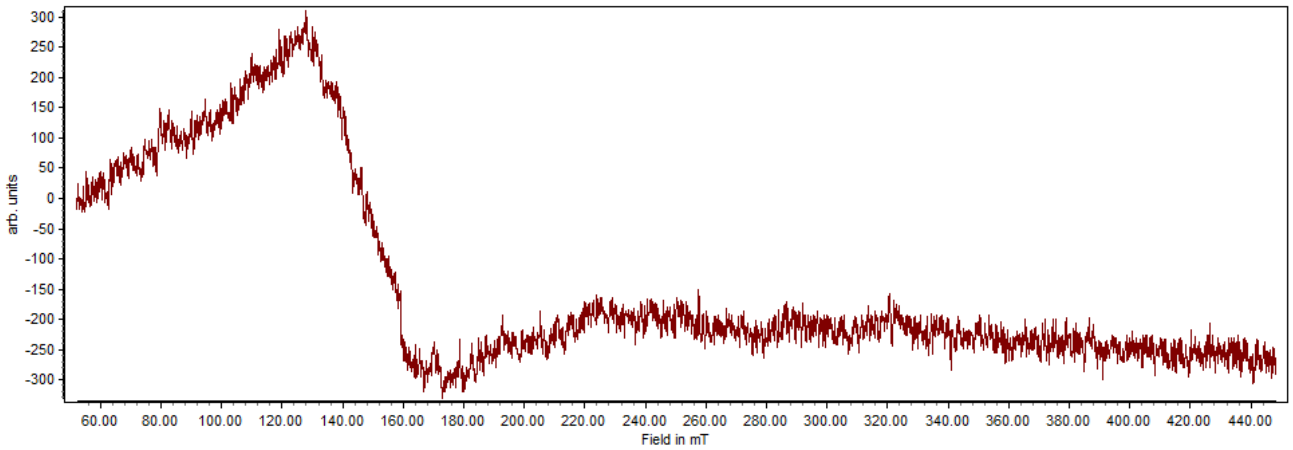

Figure S58: X-Band EPR spectrum of **5** at room temperature showing no signal. The "signal" at ~145 mT arises from the glas measuring apparatus, which was used and contains Fe.

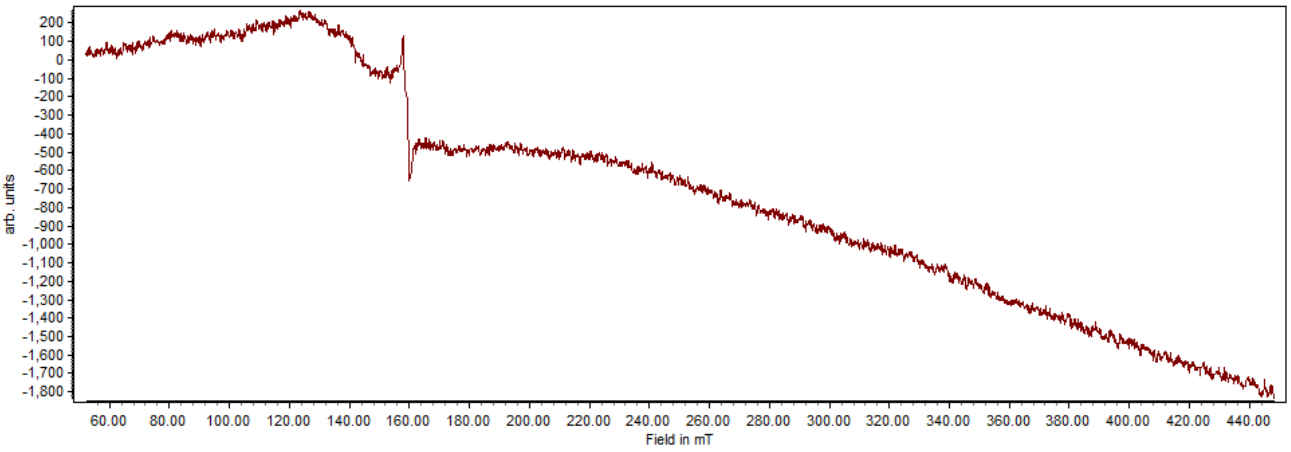

Figure S59: X-Band EPR spectrum of **5** at 77 K showing no signal. The "signal" at ~145 mT arises from the glas measuring apparatus, which was used and contains Fe.

7 X-ray crystallography

All crystal manipulations were performed under mineral oil. The diffraction experiments were performed at 123 K (if not stated otherwise) either on a Rigaku (former Agilent Technologies or Oxford Diffraction) SuperNova Single Source with an Atlas detector, a Gemini Ultra with an AtlasS2 detector, on a GV50 diffractometer with a TitanS2 detector or on a XtaLAB Synergy R DW system with a HyPix-Arc 150 detector using Cu-K_α, Cu-K_β or Mo-K_α radiation. Crystallographic data together with the details of the experiments are given in Table S1 and Table S2. The cell determination, data reduction and absorption correction for all compounds were performed with the help of the CrysAlis PRO software.[5] All structures were solved by using the programs SHELXT[6] and Olex2.[7] The full-matrix least-squares refinement against F^2 was done using SHELXL[8] and Olex2.[7] If not stated otherwise, all atoms except hydrogen atoms were refined anisotropically. The H atoms were calculated geometrically and a riding model was used during the refinement process.

CCDC-2105248 (**1**), CCDC-2105249 (**3a**), CCDC-2105250 (**3b**), CCDC-2105251 (**4a**), CCDC-2105252 (**4b**) and CCDC-2105253 (**5**), contain the supplementary crystallographic data for this paper. These data can be obtained free of charge at www.ccdc.cam.ac.uk/conts/retrieving.html (or from the Cambridge Crystallographic Data Centre, 12 Union Road, Cambridge CB2 1EZ, UK; Fax: + 44-1223-336-033; e-mail: deposit@ccdc.cam.ac.uk).

Table S1: Crystallographic details for the compounds **1**, **2**, **3a** and **4a**.

	1	**2**	**3a**	**4a**
formula	$C_{60}H_{20}Al_2As_2F_{72}Mo_4O_{16}P_2$	$C_{60}H_{20}Al_2F_{72}Mo_4O_{16}P_2Sb_2$	$C_{60}H_{20}Al_2F_{72}Mo_4O_{16}As_2Sb_2$	$C_{60.1}H_{19.2}Al_2As_{2.12}Bi_{1.88}Cl_{0.2}F_{72}Mo_4O_{16}$
weight [g·mol^{-1}]	3014.26	3277.77	3195.82	3361.68
Temperature [K]	123.0(1)	123.0(1)	100.01(10)	123.0(1)
crystal system	monoclinic	monoclinic	orthorhombic	triclinic
space group	$P2_1/n$	$P2_1/m$	*Pbca*	$P\bar{1}$
a [Å]	15.48296(15)	16.5312(16)	27.8964(2)	14.9100(3)
b [Å]	21.4711(2)	14.7868(11)	22.20040(10)	15.9359(6)
c [Å]	26.9785(3)	20.505(2)	29.7016(2)	20.4158(7)
α [°]	90	90	90	80.965(3)
β [°]	90.8706(9)	105.272(12)	90	82.393(2)
γ [°]	90	90	90	75.244(2)
Volume [Å^3]	8967.59(15)	4835.3(8)	18394.5.5(2)	4611.0(3)
Z	4	4	8	2
ρ_{calc} [g·cm^{-3}]	2.233		2.308	2.421
μ [mm^{-1}]	7.820		2.047	5.088
F(000)	5784.0		12144	3158
crystal size [mm^3]	0.260 × 0.144 × 0.100		0.174 × 0.119 × 0.109	0.606 × 0.135 × 0.13
diffractometer	SuperNova	GV50	XtaLAB Synergy R, DW system	Gemini Ultra
absorption correction	gaussian		gaussian	gaussian
T_{min} / T_{max}	0.349 / 0.602		0.727 / 1.000	0.354 / 0.760
radiation [Å]	Cu-Kα (λ = 1.54184)	Cu-Kα (λ = 1.54184)	Mo-Kα (λ = 0.71073)	Mo-Kα (λ = 0.71073)
2*Θ* range [°]	6.996 to 147.820		3.670 to 65.154	6.732 to 61.016
completeness [%]	99.3		100	99.2
reflns collected / unique	42829 / 17600		437712 / 33485	48635 / 27938
R_{int} / R_{sigma}	0.0239 / 0.0264		0.0704 / 0.0288	0.0396 / 0.0744
data / restraints / parameters	15039 / 587 / 1896		27529 / 1404 / 2548	20441 / 1724 / 2440
GooF on F^2	1.063		1.031	1.013
R_1 / wR_2 [$I \geq 2\sigma(I)$]	0.0349 / 0.0964		0.0325 / 0.0786	0.0437 / 0.0814
R_1 / wR_2 [all data]	0.0408 / 0.0985		0.0436 / 0.0831	0.0721 / 0.0920
max / min $\Delta\rho$ [e·Å^{-3}]	1.851 / –0.738		1.461 / –0.784	1.387 / −1.053
identification code	LD106_new_abs_error_model_off	LD202	LD461_oP_abs_gaus	CR500_Moa

Table S2: Crystallographic details for the compounds **5**, **3b** and **4b**.

	5	**3b**	**4b**
formula	$C_{60}H_{20}Al_2Bi_2F_{72}Mo_4O_{16}Sb_2$	$C_{60}H_{20}Al_2As_2Cl_{24}F_{48}Mo_4O_{16}Sb_2$	$C_{62}H_{24}O_{16}F_{48}Al_2Cl_{28}As_{2.07}Mo_4Bi_{1.93}$
weight [g·mol^{-1}]	3463.94	3590.62	3925.55
Temperature [K]	110.0(1)	123.0(1)	123.0(1)
crystal system	monoclinic	monoclinic	monoclinic
space group	$P2_1/n$	$P2_1/c$	$P2_1/n$
a [Å]	15.58570(10)	20.6398(2)	13.3028(2)
b [Å]	22.6461(2)	23.2138(2)	27.6708(4)
c [Å]	25.9891(2)	23.1270(2)	14.6789(3)
α [°]	90	90	90
β [°]	90.5190(10)	112.9690(10)	96.234(2)
γ [°]	90	90	90
Volume [Å^3]	9172.61(12)	10202.27(17)	5371.34(16)
Z	4	4	2
ρ_{calc} [g·cm^{-3}]	2.508	2.338	2.427
μ [mm^{-1}]	13.899	16.089	5.090
F(000)	6472.0	6840.0	3709.0
crystal size [mm^3]	0.373 × 0.109 × 0.086	0.275 × 0.122 × 0.11	0.984 × 0.237 × 0.128
diffractometer	GV50	GV50	SuperNova
absorption correction	gaussian	gaussian	gaussian
T_{min} / T_{max}	0.079 / 0.642	0.477 / 0.719	0.106 / 1.000
radiation [Å]	Cu-Kβ (λ = 1.39222)	Cu-Kα (λ = 1.54184)	Mo-Kα (λ = 0.71073)
2*Θ* range [°]	4.674 to 148.256	7.616 to 148.062	5.89 to 69.18
completeness [%]	99.6	99.6	99.8
reflns collected / unique	84463 / 24730	58041 / 20043	51984 / 21333
R_{int} / R_{sigma}	0.0457 / 0.0333	0.0525 / 0.0453	0.0391 / 0.0513
data / restraints / parameters	23965 / 656 / 1694	18107 / 587 / 1675	18316 / 0 / 743
GooF on F^2	1.165	1.033	1.068
R_1 / wR_2 [$I \geq 2\sigma(I)$]	0.0577 / 0.1524	0.0458 / 0.1181	0.0378 / 0.0816
R_1 / wR_2 [all data]	0.0589 / 0.1531	0.0523 / 0.1233	0.0484 / 0.0856
max / min $\Delta\rho$ [e·Å^{-3}]	2.412 / −1.793	1.903 / −1.166	1.920 / −1.979
identification code	LD364_mP_abs_gaus	LD196_CR014_abs	LD448_abs

Refinement details for 1:

Compound **1** can be regarded as isostructural to compound **2**, **IX** and **X**. It crystallizes in the monoclinic space group $P2_1/n$ with one dicationic complex exhibiting a central AsPPAs zigzag chain and two independent WCAs $[TEF]^-$ in the asymmetric unit. The refinement of the cationic part could be performed without any difficulty. For one $[TEF]^-$ anion (including Al1) a positional disorder for the fragment $Al\{OC(CF_3)_3\}_2$ is observed with a ratio of 90:10. Due to the low occupancy of the minor part was only the Al11 atom anisotropically refined and the U_{iso} of the O, C and F atoms was set to 0.3. The other $[TEF]^-$ anion (including Al2) shows a rotational or positional disorder of the $-OC_4F_9$ groups with ratios of 88:12, 86:14, 81:19 and 60:40, respectively. The disordered groups were during the refinement process partially restrained with DFIX, SADI and SIMU commands.

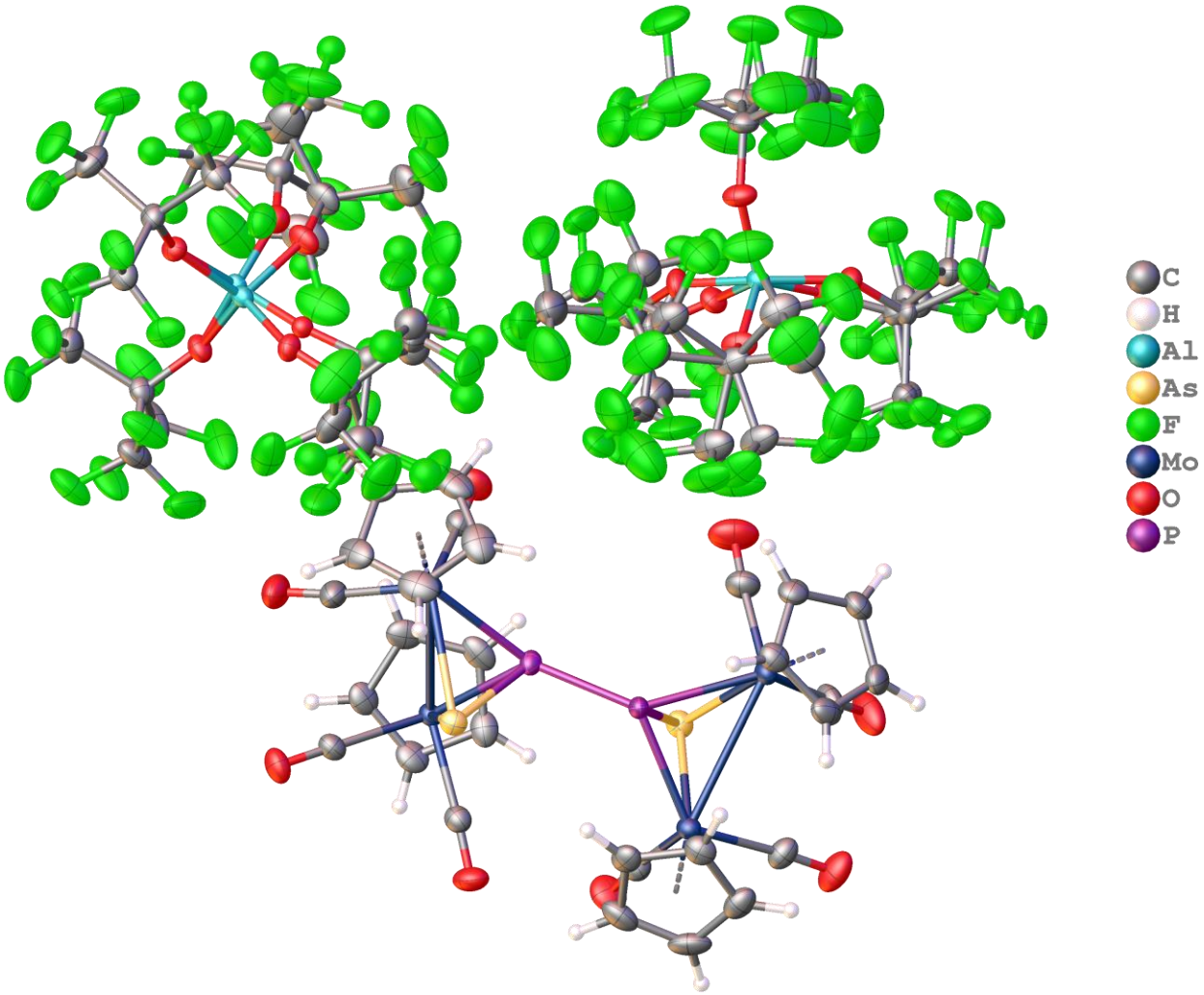

Figure S60: Molecular structure of **1**. The asymmetric unit is shown containing one dication and two $[TEF]^-$ anions, which both show disorder of several $-OC(CF_3)_3$ groups.

Refinement details for 2:

The X-ray dataset of **2** is very weak and, therefore, a proper refinement of the molecular structure was not possible. Only the heavy atom framework of the dicationic part can be identified, which suggests in combination with the spectroscopical data of **2** (*vide supra*) and the unit cell parameters that **2** also forms a dicationic SbPPSb zigzag chain upon P–P bond formation being isostructural to **1**, **IX** and **X**. The heavy atom framework of **2** is shown in Figure S61.

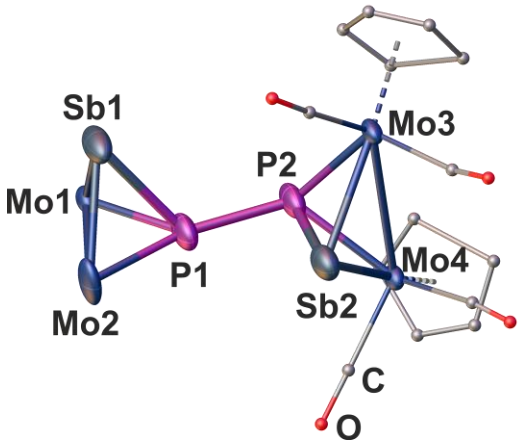

Figure S61: Heavy atom framework of the dicationic part of **2**. H atoms as well as the Cp and CO ligands of one Mo_2PSb unit are omitted for clarity. Additionally, Cp and CO ligands are drawn as small spheres.

Refinement details for 3a:

Compound **3a** crystallizes in the orthorhombic space group *Pbca* with one dication exhibiting a central AsSbSbAs chain/cage and two independent WCAs $[TEF]^-$ in the asymmetric unit. The cationic unit shows a positional disorder of the $(Mo_2AsSB)_2$ unit with a ratio of 80:20. For one $[TEF]^-$ anion (including Al1) a positional disorder for three $-OC(CF_3)_3$ groups is observed with a ratio of 60:40, 51:49 and 50:50, respectively. The other $[TEF]^-$ anion (including Al2) shows a positional disorder of two $-OC(CF_3)_3$ groups over two positions with a ratio of 70:30 and of two $-OC(CF_3)_3$ group over three positions with ratios of 50:25:25 and 47:29:24, respectively. The disordered groups were, during the refinement process, partially restrained with DFIX, SADI and SIMU commands. An interesting feature of the molecular structure in **3a** is the arrangement of the Cp substituents. While the arrangement at one of the Mo_2AsSb units resembles the respective arrangement of chain-type structures (see manuscript, Figure 2b Mo_2AsSb unit), like in **1**, the arrangement at the other Mo_2AsSb unit is similar to cage-type structures (see manuscript, Figure 2b left Mo_2AsSb unit), e.g., in **5**. This again shows that the structure of **3a** represents an intermediate stage between the chain-type structures in **1**, **2**, **VI** and **VII**, and the cage-type structures in **5**, **VIII** and **IX**.

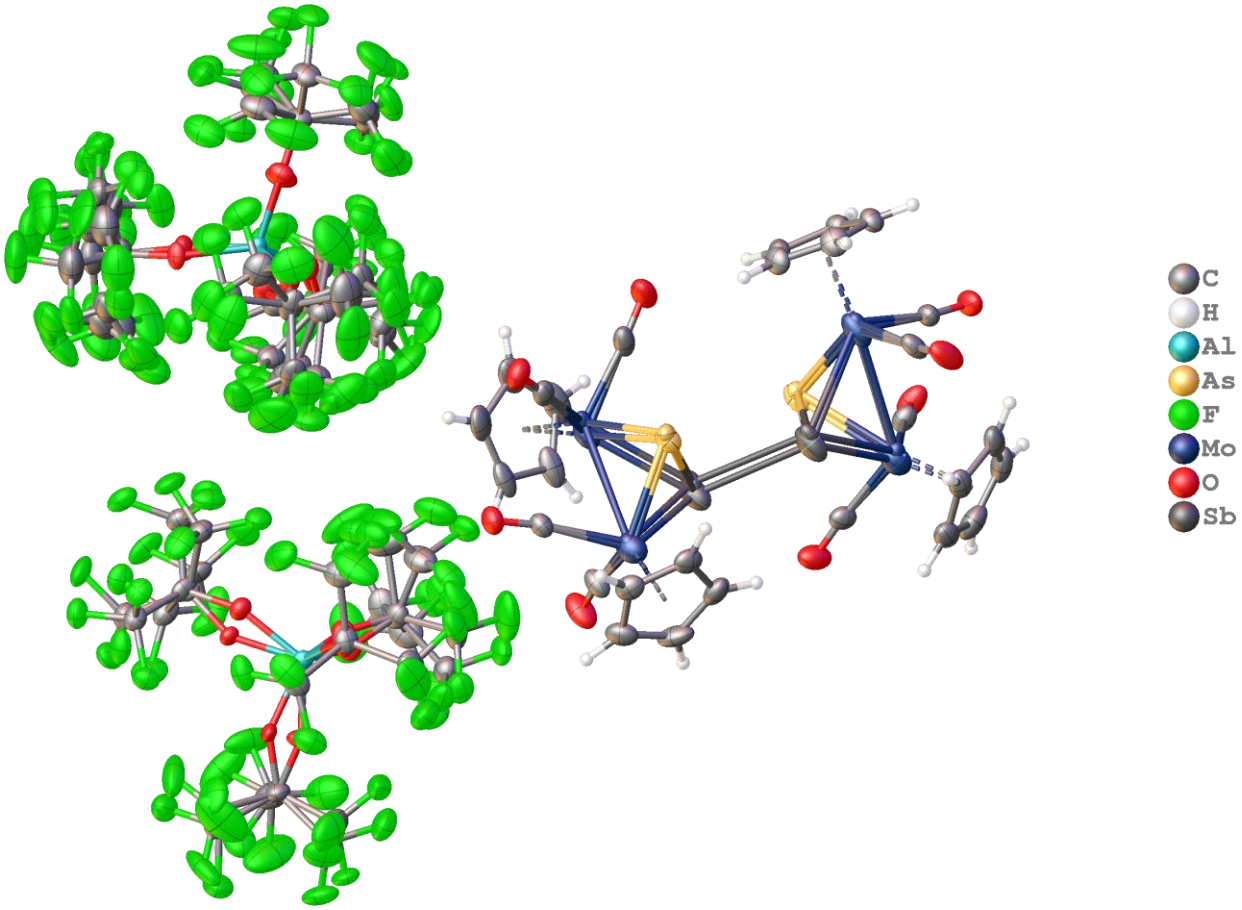

Figure S62: Molecular structure of **3**a. The asymmetric unit is shown containing one disordered dication and two disordered $[TEF]^-$ anions.

Refinement details for 3b:

Compound **3b** crystallizes in the monoclinic space group $P2_1/c$ with one dication exhibiting a central AsSbAsSb cycle and two independent WCAs $[TEF^{Cl}]^-$ in the asymmetric unit. The cationic unit shows a disorder of the As_2Sb_2 cycle in a ratio of 84:16. Further shows one of the $[TEF^{Cl}]^-$ anions (including Al1) a rotational and a positional disorder of two $OC(CF_3)_2(CCl_3)$ groups in a ratio of 85:15. The second $[TEF^{Cl}]^-$ anion (including Al2) shows a disorder of the two oxygen atoms O14 and O15 in ratios of 60:40 and 50:50, respectively. Further is the Cl atom Cl21 disordered over two positions with the ratio 70:30. The disordered groups were, during the refinement process, partially restrained with SADI, ISOR and SIMU commands.

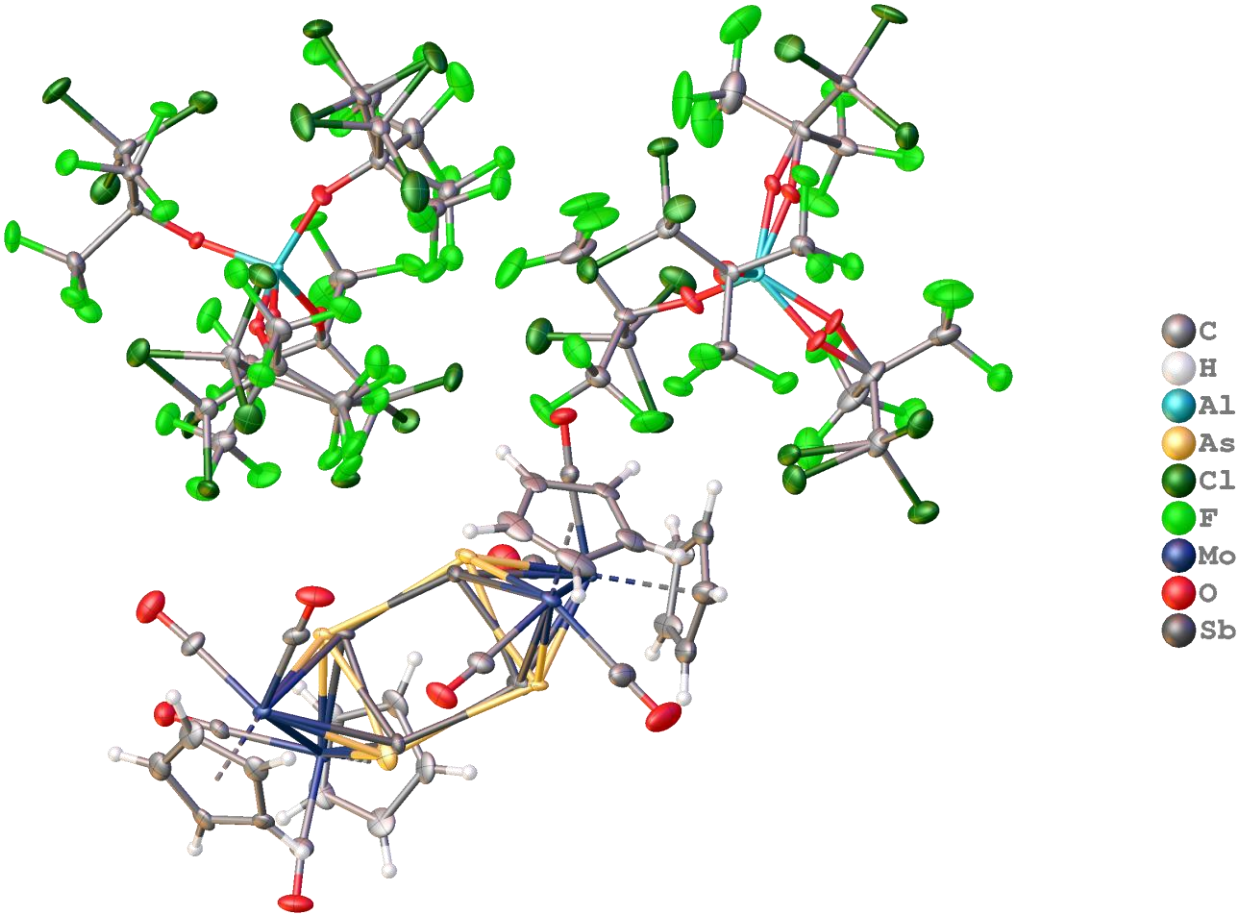

Figure S63: Molecular structure of **3b**. The asymmetric unit is shown containing one disordered dication and two disordered $[TEF^{Cl}]^-$ anions.

Refinement details for 4a:

Compound **4a** crystallizes in the triclinic space group $P\bar{1}$ with two half dications exhibiting a central AsBiBiAs ring and two independent WCAs $[TEF]^-$ as well as 0.1 molecules CH_2Cl_2 in the asymmetric unit. One of these dications co-crystalizes with the dicationic As_4 chain **X** in a ratio of 88:12. One $[TEF]^-$ anion (including Al2) shows rotational and positional disorder of all four perfluorinated *tert*-butoxy groups in a ratio of 50:50, 50:50, 63:37 and 58:42. The second $[TEF]^-$ anion (including Al1) shows also a rotational and positional disorder of all four $-OC(CF_3)_3$ groups, whereat three of these groups are disordered over two positions (88:12; 86:14; 74:26) and the third one shows a disorder over three positions (55:31:14). The disordered groups were, during the refinement process, partially restrained with DFIX, SADI and SIMU commands.

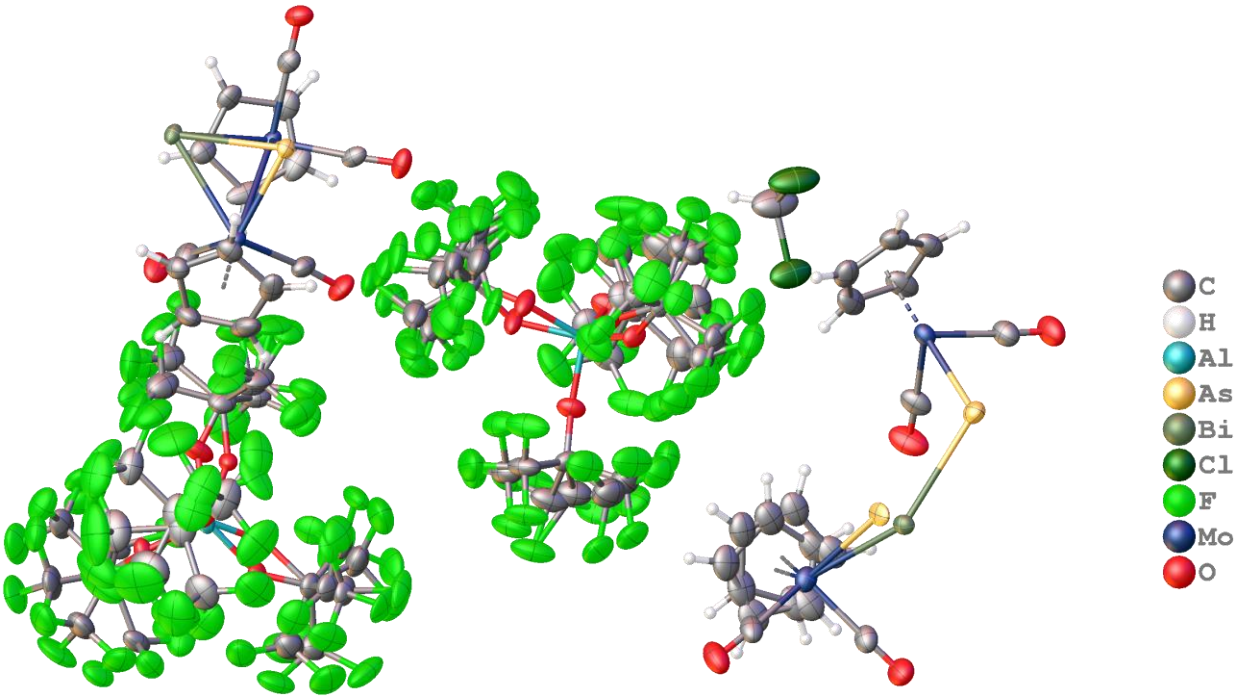

Figure S64: Molecular structure of **4a**. The asymmetric unit is shown containing two half molecules of the dication, two disordered $[TEF]^-$ anions and one solvent molecule CH_2Cl_2. One of the dications co-crystalizes with the dicationic As_4 chain **X** in a ratio of 88:12 and exhibits rotational disorder of one of its Cp ligands.

Refinement details for 4b:

Compound **4b** crystallizes in the monoclinic space group $P2_1/n$ with one half dication exhibiting a central AsBiBiAs cycle, one WCA $[TEF^{Cl}]^-$ and one solvent molecule CH_2Cl_2 in the asymmetric unit. The cyclic dication $[\{CpMo(CO)_2\}_2(\mu,\eta^2{:}\eta^2\text{-BiAs})]_2^{2+}$ co-crystalizes with the dicationic As_4 chain **X** in a ratio of 97:3. The anion $[TEF^{Cl}]^-$ shows no sign of disorder.

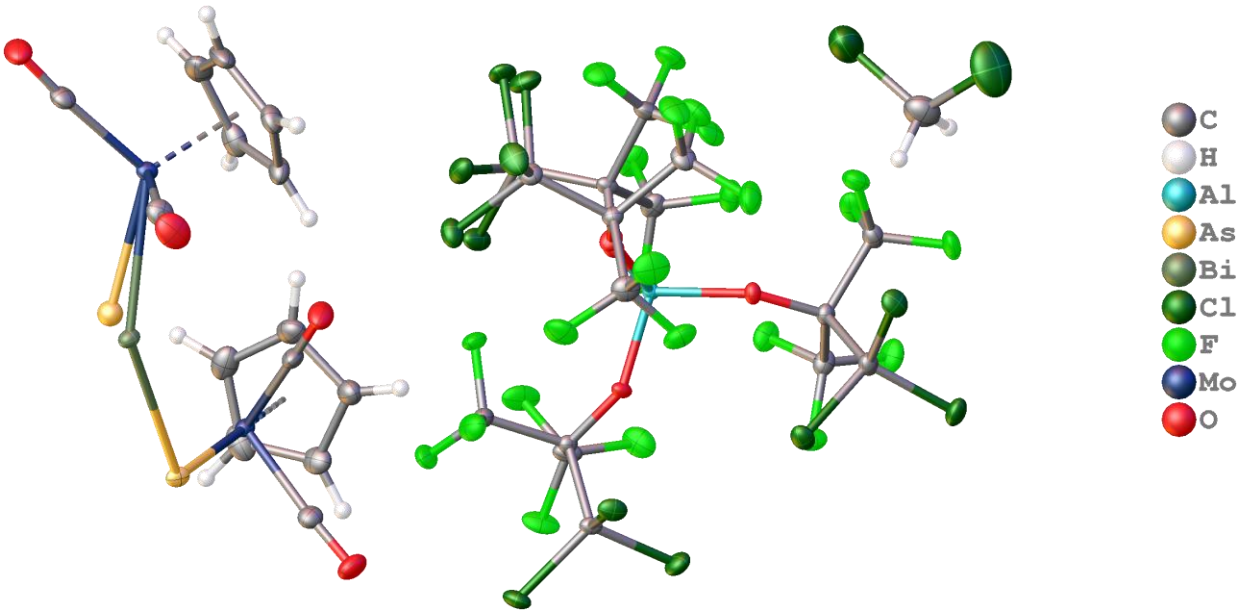

Figure S65: Molecular structure of **4b**. The asymmetric unit is shown containing one half dication, one $[TEF^{Cl}]^-$ anion and one solvent molecule CH_2Cl_2. The dication co-crystalizes with the dicationic As_4 chain **X** in a ratio of 97:3.

Refinement details for 5:

Compound **5** crystallizes in the monoclinic space group $P2_1/n$ with one dication exhibiting a central BiSbSbBi cage and two independent WCAs $[TEF]^-$ in the asymmetric unit. The dication $[\{CpMo(CO)_2\}_2(\mu,\eta^2{:}\eta^2\text{-BiSb})]_2^{2+}$ features a disorder over two positions of both BiSb dumbbells (76:24) and one Cp ligand (59:41). It could, however, also be a co-crystallization with the dicationic Sb_4 and/or Bi_4 cages **XI** and **XII**, respectively, which were also detected in the NMR spectra (*vide supra*). One $[TEF]^-$ anion (including Al2) shows rotational disorder of two perfluorinated *tert*-butoxy groups in a ratio of 52:48 and 72:28. The disordered groups were, during the refinement process, partially restrained with SADI and SIMU commands.

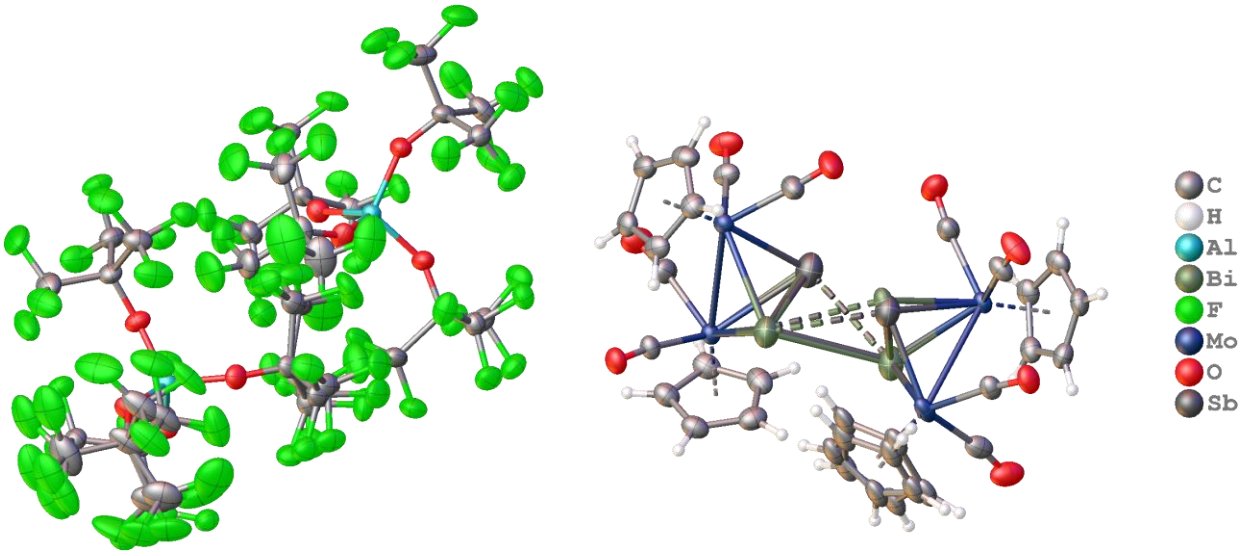

Figure S66: Molecular structure of **5**. The asymmetric unit is shown containing one disordered dication and two disordered $[TEF]^-$ anions.

8 Details of DFT Calculations

The DFT calculations have been performed with the ORCA program.[9] The geometries have been optimised with the TPSSh[10] functional together with the def2-TZVP[11] basis set. The starting point for the geometry optimisations were the coordinates obtained from the X-ray diffractions. To speed up the calculations in a first step the geometries has been optimised at the BP86[12]/def2-SVP level, than at the BP86/def2-TZVP, TPSSh/def2-TZVP (using the RIJCOSX[13] approximation) and finally at the TPSSh/def2-TZVP level (the latter without the RIJCOSX approximation). The dispersion effects have been incorporated by using the charge dependent atom-pairwise dispersion correction model (D4).[14] For the solvent effects has been accounted via the Conductor-like Polarizable Continuum Model (CPCM)[15] as implemented in Orca, using the dielectric constant of dichloromethane. The atomic orbital contribution to the frontier molecular orbitals of compounds **A**–**E** has been determined at the B3LYP[12a,16]/def2-TZVP level using Loewdin orbital population analysis. For the calculation of the reaction energies, the total SCF energies (TPSSh/def2-TZVP) have been used without further corrections.

Table S3: Total SCF energies calculated at the TPSSh/def2-TZVP level.

Compound	Total energy (ha)
$[(CpMo(CO)_2\}_2(PAs)]^+$ (**A**$^+$)	-3554.59332539731
$[(CpMo(CO)_2\}_2(PSb)]^+$ (**B**$^+$)	-1558.95030364644
$[(CpMo(CO)_2\}_2(PBi)]^+$	-1533.35568693966
$[(CpMo(CO)_2\}_2(AsSb)]^+$ (**C**$^+$)	-3453.41414884946
$[(CpMo(CO)_2\}_2(AsBi)]^+$ (**D**$^+$)	-3427.82007153905
$[(CpMo(CO)_2\}_2(SbBi)]^+$ (**E**$^+$)	-1432.18131708391
$[(CpMo(CO)_2\}_2(PAs)]_2^{2+}$ (**1**)	-7109.24276961385
$[(CpMo(CO)_2\}_2(PSb)]_2^{2+}$ (**2**)	-3117.96089582412
$[(CpMo(CO)_2\}_2(AsSb)]_2^{2+}$ (**3a**)	-6906.88267451174
$[(CpMo(CO)_2\}_2(AsBi)]_2^{2+}$ (**4a**)	-6855.69504284423
$[(CpMo(CO)_2\}_2(SbBi)]_2^{2+}$ (**5**)	-2864.42577128920

Table S4: Mulliken spin densities calculated at the TPSSh/def2-TZVP level.

$[(CpMo(CO)_2\}_2(PAs)]^+$ (**A**$^+$)			
0 As:	1P	2 Mo:	3 Mo:
0.022	0.016	0.423	0.397
$[(CpMo(CO)_2\}_2(PSb)]^+$ (**B**$^+$)			
0 Sb:	1p	2 Mo:	3 Mo:
0.157	0.138	0.238	0.402
$[(CpMo(CO)_2\}_2(PBi)]^+$			
0 Bi:	1p	2 Mo:	3 Mo:
0.206	0.155	0.211	0.370
$[(CpMo(CO)_2\}_2(AsSb)]^+$ (**C**$^+$)			
0 Sb:	1 As:	2 Mo:	3 Mo:
0.167	0.154	0.254	0.367
$[(CpMo(CO)_2\}_2(AsBi)]^+$ (**D**$^+$)			
0 Bi:	1 As:	2 Mo:	3 Mo:
0.2133	0.1724	0.22449	0.3381
$[(CpMo(CO)_2\}_2(SbBi)]^+$ (**E**$^+$)			
0 Bi:	1 Sb:	2 Mo:	3 Mo:
0.257	0.226	0.247	0.231

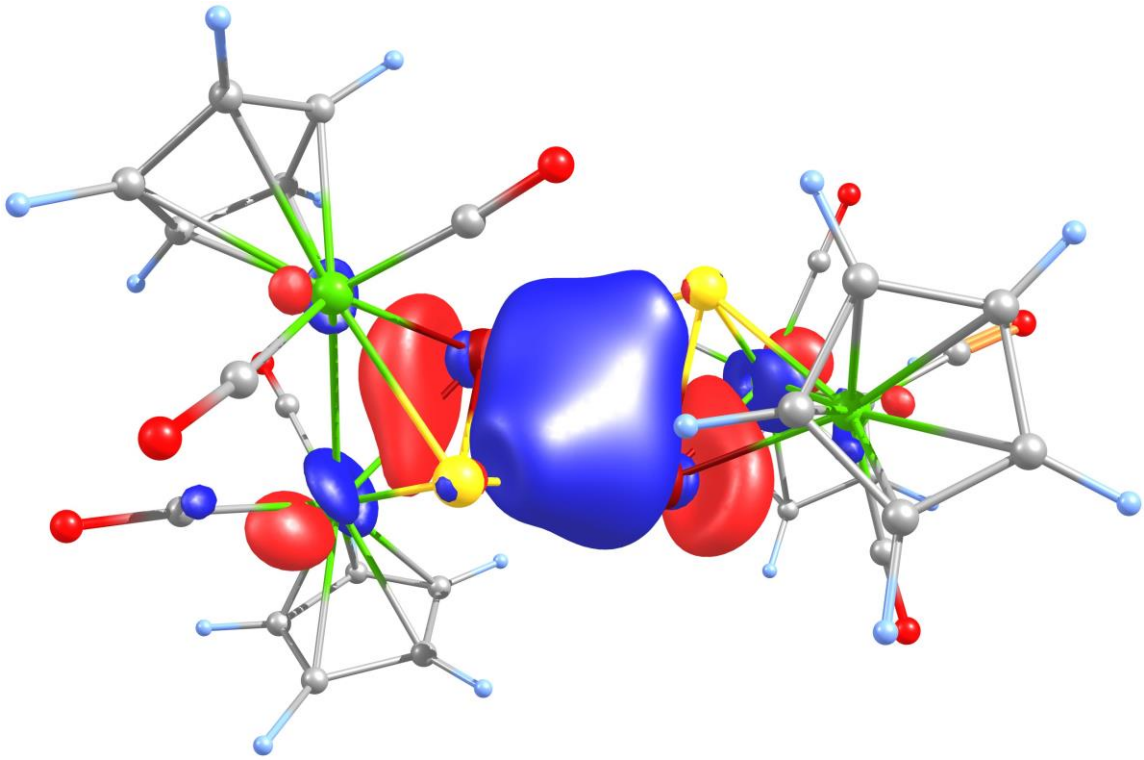

Figure S67: Intrinsic bonding orbital[17] representing a 2e4c bond in $[(CpMo(CO)_2\}_2(AsSb)]_2^{2+}$ (**3a**) (TPSSh/def2-TZVP level).

Table S5: Cartesian coordinates of the optimised geometry of $[\{CpMo(CO)_2\}_2(PAs)]^+$ (**A**$^+$) (TPSSh/def2-TZVP level).

Atom	X	Y	Z
As	-0.610966	-2.460618	-0.910819
P	-1.738249	-1.693525	0.839316
Mo	0.696782	-1.060954	0.887756
Mo	-1.269650	0.067632	-0.902140
C	-0.736118	2.029106	0.277819
H	0.093540	2.139065	0.955724
C	-2.868398	1.720693	-0.520259
H	-3.926207	1.510736	-0.564317
C	-2.043460	2.102696	-1.619976
H	-2.369461	2.250644	-2.637558
C	-0.721155	2.298408	-1.118548
H	0.127950	2.630745	-1.695596
C	-2.064790	1.670979	0.645800
H	-2.406099	1.417388	1.637066
C	-2.895926	-0.819607	-1.669453
C	-0.311624	-0.233474	-2.647801
O	-3.854636	-1.264780	-2.109284
O	0.226998	-0.334750	-3.656166
C	2.141380	0.373218	-0.284312
H	1.825427	1.140439	-0.971111
C	2.931888	-1.621741	0.538610
H	3.279795	-2.641984	0.593749
C	2.836340	-0.709105	1.630432
H	3.117111	-0.908581	2.652686
C	2.348660	0.529899	1.114140
H	2.205649	1.435221	1.683624
C	2.502476	-0.958189	-0.638294
H	2.470953	-1.385225	-1.628248
C	0.714301	-2.901218	1.687443
C	-0.054321	-0.389476	2.633019
O	0.784372	-3.942300	2.157768
O	-0.432561	0.008657	3.638929

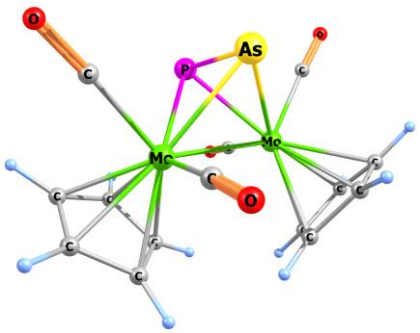

Selected Mayer bond orders larger than 0.100:

B (0-As, 1-P): 1.0872
B (0-As, 2-Mo): 0.8196
B (0-As, 3-Mo): 0.8466
B (1-P, 2-Mo): 0.8847
B (1-P, 3-Mo): 0.8635
B (2-Mo, 3-Mo): 0.5894

Table S6: Cartesian coordinates of the optimised geometry of $[(CpMo(CO)_2\}_2(PSb)]^+$ (**B**$^+$) (TPSSh/def2-TZVP level).

Atom	X	Y	Z
Sb	-0.646814	-2.509003	-0.993646
P	-1.626806	-1.422281	1.012484
Mo	0.854833	-1.113182	0.836797
Mo	-1.467061	0.156972	-0.851129
C	-1.161050	2.203875	0.262654
H	-0.280476	2.439496	0.837805
C	-3.276506	1.508541	-0.329638
H	-4.278372	1.110190	-0.283577
C	-2.640350	2.050167	-1.490277
H	-3.077465	2.133987	-2.473282
C	-1.340505	2.478097	-1.119550
H	-0.612742	2.934229	-1.772867
C	-2.362048	1.606572	0.752508
H	-2.558429	1.315752	1.771996
C	-2.548486	-0.671885	-2.317019
C	0.046022	0.150824	-2.143744
O	-3.213157	-1.052937	-3.173724
O	0.856322	0.255282	-2.958695
C	2.521566	0.100683	-0.299167
H	2.313923	0.957769	-0.918516
C	2.911148	-2.057677	0.402876
H	3.059127	-3.126348	0.404599
C	3.049345	-1.187524	1.531585
H	3.321540	-1.480579	2.533497
C	2.809236	0.141702	1.087087
H	2.848071	1.030112	1.698340
C	2.581413	-1.261010	-0.727669
H	2.460346	-1.614168	-1.738826
C	0.693822	-2.591214	2.164300
C	0.203045	0.121053	2.255930
O	0.657216	-3.442667	2.931845
O	-0.096709	0.835168	3.107023

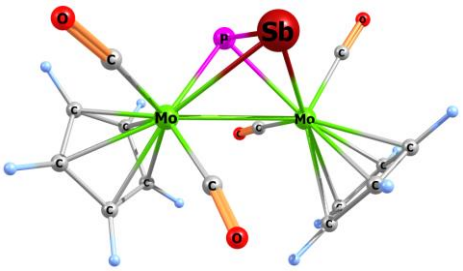

Selected Mayer bond orders larger than 0.100:
B (0-Sb, 1-P): 0.9265
B (0-Sb, 2-Mo): 0.8113
B (0-Sb, 3-Mo): 0.8238
B (1-P, 2-Mo): 0.9512
B (1-P, 3-Mo): 0.9418
B (2-Mo, 3-Mo): 0.3914

Table S7: Cartesian coordinates of the optimised geometry of $[(CpMo(CO)_2\}_2(PBi)]^+$ (TPSSh/def2-TZVP level).

Atom	X	Y	Z
Bi	-0.6625821684	-2.6088159753	-1.0549283193
P	-1.6344873557	-1.4073746242	1.0215391258
Mo	0.8428148269	-1.1220357636	0.8376144827
Mo	-1.4699544041	0.1455159764	-0.8582134695
C	-1.1215365194	2.1757054784	0.2801934741
H	-0.2442382035	2.3820982409	0.8715215283
C	-3.2452086110	1.5427336373	-0.3503658572
H	-4.2592149573	1.1748957993	-0.3209682220
C	-2.5762029141	2.0738774695	-1.4977752498
H	-2.9954029745	2.1774480669	-2.4866242779
C	-1.2708829568	2.4631442473	-1.1028905341
H	-0.5201973874	2.9037411824	-1.7407270964
C	-2.3456105654	1.6090268054	0.7465628145
H	-2.5646312463	1.3174937319	1.7612614626
C	-2.6078876151	-0.6730147803	-2.2834782462
C	0.0244885311	0.1023473750	-2.1689436117
O	-3.3143641889	-1.0350166834	-3.1169998697
O	0.8281959907	0.2006131624	-2.9936759461
C	2.4805287441	0.1214283875	-0.3178486991
H	2.2548170629	0.9576198774	-0.9589511004
C	2.9300713278	-2.0070762320	0.4361244980
H	3.1135013730	-3.0699284406	0.4618031866
C	3.0261564444	-1.1101259098	1.5481214801
H	3.2983184297	-1.3726273276	2.5583544235
C	2.7474832059	0.2018435535	1.0704583190
H	2.7525478230	1.1049685071	1.6610751851
C	2.5876807787	-1.2459933456	-0.7154449886
H	2.4941225920	-1.6230447344	-1.7209923125
C	0.6987606708	-2.6478808255	2.1081456943
C	0.1869409770	0.0525583583	2.2994442962
O	0.6776055727	-3.5223044011	2.8513561623
O	-0.1116317826	0.7381791862	3.1752512674

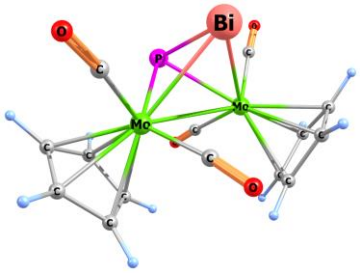

Selected Mayer bond orders larger than 0.100:
B (0-Bi, 1-P): 0.8614
B (0-Bi, 2-Mo): 0.7541
B (0-Bi, 3-Mo): 0.7880
B (0-Bi, 14-C): 0.1081
B (1-P, 2-Mo): 0.9677
B (1-P, 3-Mo): 0.9641
B (2-Mo, 3-Mo): 0.3897
B (2-Mo, 18-C): 0.4194
B (2-Mo, 20-C): 0.4489

Table S8: Cartesian coordinates of the optimised geometry of $[(CpMo(CO)_2\}_2(AsSb)]^+$ (**C**$^+$) (TPSSh/def2-TZVP level).

Atom	X	Y	Z
Sb	-0.5965984758	-2.4985963828	-1.047114392
As	-1.7203446200	-1.5105099222	1.0668385865
Mo	0.8604917699	-1.1386282867	0.8467724823
Mo	-1.4665777622	0.15705897227	-0.854185626
C	-1.1528209513	2.18939214070	0.2899482750
H	-0.2869097942	2.40613413804	0.8939309479
C	-3.2597377772	1.53259859517	-0.371902626
H	-4.2708059913	1.15591929732	-0.357322829
C	-2.5792911580	2.07022466465	-1.509812818
H	-2.9852043589	2.17189179943	-2.504339469
C	-1.2837880194	2.47382123271	-1.094497453
H	-0.5289867275	2.92444073876	-1.720285291
C	-2.3771120138	1.60757574758	0.7391791170
H	-2.6111144269	1.32325868896	1.7526869818
C	-2.6068874325	-0.6705884353	-2.271143252
C	0.01473362742	0.14437855337	-2.179186702
O	-3.3101129688	-1.0548157818	-3.095208818
O	0.81557675288	0.24899236551	-3.004108688
C	2.49203482232	0.10597687296	-0.307902221
H	2.26384902534	0.95438318298	-0.931852657
C	2.93424093958	-2.0382944923	0.4060514957
H	3.10577605642	-3.1034195077	0.4138772187
C	3.05646570746	-1.1584614030	1.5287467361
H	3.33818801562	-1.4396818753	2.5313816838
C	2.78355936659	0.16189239967	1.0773380372
H	2.80411710629	1.05512925541	1.6824651602
C	2.58211868274	-1.2564293173	-0.728141998
H	2.47002376955	-1.6178016998	-1.737552594
C	0.72594049025	-2.6192988822	2.1741847272
C	0.18314048065	0.08764881021	2.2573215909
O	0.71977977429	-3.4695914524	2.9452735209
O	-0.1137441088	0.80539958361	3.1085609799

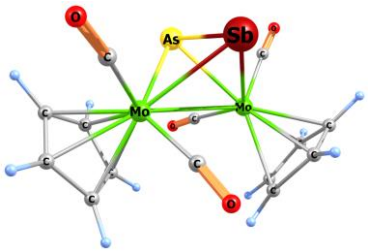

Selected Mayer bond orders larger than 0.100:
B (0-Sb, 1-As): 0.9199
B (0-Sb, 2-Mo): 0.8233
B (0-Sb, 3-Mo): 0.8456
B (1-As, 2-Mo): 0.9303
B (1-As, 3-Mo): 0.9291
B (2-Mo, 3-Mo): 0.3867

Table S9: Cartesian coordinates of the optimised geometry of $[\{CpMo(CO)_2\}_2(AsBi)]^+$ (**D**$^+$) (TPSSh/def2-TZVP level).

Atom	X	Y	Z
Bi	-0.603918104	-2.589742324	-1.107583134
As	-1.722326723	-1.493966333	1.0754222756
Mo	0.8560047290	-1.141906417	0.8488453333
Mo	-1.469296421	0.1516338376	-0.859932278
C	-1.130392082	2.1778337404	0.2895818031
H	-0.262195599	2.3827208417	0.8944445642
C	-3.245142473	1.5481278930	-0.373761792
H	-4.261235278	1.1853715877	-0.358769715
C	-2.557687975	2.0778526871	-1.511259598
H	-2.962054522	2.1857565486	-2.505699547
C	-1.257258219	2.4648177160	-1.094902483
H	-0.496750891	2.9065686003	-1.720139267
C	-2.361984823	1.6114948180	0.7375567709
H	-2.599716564	1.3295323643	1.7509272469
C	-2.638550828	-0.671481249	-2.251630111
C	0.0065030683	0.1217215086	-2.187642270
O	-3.367329542	-1.037762964	-3.064310170
O	0.8063888107	0.2321203226	-3.015353276
C	2.4745275071	0.1161577182	-0.314757703
H	2.2390836685	0.9538718243	-0.950081052
C	2.9436232771	-2.013251790	0.4267731745
H	3.1323589457	-3.075294567	0.4466910979
C	3.0445012377	-1.120201693	1.5408416521
H	3.3249944344	-1.385609029	2.5480420005
C	2.7537527271	0.1914336276	1.0718795617
H	2.7588689409	1.0919486914	1.6664825819
C	2.5877915111	-1.248885966	-0.719053963
H	2.4932938289	-1.620865370	-1.726441167
C	0.7229971655	-2.647213218	2.1445075938
C	0.1800667500	0.0584352312	2.2784829458
O	0.7231864748	-3.510398078	2.9026360970
O	-0.112103223	0.7691790457	3.1382029348

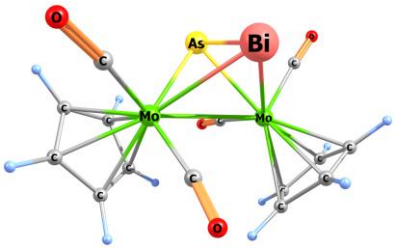

Selected Mayer bond orders larger than 0.100:
B (0-Bi, 1-As): 0.8587
B (0-Bi, 2-Mo): 0.7675
B (0-Bi, 3-Mo): 0.8031
B (1-As, 2-Mo): 0.9447
B (1-As, 3-Mo): 0.9533
B (2-Mo, 3-Mo): 0.3837

Table S10: Cartesian coordinates of the optimised geometry of $[(CpMo(CO)_2\}_2(SbBi)]^+$ (**E**$^+$) (TPSSh/def2-TZVP level).

Atom	X	Y	Z
Bi	0.442370	5.922866	7.856550
Sb	1.502950	5.823532	5.190276
Mo	-0.481483	4.043711	5.858225
Mo	2.446205	4.041462	7.137506
O	-1.265329	2.819391	8.633455
O	-2.864302	6.069579	6.101510
C	-0.915092	3.328204	7.654623
C	-1.949739	5.368853	6.064337
O	3.265132	2.818340	4.373432
O	4.807131	6.087872	6.869914
C	2.906828	3.321731	5.350780
C	3.902366	5.376883	6.923360
C	1.882128	2.129192	8.393628
H	1.010716	1.523835	8.206782
C	3.160723	1.931421	7.814368
H	3.420541	1.159235	7.106848
C	4.045553	2.913208	8.338159
H	5.095447	3.006570	8.108777
C	3.304350	3.725944	9.252236
H	3.697926	4.543511	9.835940
C	1.966434	3.241724	9.284936
H	1.179021	3.595693	9.930958
C	0.086532	2.118151	4.629259
H	0.949502	1.507809	4.838768
C	-1.205516	1.934681	5.184531
H	-1.484529	1.171941	5.894956
C	-2.070915	2.918437	4.635249
H	-3.123708	3.023879	4.845715
C	-1.306166	3.717637	3.728497
H	-1.680964	4.534462	3.131552
C	0.027277	3.222841	3.726041
H	0.831212	3.571607	3.097631

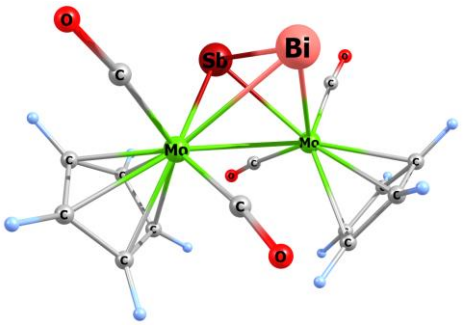

Selected Mayer bond orders larger than 0.100:
B (0-Bi, 1-Sb): 0.8384
B (0-Bi, 2-Mo): 0.8133
B (0-Bi, 3-Mo): 0.7789
B (1-Sb, 2-Mo): 0.8574
B (1-Sb, 3-Mo): 0.8735
B (2-Mo, 3-Mo): 0.3761

Table S11: Cartesian coordinates of the optimised geometry of $[(CpMo(CO)_2\}_2(PAs)]_2^{2+}$ (**1**) (TPSSh/def2-TZVP level).

Atom	X	Y	Z
Mo	14.252187352	4.366093139	33.879736289
Mo	12.719242027	1.673549128	33.423942471
Mo	11.032047162	3.240545620	28.431425382
Mo	12.332175263	6.115833348	28.691846086
As	11.648135636	3.974739134	34.097143512
P	12.686417117	3.741846276	32.142838214
P	11.606853263	4.533892131	30.400086307
As	13.435361153	3.831699419	29.131267425
O	14.840631237	7.080647437	30.297906410
O	14.993249815	0.950344458	31.380525909
C	14.196707505	1.245460857	32.154963587
O	12.453558923	3.218794140	25.614419886
O	14.278376463	5.706785768	26.246252726
C	11.972606298	3.245096831	26.652778292
C	13.939620136	6.679553527	29.711953417
C	16.380610944	3.936293870	34.671673883
H	16.559534856	3.533863530	35.656611996
C	16.048519505	4.081486951	32.397461962
H	15.931075430	3.812291913	31.359458812
O	12.359467696	0.473980854	29.064902079
C	10.341617694	7.256227417	29.124026513
H	9.6108203526	6.912545199	29.839277948
C	13.565593311	5.807980763	27.137671485
O	13.597906929	4.412470114	36.965347128
C	16.261809797	3.181323852	33.474921664
H	16.343097318	2.109432260	33.404327807
C	11.920959779	1.513075639	28.843442420
C	9.1528092841	3.620955807	27.151152084
H	9.1862893398	4.169072364	26.222431980
C	11.451045297	8.097754412	29.422259401
H	11.693673271	8.509372138	30.389421282
C	8.8716308984	3.082920717	29.372183296
H	8.6729191068	3.169262695	30.428972048
O	14.727282166	1.272457942	35.797546820
C	10.351605100	6.985164490	27.727457695
H	9.6272392324	6.414802891	27.171521191
C	16.272688230	5.319233772	34.335559325
H	16.365719467	6.150302361	35.016808424
C	16.059570232	5.404150824	32.923385074

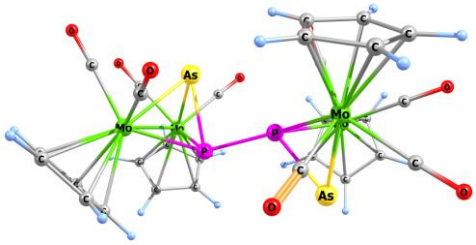

H	15.967224006	6.314935220	32.354976615
C	9.1603366819	1.885069952	28.670287433
H	9.2138725133	0.895163347	29.096558991
C	9.3319018200	2.207789470	27.292808116
H	9.5271744592	1.505549816	26.497588745
C	14.023937848	1.525540285	34.916120622
C	13.551649248	6.234159164	33.818338328
C	8.8690024394	4.154784001	28.437865348
H	8.6301552173	5.177635656	28.671785366
C	12.206782558	-0.51555587	33.779131134
H	12.964776272	-1.24955723	34.002723729
C	11.469377660	7.649105654	27.161166068
H	11.739957005	7.644303237	26.116475650
C	13.791157340	4.378517967	35.835359879
C	10.697359498	0.793683139	32.631002834
H	10.132625782	1.252921725	31.835055486
C	11.730437106	-0.17005007	32.477336597
H	12.070329330	-0.59505810	31.546265192
C	12.152884708	8.344545731	28.199562327
H	13.022133983	8.971660146	28.077515774
O	13.203219062	7.324472412	33.760787150
C	10.522262618	1.043252717	34.021699648
H	9.7773984137	1.688366719	34.459436060
C	11.459784626	0.247125972	34.732303111
H	11.561305190	0.198034940	35.805041535

Selected Mayer bond orders larger than 0.100:

B (0-Mo, 1-Mo): 0.4639;	B (0-Mo, 4-As): 0.9126;	B (0-Mo, 5-P): 0.7025
B (0-Mo, 15-C): 0.4683;	B (0-Mo, 17-C): 0.4385;	B (0-Mo, 23-O): 0.1064
B (0-Mo, 24-C): 0.4137;	B (0-Mo, 36-C): 0.4923;	B (0-Mo, 38-C): 0.4706
B (0-Mo, 44-C): 0.1611;	B (0-Mo, 45-C): 1.1261;	B (0-Mo, 52-C): 1.1123
B (0-Mo, 59-O): 0.1049;	B (1-Mo, 4-As): 0.7679;	B (1-Mo, 5-P): 0.7405
B (1-Mo, 9-O): 0.1056;	B (1-Mo, 10-C): 1.1022;	B (1-Mo, 33-O): 0.1029
B (1-Mo, 44-C): 1.1495;	B (1-Mo, 48-C): 0.5140;	B (1-Mo, 53-C): 0.4387
B (1-Mo, 55-C): 0.4196;	B (1-Mo, 60-C): 0.3806;	B (1-Mo, 62-C): 0.4601
B (2-Mo, 3-Mo): 0.3970;	B (2-Mo, 6-P): 0.6984;	B (2-Mo, 7-As): 0.8701
B (2-Mo, 13-C): 1.0731;	B (2-Mo,19-O): 0.1111;	B (2-Mo, 26-C): 1.1755
B (2-Mo, 27-C): 0.4806;	B (2-Mo, 31-C): 0.4223;	B (2-Mo, 40-C): 0.4536
B (2-Mo, 42-C): 0.4787;	B (2-Mo, 46-C): 0.4246;	B (3-Mo, 6-P): 0.7604
B (3-Mo, 7-As): 0.8495;	B (3-Mo, 8-O): 0.1037;	B (3-Mo, 12-O): 0.1001
B (3-Mo, 14-C): 1.1852;	B (3-Mo, 20-C): 0.4461;	B (3-Mo, 22-C): 1.0967
B (3-Mo, 29-C): 0.4651;	B (3-Mo, 34-C): 0.4056;	B (3-Mo, 50-C): 0.4380
B (3-Mo, 57-C): 0.5006;	B (4-As, 5-P): 0.9632;	B (5-P, 6-P): 0.7926
B (6-P, 7-As): 0.9394;	B (8-O, 14-C): 2.2029;	B (9-O, 10-C): 2.1706

Table S12: Cartesian coordinates of the optimised geometry of $[(CpMo(CO)_2\}_2(PSb)]_2^{2+}$ (**2**) (TPSSh/def2-TZVP level).

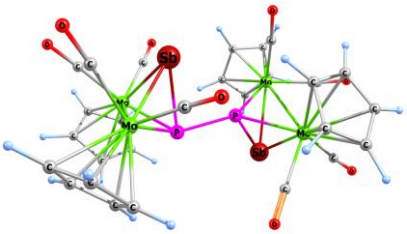

Atom	X	Y	Z
Mo	13.573928448	4.5505328779	34.167699904
Mo	12.683932903	1.5897439346	33.521561451
Mo	10.690541879	3.2835820213	28.505503938
Mo	12.683251444	5.7582498316	28.598355424
Sb	10.883815427	3.6670270672	34.180975307
P	12.362527993	3.6452456575	32.251522740
P	11.550433041	4.5340636369	30.408769058
Sb	13.352255202	3.1620569334	29.235635676
O	15.376165273	6.2271448764	30.116661493
O	15.423291225	1.3698062795	32.013795986
C	14.440049360	1.5038718778	32.598430277
O	11.923475756	3.0302270455	25.615075668
O	14.444388051	4.7968410382	26.176380179
C	11.534868092	3.1360944867	26.688814600
C	14.388965612	5.9945741463	29.574757891
C	15.611935393	4.6110738282	35.276534940
H	15.717003034	4.3188371311	36.309914992
C	15.591228722	4.5366992050	32.975974185
H	15.689558510	4.1816036000	31.963285754
O	11.293588911	0.2539417214	28.978105140
C	11.024567093	7.3701224568	28.969306617
H	10.251261628	7.2595512624	29.713087725
C	13.788211223	5.0788664146	27.076771120
O	12.591968797	4.5806266082	37.155513621
C	15.813181710	3.7707893034	34.153267425
H	16.105927003	2.7350024351	34.195471332
C	11.154955773	1.3908353051	28.832698444
C	8.8834853425	4.0348700157	27.279692557
H	8.9929641197	4.5133248275	26.318754382
C	12.308724058	7.9387540496	29.196057895
H	12.668374687	8.3452384566	30.128362538
C	8.6065040818	3.6897222937	29.539397200
H	8.4881937876	3.8689713488	30.596441974
O	14.209905194	1.5933386901	36.265569588
C	10.933668921	7.0074189612	27.596841392
H	10.078365598	6.5912184758	27.092753902
C	15.286604063	5.9165945667	34.801560813
H	15.118198978	6.7912670882	35.409841500
C	15.274133229	5.8654243327	33.371107381

H	15.096505755	6.6996153978	32.712122861
C	8.5752454060	2.4240770669	28.901867001
H	8.4220178193	1.4729493792	29.387649823
C	8.7431779241	2.6280831716	27.499731140
H	8.7298207670	1.8611581500	26.741248408
C	13.663233520	1.6964506600	35.252873607
C	12.562848310	6.2452258277	33.913150636
C	8.7996009812	4.6844942988	28.539559644
H	8.8217750510	5.7457660559	28.718057338
C	12.624472235	-0.682958717	33.589129617
H	13.497932988	-1.271521730	33.821267169
C	12.162147433	7.3450615849	26.973543864
H	12.396535415	7.2064394337	25.929334080
C	12.875681748	4.5256440313	36.040499639
C	10.976616540	0.4282192970	32.419154563
H	10.394137272	0.8577427752	31.620281855
C	12.205557090	-0.272128648	32.282512386
H	12.711690541	-0.495617654	31.356814863
C	13.017988189	7.9262021695	27.952710408
H	14.007262890	8.3192497744	27.778256167
O	12.049073153	7.2588805817	33.747764033
C	10.623127704	0.4486310746	33.799082346
H	9.7046688485	0.8337462754	34.212425359
C	11.646563128	-0.222672644	34.520846146
H	11.662079663	-0.384559448	35.587381343

Selected Mayer bond orders larger than 0.100:

B (0-Mo, 1-Mo): 0.4478	B (0-Mo, 4-Sb): 0.8107	B (0-Mo, 5-P): 0.7395
B (0-Mo, 15-C): 0.4550	B (0-Mo, 17-C): 0.4455	B (0-Mo, 23-O): 0.1247
B (0-Mo, 24-C): 0.4070	B (0-Mo, 36-C): 0.4779	B (0-Mo, 38-C): 0.4686
B (0-Mo, 44-C): 0.1478	B (0-Mo, 45-C): 1.1633	B (0-Mo, 52-C): 1.1713
B (0-Mo, 59-O): 0.1121	B (1-Mo, 4-Sb): 0.7059	B (1-Mo, 5-P): 0.7256
B (1-Mo, 9-O): 0.1079	B (1-Mo, 10-C): 1.1350	B (1-Mo, 33-O): 0.1008
B (1-Mo, 44-C): 1.1210	B (1-Mo, 48-C): 0.4983	B (1-Mo, 53-C): 0.4303
B (1-Mo, 55-C): 0.4561	B (1-Mo, 60-C): 0.3844	B (1-Mo, 62-C): 0.4600
B (2-Mo, 3-Mo): 0.3905	B (2-Mo, 6-P): 0.7275	B (2-Mo, 7-Sb): 0.7968
B (2-Mo, 11-O): 0.1035	B (2-Mo, 13-C): 1.1107	B (2-Mo, 19-O): 0.1287
B (2-Mo, 26-C): 1.2287	B (2-Mo, 27-C): 0.4660	B (2-Mo, 31-C): 0.4157
B (2-Mo, 34-C): 0.1064	B (2-Mo, 40-C): 0.4500	B (2-Mo, 42-C): 0.4836
B (2-Mo, 46-C): 0.4375	B (3-Mo, 6-P): 0.7250	B (3-Mo, 7-Sb): 0.8156
B (3-Mo, 8-O): 0.1114	B (3-Mo, 12-O): 0.1128	B (3-Mo, 14-C): 1.2217
B (3-Mo, 20-C): 0.4344	B (3-Mo, 22-C): 1.1425	B (3-Mo, 29-C): 0.4641
B (3-Mo, 34-C): 0.4157	B (3-Mo, 50-C): 0.4261	B (3-Mo, 57-C): 0.5000
B (4-Sb, 5-P): 0.8695	B (4-Sb, 52-C): 0.1474	B (4-Sb, 60-C): 0.1551
B (5-P, 6-P): 0.8140	B (5-P, 7-Sb): 0.1198	B (6-P, 7-Sb): 0.8336

Table S13: Cartesian coordinates of the optimised geometry of $[(CpMo(CO)_2\}_2(AsSb)]_2^{2+}$ (**3a**/**b**) (TPSSh/def2-TZVP level).

Atom	X	Y	Z
Mo	6.142986837	13.593613669	16.09400084
Mo	3.134279550	12.718727674	16.21814789
Mo	3.038399406	18.872109769	13.51493045
Mo	1.741117505	18.786169551	16.38179660
Sb	4.081148353	14.771770445	14.59044227
As	4.176988947	14.767681157	17.28475449
Sb	4.173303120	17.606953815	15.74219033
As	1.816967434	16.941798080	14.57916041
O	4.721976566	21.197887760	14.78278281
O	0.539853495	20.777054312	13.41121452
O	-1.17240653	18.622999863	15.21235078
O	3.780242452	11.260408574	13.51677478
O	6.581531159	12.996093726	19.14887194
O	1.009523569	16.329680696	18.17344438
C	4.322233534	11.410080650	17.14068003
O	4.869163946	10.554648196	17.68864477
C	3.100060992	20.341702195	17.47725051
C	3.610827422	11.820939888	14.50892720
C	2.184920523	21.090340955	16.68177128
H	2.436924978	21.772473461	15.88692131
C	7.772332633	13.621797642	14.48248257
H	8.093210077	14.535282259	14.00664054
C	1.281323211	17.197374580	17.47241805
C	4.063043521	20.339461125	14.38695237
C	6.765172676	12.736814935	14.00225961
H	6.199866656	12.854797101	13.09138498
C	1.429949023	20.054253297	13.52584477
C	7.644779489	11.828380365	15.92686138
H	7.836525739	11.152810388	16.74627155
C	-0.08838960	18.657465889	15.58718389
C	2.346182588	19.605511906	18.43523311
H	2.751741457	18.973359500	19.20965729
O	7.370515419	16.420407057	16.64400808
C	8.323206162	13.057809371	15.67854981
H	9.131802674	13.466075895	16.26402730
C	2.528174614	18.558519050	11.29028144
H	1.518900016	18.628840204	10.91565163
C	6.695182489	11.629374916	14.89406546

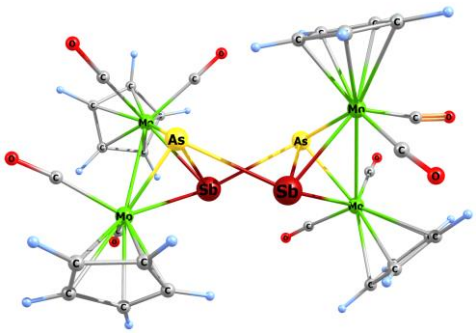

H	6.049514598	10.772247860	14.79662792
C	0.872361831	20.812744526	17.13552223
C	0.959798585	19.896770708	18.22363809
H	0.132528697	19.524706648	18.80727655
C	6.888417844	15.393446217	16.46435654
C	3.176201842	17.367315264	11.71884874
H	2.747604235	16.377491926	11.70983941
C	1.334598858	13.198604515	17.66552212
H	1.389146366	13.866015981	18.50919492
C	3.462167458	19.636309544	11.40371387
H	3.287073035	20.663156108	11.12362602
C	4.682340849	19.099720534	11.91059809
H	5.591629103	19.650888935	12.09373118
C	4.505865555	17.703193958	12.10261311
H	5.258574853	17.016637648	12.45870720
C	6.362105922	13.220897088	18.04532378
C	1.595166250	11.803283452	17.69484850
H	1.893517264	11.237783019	18.56407132
C	1.367423675	11.275443850	16.39012863
H	1.450597233	10.239585466	16.10063463
C	0.954916705	13.542631273	16.33725268
H	0.686534336	14.526404218	15.98541929
C	0.973853877	12.360131906	15.54581663
H	0.701284475	12.290557684	14.50437207
H	-0.03552323	21.240218612	16.73825460
H	4.176058423	20.375473403	17.41025577

Selected Mayer bond orders larger than 0.100

B (0-Mo, 1-Mo): 0.4179	B(0-Mo, 4-Sb): 0.6313	B(0-Mo, 5-As): 0.9770
B (0-Mo, 12-O): 0.1104	B (0-Mo, 14-C): 0.1529	B (0-Mo, 20-C): 0.4710
B (0-Mo, 24-C): 0.4433	B (0-Mo, 27-C): 0.4422	B (0-Mo, 32-O): 0.1020
B (0-Mo, 33-C): 0.4902	B (0-Mo, 37-C): 0.4249	B (0-Mo, 42-C): 1.1453
B (0-Mo, 53-C): 1.1299	B (1-Mo, 4-Sb): 0.7173	B (1-Mo, 5-As): 0.8696
B (1-Mo, 11-O): 0.1132	B (1-Mo, 14-C): 1.1338	B (1-Mo, 17-C): 1.1708
B (1-Mo, 45-C): 0.3930	B (1-Mo, 54-C): 0.4391	B (1-Mo, 56-C): 0.5086
B (1-Mo, 58-C): 0.4320	B (1-Mo, 60-C): 0.4435	B (2-Mo, 3-Mo): 0.4229
B (2-Mo, 6-Sb): 0.6956	B (2-Mo, 7-As): 0.9153	B (2-Mo, 8-O): 0.1082
B (2-Mo, 23-C): 1.1452	B (2-Mo, 26-C): 1.1408	B (2-Mo, 35-C): 0.4523
B (2-Mo, 43-C): 0.4016	B (2-Mo, 47-C): 0.5084	B (2-Mo, 49-C): 0.4394
B (2-Mo, 51-C): 0.4049	B (3-Mo, 6-Sb): 0.6826	B (3-Mo, 7-As): 0.9160
B (3-Mo, 10-O): 0.1147	B (3-Mo, 13-O): 0.1000	B (3-Mo, 16-C): 0.4521
B (3-Mo, 18-C): 0.4323	B (3-Mo, 22-C): 1.1602	B (3-Mo, 26-C): 0.1146
B (3-Mo, 29-C): 1.1252	B (3-Mo, 30-C): 0.4650	B (3-Mo, 39-C): 0.4374
B (3-Mo, 40-C): 0.4915	B (4-Sb, 5-As): 0.6726	B (4-Sb, 6-Sb): 0.5246
B (4-Sb, 7-As): 0.2447	B (5-As, 6-Sb): 0.2145	B (6-Sb, 7-As): 0.6481

Table S14: Cartesian coordinates of the optimised geometry of $[(CpMo(CO)_2\}_2(AsBi)]_2^{2+}$ (**4a**/**b**) (TPSSh/def2-TZVP level).

Atom	X	Y	Z
Bi	9.881866893	-0.24595191	9.997197629
Mo	12.34781796	1.217599458	9.543526603
Mo	10.51625159	0.147943673	7.222442932
As	10.20246271	2.229827168	8.711089346
O	11.09961397	2.613309664	5.365623435
O	13.28469276	-1.77690408	9.645966329
O	13.92028485	1.600930318	6.853415141
C	10.89739102	1.750819717	6.096423749
C	12.88945273	-0.69754867	9.548134303
C	12.33028744	3.116769464	10.92539412
H	11.57521483	3.887043716	10.90648262
C	13.27098109	1.431333850	7.791828329
C	9.876578363	-1.93250054	6.500640218
H	8.888623226	-2.32675033	6.680463888
C	11.01976138	-2.13693751	7.325249459
H	11.05342359	-2.73165159	8.224546573
C	12.34494710	1.971398933	11.77138723
H	11.59296917	1.703759010	12.49773174
C	13.52164382	3.105689602	10.14882569
H	13.81406903	3.855552443	9.430515449
C	12.13001684	-1.50122162	6.697608403
H	13.14746880	-1.49628766	7.051859393
C	11.67743951	-0.89668367	5.499740217
H	12.28982754	-0.35111686	4.798294624
C	14.28059353	1.951151221	10.51905148
H	15.25044369	1.676389323	10.13518089
C	10.28242361	-1.16071194	5.364773461
H	9.658605447	-0.86779799	4.535090108
C	13.54431030	1.251741387	11.51910252
H	13.85283391	0.346812531	12.01910838
O	7.475382534	0.636665206	6.684579540
C	8.591299040	0.501699342	6.921821807
Bi	8.459919146	2.337259885	11.37800336
Mo	5.799337324	2.812055038	10.41483753
Mo	6.399326901	0.824082994	12.76396327
As	6.724311141	0.468325697	10.22403468
O	4.112803749	-1.16158179	11.93012118
O	6.205285464	5.002717880	12.62247780
O	3.096677061	2.019820965	11.79956248

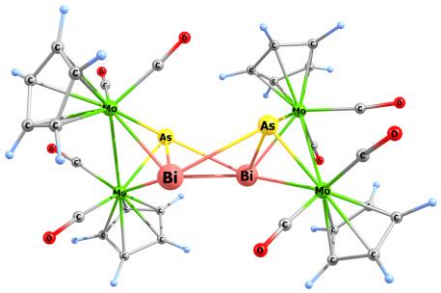

C	4.950790786	-0.41574889	12.17394334
C	6.078710926	4.143235132	11.86332314
C	5.378295177	2.575976149	8.107020486
H	5.368872301	1.635823090	7.581618099
C	4.140267125	2.235588885	11.35545968
C	7.278189201	1.012068236	14.87234202
H	8.275713145	0.678644763	15.11252752
C	6.909330730	2.332718224	14.48549445
H	7.574200865	3.178422725	14.40467819
C	6.498442025	3.438089504	8.280294360
H	7.500161797	3.262081393	7.920632880
C	4.256573814	3.193749475	8.719748838
H	3.255717474	2.791265881	8.749113683
C	5.494770779	2.359737115	14.32181898
H	4.899537798	3.218753381	14.05935007
C	4.989908434	1.064095504	14.59310662
H	3.951008972	0.773419566	14.56509921
C	4.671506626	4.442991197	9.263758243
H	4.038986656	5.157856985	9.766369858
C	6.086552357	0.221180255	14.94237600
H	6.022392290	-0.81225426	15.24434464
C	6.067573131	4.591835174	8.994396342
H	6.678309388	5.443393730	9.250598100
O	8.318747206	-1.64634956	12.76044870
C	7.612001777	-0.73952591	12.71994048

Selected Mayer bond orders larger than 0.100:

B (0-Bi, 1-Mo): 0.6362	B (0-Bi, 2-Mo): 0.6487	B (0-Bi, 3-As): 0.5781
B (0-Bi, 32-Bi): 0.4243	B (0-Bi, 35-As): 0.2528	B (1-Mo, 2-Mo): 0.4266
B (1-Mo, 3-As): 0.9562	B (1-Mo, 5-O): 0.1099	B (1-Mo, 8-C): 1.1449
B (1-Mo, 9-C): 0.3956	B (1-Mo, 11-C): 1.1541	B (1-Mo, 16-C): 0.4100
B (1-Mo, 18-C): 0.4487	B (1-Mo, 24-C): 0.4985	B (1-Mo, 28-C): 0.4308
B (2-Mo, 3-As): 0.9279	B (2-Mo, 4-O): 0.1197	B (2-Mo, 7-C): 1.1412
B (2-Mo, 11-C): 0.1223	B (2-Mo, 12-C): 0.4646	B (2-Mo, 14-C): 0.4524
B (2-Mo, 20-C): 0.4275	B (2-Mo, 22-C): 0.4397	B (2-Mo, 26-C): 0.4860
B (2-Mo, 30-O): 0.1009	B (2-Mo, 31-C): 1.1651	B (3-As, 32-Bi): 0.2583
B (4-O, 7-C): 2.2021	B (5-O, 8-C): 2.1529	B (6-O, 11-C): 2.1628
B (9-C, 10-H): 0.9541	B (9-C, 16-C): 1.1391	B (9-C, 18-C): 1.1960
B (2-C, 13-H): 0.9451	B (12-C, 14-C): 1.1330	B (12-C, 26-C): 1.0903
B (14-C, 15-H): 0.9654	B (14-C, 20-C): 1.1149	B (16-C, 17-H): 0.9564
B (16-C, 28-C): 1.1768	B (18-C, 19-H): 0.9370	B (18-C, 24-C): 1.1200
B (20-C, 21-H): 0.9522	B (20-C, 22-C): 1.1983	B (22-C, 23-H): 0.9351
B (22-C, 26-C): 1.1431	B (24-C, 25-H): 0.9427	B (24-C, 28-C): 1.1780
B (26-C, 27-H): 0.9466	B (28-C, 29-H): 0.9378	B (30-O, 31-C): 2.1823
B (32-Bi, 33-Mo): 0.6822	B (32-Bi, 34-Mo): 0.5968	B (32-Bi, 35-As): 0.5872
B (33-Mo, 34-Mo): 0.4243	B (33-Mo, 35-As): 0.9175	B (33-Mo, 37-O): 0.1159
B (33-Mo, 40-C): 1.1766	B (33-Mo, 41-C): 0.3908	B (33-Mo, 43-C): 1.1372
B (33-Mo, 48-C): 0.4356	B (33-Mo, 50-C): 0.4398	B (33-Mo, 56-C): 0.4936
B (33-Mo, 60-C): 0.4423	B (34-Mo, 35-As): 0.9741	B (34-Mo, 36-O): 0.1140

Table S15: Cartesian coordinates of the optimised geometry of $[(CpMo(CO)_2\}_2(SbBi)]_2^{2+}$ (**5**) (TPSSh/def2-TZVP level).

Atom	X	Y	Z
Mo	12.43764954	1.920669270	16.087072078
Mo	9.365691405	2.760065882	15.807595321
Mo	11.77827166	7.969998648	12.929527995
Mo	13.08195055	8.511228604	15.798543996
Sb	11.43386581	3.800094698	14.281253808
Bi	11.26099019	4.286874049	17.232507149
Sb	10.89778746	6.845918024	15.304447108
Bi	13.59077128	6.194783758	14.162508455
O	12.38364563	1.467828160	19.191437506
O	9.426527704	0.653646808	13.489976645
O	9.548367102	0.424491379	17.893231706
O	14.00854580	10.14783309	12.576959514
O	16.03234589	8.793023260	14.766701692
O	14.10416076	6.454817007	17.916362963
O	14.95396385	3.728114430	16.488608848
O	9.798381999	10.20511124	13.873376014
C	10.57223640	9.392072873	13.607169422
C	13.53915546	10.73214762	16.319098161
H	14.38140841	11.26396802	15.904047850
C	13.54778441	9.950150807	17.509955158
H	14.39229214	9.799455747	18.163652203
C	12.34410014	1.699960624	18.063614394
C	9.492411602	1.410810992	14.357732768
C	9.592070647	1.288962343	17.127878932
C	13.22525123	9.330872870	12.808287230
C	14.93625369	8.630433598	15.081672444
C	13.74132357	7.162474258	17.081362458
C	13.98396939	3.116732728	16.368261895
C	12.22351616	9.443947276	17.706213588
H	11.88966245	8.842955917	18.537504800
C	11.41044398	9.916204271	16.636289415
H	10.34974089	9.752602979	16.529483184
C	12.22724016	10.71749757	15.786436443
H	11.91017112	11.24277392	14.900875190
C	11.94883947	-0.19925718	15.155335748
H	10.96340636	-0.63170742	15.105571430
C	12.85840061	-0.36266020	16.228136923
H	12.67632848	-0.93195104	17.126625955
C	14.06219611	0.327204403	15.903265056

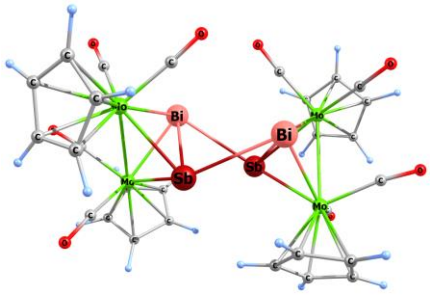

H	14.95747943	0.358257394	16.503894655
C	13.88443093	0.926511306	14.615703556
H	14.62434324	1.490800476	14.069950692
C	12.57483454	0.604040788	14.158212401
H	12.15962840	0.863452096	13.197224654
C	11.89061167	6.300288132	11.272534432
H	12.48561265	5.400913392	11.296941692
C	12.29065572	7.552668744	10.724283804
H	13.25931284	7.775622493	10.304921754
C	11.17591083	8.442442948	10.784277845
H	11.14642159	9.453749373	10.410599648
C	10.09044798	7.733636141	11.385417978
H	9.096379030	8.117547436	11.554147207
C	10.53200479	6.417561495	11.682596859
H	9.932899193	5.634024266	12.120333490
C	7.107972236	2.478370851	15.919748482
H	6.657776342	1.499088926	15.957934710
C	7.491301975	3.275693304	17.040203165
H	7.390562714	3.001668497	18.078804513
C	7.988576910	4.518684650	16.553050662
H	8.282819544	5.363187219	17.156441994
C	7.923981146	4.486919378	15.130939437
H	8.211791444	5.286520444	14.465925331
C	7.384904964	3.233584596	14.738777446
H	7.187420146	2.922614335	13.724652113

Selected Mayer bond orders larger than 0.100:

B (0-Mo, 1-Mo): 0.3910	B (0-Mo, 4-Sb): 0.7379	B (0-Mo, 5-Bi): 0.7715
B (0-Mo, 8-O): 0.1249	B (0-Mo, 14-O): 0.1146	B (0-Mo, 21-C): 1.1933
B (0-Mo, 23-C): 0.1294	B (0-Mo, 27-C): 1.2087	B (0-Mo, 34-C): 0.4272
B (0-Mo, 36-C): 0.4349	B (0-Mo, 38-C): 0.4924	B (0-Mo, 40-C): 0.4545
B (0-Mo, 42-C): 0.4564	B (1-Mo, 4-Sb): 0.7364	B (1-Mo, 5-Bi): 0.7569
B (1-Mo, 9-O): 0.1146	B (1-Mo, 10-O): 0.1074	B (1-Mo, 22-C): 1.1817
B (1-Mo, 23-C): 1.1591	B (1-Mo, 54-C): 0.5044	B (1-Mo, 56-C): 0.4556
B (1-Mo, 58-C): 0.4181	B (1-Mo, 60-C): 0.3996	B (1-Mo, 62-C): 0.4469
B (2-Mo, 3-Mo): 0.3909	B (2-Mo, 6-Sb): 0.7371	B (2-Mo, 7-Bi): 0.7560
B (2-Mo, 11-O): 0.1069	B (2-Mo, 15-O): 0.1152	B (2-Mo, 16-C): 1.1849
B (2-Mo, 24-C): 1.1570	B (2-Mo, 44-C): 0.4177	B (2-Mo, 46-C): 0.4557
B (2-Mo, 48-C): 0.5053	B (2-Mo, 50-C): 0.4462	B (2-Mo, 52-C): 0.4002
B (3-Mo, 6-Sb): 0.7401	B (3-Mo, 7-Bi): 0.7723	B (3-Mo, 12-O): 0.1240
B (3-Mo, 13-O): 0.1148	B (3-Mo, 17-C): 0.4348	B (3-Mo, 19-C): 0.4915
B (3-Mo, 24-C): 0.1270	B (3-Mo, 25-C): 1.1902	B (3-Mo, 26-C): 1.2110
B (3-Mo, 28-C): 0.4542	B (3-Mo, 30-C): 0.4573	B (3-Mo, 32-C): 0.4264
B (4-Sb, 5-Bi): 0.5389	B (4-Sb, 6-Sb): 0.4557	B (4-Sb, 7-Bi): 0.3460
B (5-Bi, 6-Sb): 0.3451	B (5-Bi, 21-C): 0.1037	B (5-Bi, 58-C): 0.1143
B (6-Sb, 7-Bi): 0.5374	B (7-Bi, 25-C): 0.1020	B (7-Bi, 44-C): 0.1149

Table S16: Natural charge distribution of the $E_2E'_2$ core in **1**-**5**, calculated at the TPSSh/def2-TZVP level.

$[(CpMo(CO)_2\}_2(PAs)]_2^{2+}$ (**1**)		$[(CpMo(CO)_2\}_2(PSb)]_2^{2+}$ (**2**)		$[(CpMo(CO)_2\}_2(AsSb)]_2^{2+}$ (**3a**)		$[(CpMo(CO)_2\}_2(AsBi)]_2^{2+}$ (**4a**)		$[(CpMo(CO)_2\}_2(SbBi)]_2^{2+}$ (**5**)	
Atom	Nat. charge	Atom	Nat. charge	Atom	Nat. charge	Atom	Nat. charge	Atom	Nat. charge
As 5	0.434	Sb 5	0.736	Sb 5	0.565	Bi 1	0.720	Sb 5	0.408
P 6	0.159	P 6	0.037	As 6	0.358	As 4	0.286	Bi 6	0.857
P 7	0.257	P 7	0.174	Sb 7	0.628	Bi 33	0.680	Sb 7	0.412
As 8	0.562	Sb 8	0.938	As 8	0.330	As 36	0.318	Bi 8	0.856
Sum	1.412	Sum	1.885	Sum	1.882	Sum	2.004	Sum	2.533

9 References

1 X. Zheng, Z. Zhang, G. Tan and X. Wang, *Inorg. Chem.* 2016, **55**, 1008-1010.

2 L. Dütsch, M. Fleischmann, S. Welsch, G. Balázs, W. Kremer and M. Scheer, *Angew. Chem. Int. Ed.* 2018, **57**, 3256-3261.

3 L. Dütsch, C. Riesinger, G. Balázs and M. Scheer, *Chem. Eur. J.* 2021, **27**, 8804-8810.

4 N. G. Connelly and W. E. Geiger, *Chem. Rev.* 1996, **96**, 877-910.

5 Agilent (2014). CrysAlis PRO. Agilent Technologies Ltd., Yarnton, Oxfordshire, England.

6 G. Sheldrick, *Acta Crystallographica Section A* **2015**, *71*, 3-8.

7 O. V. Dolomanov, L. J. Bourhis, R. J. Gildea, J. A. K. Howard and H. Puschmann, *J. Appl. Cryst.* 2009, **42**, 339-341.

8 G. Sheldrick, *Acta Crystallographica Section C* 2015, **71**, 3-8.

9 F. Neese, *WIREs Comput. Mol. Sci.* 2018, **8**, e1327.

10 a) J. Tao, J. P. Perdew, V. N. Staroverov, G. E. Scuseria, *Phys. Rev. Lett.* **2003**, *91*, 146401; b) V. N. Staroverov, G. E. Scuseria, J. Tao and J. P. Perdew, *J. Chem. Phys.* 2003, **119**, 12129-12137; Erratum: *J. Chem. Phys.* 2004, **121**, 11507.

11 a) F. Weigend, M. Häser, H. Patzelt and R. Ahlrichs, *Chem. Phys. Lett.* 1998, **294**, 143; b) F. Weigend and R. Ahlrichs, *PCCP* 2005, **7**, 3297-3305.

12 a) A. D. Becke, *Physical Review A* 1988, **38**, 3098-3100; b) J. P. Perdew, *Physical Review B* 1986, **33**, 8822-8824; Erratum: *Physical Review B* 1986, **8834**, 7406.

13 F. Neese, F. Wennmohs, A. Hansen and U. Becker, *Chem. Phys.* 2009, **356**, 98.

14 E. Caldeweyher, S. Ehlert, A. Hansen, H. Neugebauer, S. Spicher, C. Bannwarth and S. Grimme, *J. Chem. Phys.* 2019, **150**, 154122.

15 V. Barone and M. Cossi, *J. Phys. Chem. A* 1998, **102**, 1995-2001.

16 a) P. J. Stephens, F. J. Devlin, C. F. Chabalowski and M. J. Frisch, *J. Phys. Chem.* 1994, **98**, 11623-11627; b) C. Lee, W. Yang and R. G. Parr, *Physical Review B* 1988, **37**, 785-789.

17 G. Knizia, *J. Chem. Theory Comput.* 2013, **9**, 4834-4843.